Cavitation monitoring and spatial mapping for pulsed high-intensity focused ultrasound enhanced drug delivery

Tong Li

A dissertation

submitted in partial fulfillment of the

requirements for the degree of

Doctor of Philosophy
University of Washington

2014

Reading Committee:

Joo Ha Hwang, Chair

Lawrence A. Crum

Matthew O'Donnell

Program Authorized to Offer Degree:

Bioengineering

University of Washington

Abstract

Cavitation Monitoring and Spatial Mapping for Pulsed High-Intensity Focused Ultrasound Enhanced Drug Delivery

Tong Li

Chair of the Supervisory Committee:
Dr. Joo Ha Hwang
Department of Bioengineering

High intensity focused ultrasound (HIFU) is an emerging non-invasive ablation modality, in which high amplitude ultrasound waves are focused inside the human body to thermally ablate or mechanically disrupt the tissue at the focus. Ultrasound-enhanced drug delivery is an active and promising area of research. Enhanced drug diffusion and vascular permeability following HIFU is largely attributed to mechanical tissue disruption caused by ultrasound-induced bubble activity- cavitation. Although cavitation can be beneficial, the violent collapsing of bubbles may cause undesired tissue damage. Therefore, it is very important to monitor cavitation activity during pHIFU treatments and know the ultrasound pressure levels sufficient to reliably induce cavitation in a given tissue. Correlating the quantity and depth of drug penetration with the degree of cavitation is a significant challenge during *in vivo* treatment due to the highly complex dynamics of cavitation in different types of tissue. Furthermore, the current methods of cavitation detection are of either limited sensitivity or spatial mapping capability to monitor the site of occurrence and the extent of bubble activity in tissue.

In this dissertation, three metrics of cavitation activity induced by pHIFU and evaluated by confocal passive cavitation detection were introduced: cavitation probability, cavitation persistence and the level of broadband acoustic emissions. These metrics were used to characterize cavitation activity in gel phantoms, *ex vivo* tissue and *in vivo* transgenic pancreatic tumors at varying peak-rarefactional focal pressures. Cavitation thresholds were also determined in various media. In order to find the ideal HIFU parameters for drug delivery, cavitation metrics were measured and correlated with the degree of chemotherapeutic drug uptake in *in vivo* tumors immediately after HIFU exposures and systematic administration of chemotherapeutic drug. The study demonstrated that reliable and intense cavitation activity induced by pHIFU is a sufficient and necessary condition for enhanced drug delivery. To spatially detect cavitation, a new ultrasound imaging method termed "Bubble Doppler" was developed to detect microbubbles using a modification of Doppler processing. This method was shown to provide sensitivity superior to that of existing cavitation detection methods, and has high spatial resolution inherent to conventional Doppler imaging.

Table of Contents

Page

List of Figures

Figure number Page

List of Tables Page

ACKNOWLEDGEMENTS

I would like to thank everyone from Center for Industrial and Medical Ultrasound who helped me for pursuing my Ph.D degree. In particular, I first would like to thank my advisor Dr. Joo Ha Hwang for giving me unreserved guidance and opportunities to grow as a researcher. I truly appreciated the trust and flexibility he gave me to explore many projects. I'd like to thank Dr. Lawrence Crum for his encouragement, support and wisdom in both my work and life. The discussion with him always excited me to move forward. Thanks to Dr. Francesco Curra for teaching me both rigorous research skills and critical thinking skills as a young scientist. I'd also like to thank my supervisory committee members Dr. Matthew O'Donnell and Dr. Raymond Yeung for their advice and time.

I'd like to thank Dr. Tatianna Khokhlova for her generous training of my experimental, writing and public speaking skills. Her enthusiasm for research motivated me to keep improving and finding new directions. I'd also like to thank Dr. Yak-Nam Wang for her guidance in designing my mouse experiment and teaching me all the histology analysis skills. I was influenced greatly by her resourcefulness and careful attitude in research studies. Thanks to Dr. Hong Chen for frequently sharing her knowledge, findings and inspirations. Thanks to Dr. Oleg Sapozhnikov and Dr. Matthew O'Donnell for giving their advice and prompt feedback in the bubble Doppler project. I'd like to further thank Marla Paun, Frank Starr and Samantha D'Andrea for all their expert skills and experience with the animal studies, as well as, Dr. Andrew Brayman, Dr. Wayne Kreider, Dr. John Kucewicz and Barbrina Dunmire for their valuable consultation in papers, algorithms and experiment setup. I also want to thank all the staff and students, Dr. Julianna Simon, Navid Farr, Camilo Perez and Dr. Wei Lu for creating such a supportive working environment, it's lucky for me to work with so many smart, humble and resourceful people throughout these five years. Lastly, I would like to thank my parents, my fiancé and my family, for their unconditional support.

DEDICATION

To my loving parents, my father Gang Li, who introduced the world of science to me and my mother Jun Yao, who encouraged me with love and caring, although we are thousands of miles apart your love has always been with me.

To my fiancé, Weilan, who kept me continuously motivated and shared every difficulty and happiness with me.

Chapter 1

Introduction

1.1 Motivation

The use of pulsed high-intensity focused ultrasound (pHIFU) to enhance the penetration of chemotherapeutic agents into solid tumors is a promising new approach in cancer therapy [1]–[3]. Cavitation is commonly considered to be the key mechanism in pHIFU-mediated drug delivery, which increases vascular permeability and affects drug transport through the interstituum. The collapse of bubbles could disrupt stromal tissue and facilitate the diffusion of drug molecules into solid tumors. The pHIFU treatment protocols are designed to promote cavitation, but suppress tissue heating by using short pHIFU pulses, and delivering ultrasound at low pulse repetition frequencies. Ultrasound contrast agents (UCAs) are often administered to efficiently enhance cavitation activity and reduce the cavitation threshold [4], however, reports of quantitative cavitation activity measurements during *in vivo* studies without UCAs are scarce. Addtionally, cavitation activity and the threshold for cavitation nucleation also depend significantly on tissue composition [5] and tissue viability and perfusion (*ex vivo* vs. *in vivo*); therefore, the results obtained for a single tissue type may not be uniformly applicable to other tissues. Furthermore, although cavitation has been demonstated beneficial to tumor drug delivery recently [6], [7], the pressures required to generate cavitation in vivo are generally very high and tissue-specific. Due to the stochastic nature of cavitation, the predicted delivery cannot be enhanced without controlled and monitored cavitation [8]. The overall goal of this study is to characterize, optimize and monitor cavitation activity, to correlate it with drug penetration, and to spatially image cavitation in pHIFU drug delivery treatments of one of the most resilient and lethal cancers – pancreatic carcinoma. The studies are performed in genetically modified mice (KPC model) that spontaneously develop pancreatic tumors which are morphologically very similar to human disease.

Multiple techniques are available and have been shown useful for characterizing cavitation activity during HIFU exposures[9], but passive cavitation detection (PCD) of broadband noise,

produced by collapsing bubbles during inertial cavitation, is by far the most widely used technique [10], [11]. Several different ways to interpret the signals acquired by PCD, i.e. cavitation activity metrics, are currently in use. Inertial cavitation dose - the root-mean-square (RMS) amplitude, in the frequency domain, of the broadband noise within a frequency window located between the harmonic peaks - was introduced and correlated to endothelial cell damage and hemolysis *in vivo* in several studies [11], [12]. Probability of cavitation occurrence is another metric, which indicates the likelihood of observing a cavitation event at a given HIFU peak negative pressure level and pulse duration and was used to study cavitation thresholds in different *ex vivo* tissues and gel phantoms [5], [13], [14]. A third metric – cavitation persistence - should be introduced to describe how long cavitation lasts when pHIFU is consistently delivered at a single treatment location. This indicator is useful for optimization of the treatment duration. Cavitation noise level relates to the intensity of bubble collapse, the cavitation probablity applies to the presence of cavitation nuclei while the cavitation persistence pertians to the replenishement of nuclei. If one considers these three metrics with respect to the design of exposures for cavitation-mediated drug delivery, all of them appear equally important and complementary. Thus, the first goal of this chapter is to compare the different metrics of cavitation activity in *ex vivo* and *in vivo* pancreatic tumor tissue, and to compare these metrics among different types of *ex vivo* tissues.

In the context of pHIFU enhanced drug delivery, correlation of the acoustic cavitation with the efficacy of drug uptake for cancer is still a question. To treat against cancerous tumors, the therapeutic agents must not only reach the tumor tissue but also penetrate in effective quantities without causing systematic toxicity to other tissues [2]. So it is important to optimize acoustic parameters for effective localized pHIFU drug delivery in the tumor. On the other hand, although several *in vivo* studies have been performed in various xenograft and syngenic autograft animal models that have demonstrated that ultrasound enhanced drug delivery is effective in decreasing tumor size [1], [15], these tumor models, especially for pancreatic cancer, have been criticized for being unrealistic and not representative of the true *in vivo* environment seen in the human disease. So the second goal of the work is to control the amount of cavitation activity

needed to improve tumor penetration of these chemotherapeutic agents in a realistic mouse model (KPC mouse model).

While PCD offers a relatively simple and well characterized way to quantify the amount of cavitation that occurred within the targeted tissue, it does not allow to spatially localize the site of cavitation occurrence. Existing methods of detecting microbubbles, such as passive cavitation detection or B-mode imaging have limited sensitivity, especially to small-size and non-violently collapsing microbubbles. The "Twinkling Artifact" (TA) occurs when one uses color Doppler ultrasound, which is usually employed to display moving blood as color on the screen to image a stone [16]. The artifact appears when color Doppler ultrasound is used to image calcifications in soft tissue, kidney stones or other hard concretions. The artifact is displayed as brightly colored spots on a black-and-white background of imaging area of tissue. One of the mechanisms for the appearance of TA is irregular scattering of the Doppler ensemble pulses from the fluctuating microbubbles [17]. Therefore, TA may be used not only to detect hard concretions in tissue, but also to visualize bubbles that exist or appear in the bulk of soft tissue, far from the rigid objects. Because the Doppler imaging is designed to detect scattering from weak scatters (*viz*, red blood cells), it is very sensitive to the presence of small-size bubbles. Therefore, the study will use TA to detect the presence and monitor the appearance of microbubbles in tissue spatially during HIFU enhanced drug delivery and determine acoustic cavitation threshold in tissue using Doppler imaging mode.

In summary, the study will characterize the cavitation activity in gel phantoms, *ex vivo* tissues and *in vivo* pancreatic tumors by studying cavitation probability, cavitation persistence and cavitation noise level. After cavitation thresholds are determined and compared between *ex vivo* and *in vivo* pancreatic tumors, the correlation of between chemotherapeutic drug uptake and pHIFU induced cavitation will be studied in an *in vivo* mouse model pancreatic tumor. Once pHIFU enhance drug delivery is demonstrated in a realistic mouse model, methods for targeting and spatially monitoring cavitation occurrence during treatment will be developed to enable clinical translation.

1.2 Background

1.2.1 High-Intensity Focused Ultrasound (HIFU)

High-Intensity Focused Ultrasound (HIFU)

Ultrasound is a form of mechanical vibration above the threshold of human hearing (20 KHz). Medical Ultrasound is typically generated by piezoelectric material which oscillated in the same frequency as the driving electrical current. The resulting ultrasound wave propagates through tissue, causing alternating cycles of compression and rarefraction pressure wave. In high-intensity focused ultrasound HIFU, ultrasound waves are focused into a given point and induce bioeffects in tissues without damaging the intervening path (Fig. 1.1). Diagnostic ultrasound usually uses frequencies in the range 1-20 MHz. In the clinical application of HIFU, a frequency range of 0.5-3.5MHz is commonly used. Another significant difference between HIFU and diagnostic ultrasound is that the time averaged acoustic intensity at the focus is several orders of magnitude greater with HIFU. The focal acoustic intensities of HIFU range from 100 to 10,000 W/cm2 and focal regions are typically 2-5 mm in diameter and 6-10 mm in length. Two predominant mechanisms of HIFU induced bioeffects can be categorized into thermal (heating) and mechanical (acoustic cavitation or radiation force). The mechanical mechanism of cavitation has becoming an emerging technique for drug delivery [18]. Cavitation is the generation of gas and/or vapor bubbles in a liquid by ultrasound. Inertial cavitation is associated with the violent collapse of bubbles due to the ultrasound field and often results in the formation of high-speed liquid jets created from an asymmetric collapse of the bubbles.

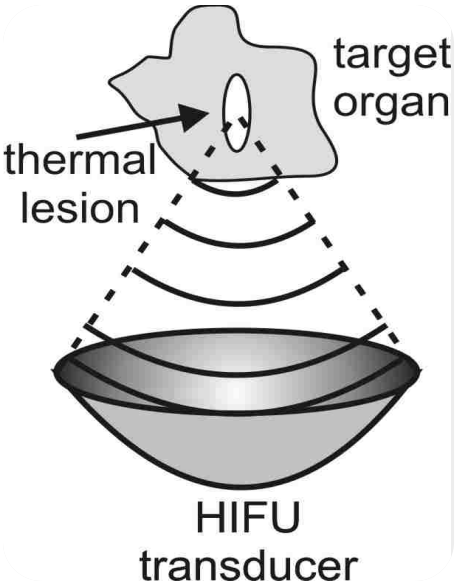

Figure 1.1: High amplitude ultrasound waves are focused inside the human body to thermally ablate or mechanically disrupt the tissue at the focus.

Pulsed High-Intensity Focused Ultrasound (pHIFU) Induced Cavitation

HIFU wave is an alternation of compressional and rarefactional pressure wave. The negative phase causes cavitation nuclei to expand. The positive phase makes it contract. When negative pressure amplitude becomes large, it could initiate unstable bubble growth, resulting in a violent collapse (Fig. 1.2). Pulsed high-intensity focused ultrasound (pHIFU) uses short pulses, delivered at low pulse repetition frequency, to cause transient bubble activity. This transient effect of bubble collapse is a key factor in pHIFU enhanced drug delivery. The pulsed exposures also reduce the temporal average intensity at the HIFU focus, so heating buildup is suppressed. pHIFU, designed to promote cavitation effect while minimizing thermal effect, has been extensively used to enhance drug/gene delivery to tumors with and without the assistance of microbubbles. pHIFU could temporarily increase the permeability of the biological tissue to the therapeutic agent through acousto-mechanical effect. Although the evidence of therapeutic benefits has been shown, the mechanism remains in dispute and uncharacterized.

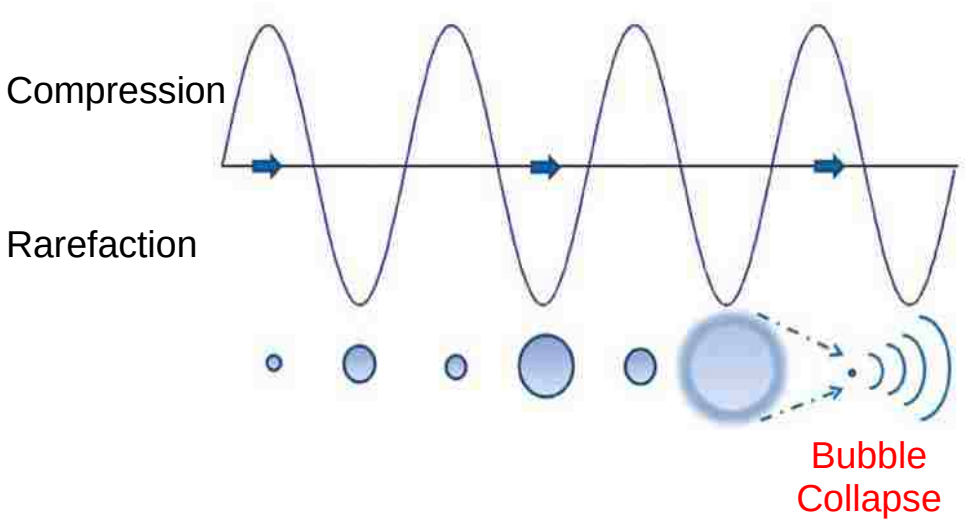

Figure 1.2 The growth and violent collapse of bubbles due to the acoustic pressure wave. HIFU pressure waveform is an alternation of compressional and rarefactional pressure waves. Cavitation nucleus grows with the rarefactional phase of the HIFU wave and collapse in compression.

1.2.2 Pancreatic Cancer and Chemotherapeutic Drug Delivery

Pancreatic Cancer

Pancreatic ductal adenocarcinoma (PDA) is the fourth leading cause of cancer-related mortality in the United States. It is one of the deadliest cancer types. Most pancreatic cancer patients will die within the first year of diagnosis. In 2013, more than 45,000 Americans are diagnosed with cancer of the pancreas [19]. Unlike many other cancers, the survival rate for the disease has not improved substantially. Since 1975, the five-year relative survival rate for pancreatic cancer has moved from 2 % to only 6 % while the overall five-year relative survival rate has moved from 49 % to 68 %. The causes of pancreatic cancer are not well understood, although there are several factors known to increase the risk, such as obesity, cigarette smoking or genetic factors. The treatment options include surgery (pancreatectomy) and chemotherapy, either alone or in combination with radiation therapy.

Chemotherapeutic Drug Delivery

Current treatment with chemotherapeutic agents in cancer therapy usually relies on systemic delivery with limited tumor specificity, and therefore may result in adverse side effects in normal tissues and insufficient drug delivery to the target tumor. Gemcitabine, a deoxycytosine analog, is the current standard chemotherapy for advanced disease. Gemcatibine has been shown to be effective in pancreatic cancer cell cultures and mouse models bearing transplanted pancreatic tumors. However, it has not been translated into an effective systemic treatment in humans.

Studies suggested that insufficient delivery of gemcitabine into the tumor is an important mechanism for the apparent chemoresistance. One of the major barriers to drug delivery in pancreas cancer appears to be the presence of a prominent stromal matrix that separates blood vessels from tumor cells (Fig. 1.3). Pancreatic adenocarcinoma is characterized by a very potent proliferation of fibroblasts. Olive *et. al* [20] hypothesized that the stromal cells might create a physical barrier against drug entry. In his study, mice were treated with a small molecule inhibitor of hedgehog pathway which was critical for fibroblast proliferation. And indeed, it's found that when fibroblast growth was inhibited, pancreatic tumors became more vascularized, more perfused with chemotherapeutic drugs, and the mice lived longer. Therefore, effective therapy for disrupting the stromal matrix is needed.

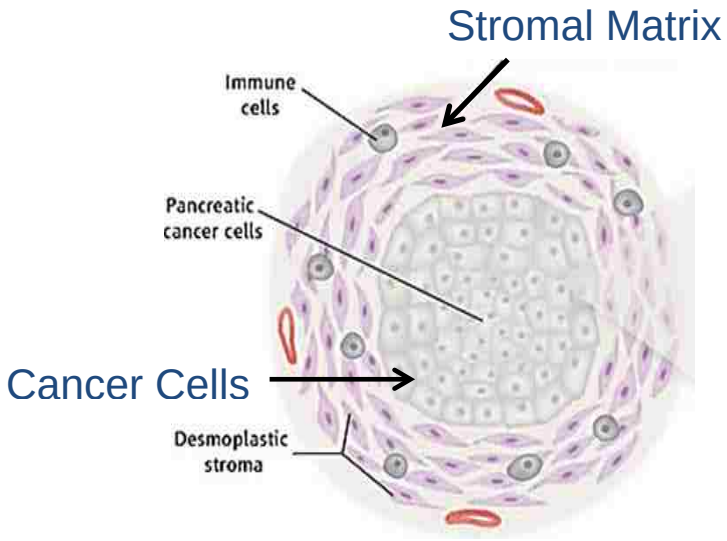

Figure 1.3: Illustration of pancreatic tumor. Stromal matrix is a highly fibrotic area that separates blood vessels from pancreatic cancer cells, leading to insufficient drug penetration. Figure cited and edited from Olsen and Hanahan, Science, 2009.

In another study, Jain showed that depleting the stromal matrix in tumor could improve the perfusion of anticancer drug and improve survival rate [21], [22]. He proposed the mechanism of chemoresistance of matrix-rich tumor, such as pancreatic tumor, was due to the fibrous matrix that compressed tumor blood vessels with solid stress. The tumor consists of the abnormally stiff stromal matrix that can squeeze blood vessels shut, preventing them from delivering anticancer drugs to many parts of the tumor mass (Fig. 1.4a). Squashing of blood vessels can, moreover, deprive tumors of oxygen, an effect that can increase the aggressive behavior of cancer cells. Therefore, when depleting the collagen in the matrix, the blood vessels in matrix rich tumors could open up enough to improve the delivery and efficacy of chemotherapies used to treat these cancers (Fig. 1.4b). If the solid stress of the abnormally stiff matrix could be removed by using pulsed HIFU induced cavitation to "loosen" up the fibrotic matrix, the drug delivery could be potentially improved.

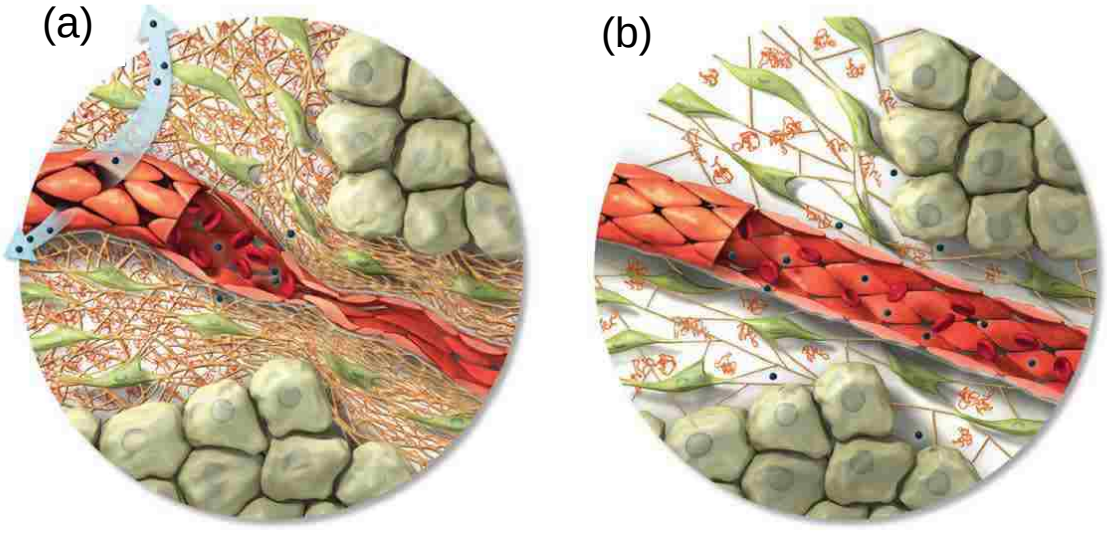

Figure 1.4 Illustration of tumor vessels crushed by fibrotic matrix. When the matrix and cells squeeze tumor vessels, they impede blood flow and thus prevent anticancer drugs from reaching malignant cells beyond the crushed region (a). Substances that deplete the matrix have been shown in mice to reduce solid stress and thus enhance tumor blood flow and the dispersal of

anticancer drugs, potentially improving the effectiveness of anticancer drugs (b). Figure cited from Jain, Scientific American, 2014

1.2.3 Pulsed HIFU Enhanced Drug Delivery

Pulsed HIFU (pHIFU) has recently been demonstrated to increase the efficacy of a variety of drug therapies. It reduces the generation of heat and allows microbubble generation or non-lethal temperature elevations. Several studies have used pHIFU in combination with temperature sensitive drugs to enhanced targeted drug delivery [23]. In such studies, a duty cycle of around 10% was used to induce a mild hyperthermia of about 4 °C to 5 °C temperature elevation. In this way, temperature sensitive drugs could be released at the targeted location.

pHIFU can also be used to cause acoustic cavitation, in which small cavities nucleate inside the biological tissues and pulsate by the acoustic pressure applied. These induced bubbles can be oscillating or collapsing violently, causing significant bioeffects in tissue. This mechanism could potentially cause many beneficial effects, such as acoustic hemostatsis, opening of blood brain barrier, sonoporation and sonophoresis, as well as thrombolysis. It has also been shown to enhance drug delivery by mechanical disrupting tissues, enhance vascular permeability. The FDA has already approved sonophoresis method for ultrasonically enhancing drug delivery, which uses ultrasound transdermally to facilitate transport of drugs through the skin and into soft tissues and blood vessels [24].

1.2.4 The KPC Mouse Model

In the *in vivo* experiments, a transgenic mouse model of pancreatic ductal adenocarcinoma was used. The KrasLSL.G12D/+; p53R172H/+; PdxCretg/+ (or KPC) model closely recapitulates the genetic mutations, clinical symptoms and histopathology found in human pancreatic cancer, unlike xenograft or orthotopic models [20]. The tumors generally have a moderately differentiated ductal morphology with extensive dense stromal matrix. The dense stromal matrix together with the poorly developed vasculature in pancreatic tumor is a major obstacle to chemotherapeutic drug penetration. The KPC mouse model is thus the most relevant in the studies on ultrasound-induced chemotherapeutic drug delivery in pancreatic cancer. All of the

animal experimental procedures were approved by the Institutional Animal Care and Use Committee at the University of Washington. KPC mice were used for this study when their tumor size reached 1 cm according to diagnostic ultrasound examination.

1.2.5 Methods for Cavitation Monitoring

Passive cavitation detection (PCD) is considered to be the most reliable, cost-effective and sensitive means of real-time cavitation detection method [8]. It is by far the most widely used technique [10], [25]. For example, the transcranial cavitation threshold in the presence of microbubbles in mouse brain was found to be 0.45 MPa at frequency of 1.5 MHz using PCD [26].

As PCD is single element focused transducer, it can only detect cavitation along one single axis and provides minimal spatial information. Therefore, techniques of using multielement arrays as passive receivers were developed to offer spatial and temporal information. Recently a passive acoustic mapping (PAM) method has been proposed. Broad and harmonic emissions during HIFU therapy from radiofrequency data were investigated using ex vivo samples of bovine tissue [27]. It serves as a detector of lesion occurrence and a method of mapping the position of ablated tissue during HIFU therapy. However, the method uses continuous waves for HIFU exposures, which is not suitable for drug delivery. In order to promote cavitation, but suppress tissue heating, the drug delivery treatments use short HIFU pulses, and deliver ultrasound at low pulse repetition frequencies. Moreover, the image reconstruction technique requires a large aperture transducer in order to achieve reasonable image quality; it's not readily practical in clinical settings. Therefore, a monitoring technique for drug delivery in real-time HIFU exposures is needed.

1.3 Scope of the Thesis

The overall goal of the thesis was to use pHIFU to enhance drug delivery into an *in vivo* pancreatic tumor in a realistic pancreatic cancer model. As pHIFU induced cavitation is a stochastic phenomenon and is often tissue specific, the study first characterized the cavitation activity in gel phantoms, *ex vivo* tissues and *in vivo* pancreatic tumors by studying cavitation

probability, cavitation persistence and cavitation noise level (Chapter 2). After cavitation was fully characterized by these cavitation metrics in the media such as *ex vivo* and *in vivo* pancreatic tumors, the correlation between chemotherapeutic drug uptake and pHIFU induced cavitation was studied in an *in vivo* mouse model of pancreatic tumor, the KPC mouse model (Chapter 3). Once pHIFU enhanced drug penetration is demonstrated to be statistically significant in the realistic KPC mouse model, methods for spatially monitoring cavitation occurrence during treatment was developed to enable clinical translation of pHIFU aided drug delivery (Chapter 4).

In Chapter 2, we introduced three cavitation metrics - probability, persistence and broadband noise level – to comprehensively characterize cavitation activity in different media (gel phantoms, *ex vivo* tissues and *in vivo* pancreatic tumors) and determine the pressure thresholds to reliably induce cavitation during pHIFU exposures. Experimental setup for detecting cavitation during pHIFU treatment was developed. Post processing algorithm for extracting inertial cavitation from acquired signals was designed. Three metrics - cavitation probability, cavitation persistence and broadband noise level - were established to fully characterize cavitation activity. Pulsing protocols were developed for reliably inducing cavitation in *in vivo* pancreatic tumors.

In Chapter 3, we demonstrated that reliable, intense cavitation activity induced by pulsed HIFU is a sufficient and necessary condition for enhanced drug uptake by the highly fibrotic pancreatic tumor. A range of pressure levels was used for enhancing drug penetration in a genetically modified mouse pancreatic tumors (KPC mouse) in *vivo*. Uptake levels of Doxorubicin (Dox) were evaluated by the three different methods: fluorescent imaging, fluorescent microscopy and high performance liquid chromatography (HPLC). The results of these methods indicated pHIFU induced blood vessel damage and increased stroma matrix permeability by cavitation effect. The relative ratio of Dox concentration in treated and control tumor tissue volumes was linearly correlated with the persistence of cavitation occurrence and the cavitation noise level.

In Chapter 4, a new active cavitation mapping technique termed bubble Doppler was developed to spatially monitor cavitation occurrence in pHIFU-aided drug delivery treatments. The bubble Doppler method was based on a fusion of the adaptations of three Doppler techniques that had been previously developed for imaging of ultrasound contrast agents – color Doppler, pulse

inversion Doppler, and decorrelation Doppler. Doppler ensemble pulses were interleaved with therapeutic pHIFU pulses using three different pulse sequences and standard Doppler processing was applied to the received echoes. The method could quantify the bubble nonlinearity and map bubble presence at the same time. It provided superior sensitivity compared to PCD methods. It would also be readily translatable for clinical use, because it uses a commercially available imaging probe, which can be incorporated into a HIFU system.

In summary, the study has shown that pulsed HIFU induced cavitation overcomes barriers to drug delivery, by increasing local delivery of chemotherapeutic agents in a targeted fashion and improve the efficacy of existing chemotherapeutic agents in a realistic mouse model. The characterization of pHIFU treatment by passive cavitation detection and the mechanisms of chemotherapeutic drug uptake were studied. The potential of clinical translation of this technology could be aided by the spatial mapping of pHIFU induced cavitation.

Chapter 2

Characterization of Cavitation Activities in Gel Phantoms, *Ex Vivo* Tissues and *In Vivo* Pancreatic Tumors

2.1 Introduction

The use of pulsed high-intensity focused ultrasound (pHIFU) to enhance the penetration of chemotherapeutic agents into solid tumors is a promising new approach in cancer therapy [1]–[3]. Cavitation is commonly considered to be the key mechanism in pHIFU-mediated drug delivery, and the treatment protocols are designed to promote cavitation, but suppress tissue heating by using short pHIFU pulses, and delivering ultrasound at low pulse repetition frequencies. Ultrasound contrast agents (UCAs) are often administered to efficiently enhance cavitation activity and reduce the cavitation threshold [4]. It has also been demonstrated that pHIFU can be used without the aid of UCAs to induce cavitation in the brain and open the blood brain barrier [28] or, in combination with tissue plasminogen activator, to improve the rate of thrombolysis *in vivo* [29]. However, reports of quantitative cavitation activity measurements during *in vivo* studies without UCAs are scarce. The major goal of this chaper was to characterize the cavitation activity induced by 1.1 MHz pHIFU exposures for *in vivo* murine pancreatic tumors, with a long term perspective of applying this treatment for chemotherapeutic drug delivery to treat pancreatic cancer.

In ultrasound therapy studies, it is often useful to perform pilot experiments in a better controlled environment of *ex vivo* tissues and tissue-mimicking gel phantoms, before pursuing the

Work published part in:

Li T, Chen H, Khokhlova T, Wang Y-N, Kreider W, He X, Hwang JH. Passive Cavitation Detection during Pulsed HIFU Exposures of *Ex Vivo* Tissues and *In Vivo* Mouse Pancreatic Tumors. Ultrasound Med Biol. 2014;1–12.

Li T., Khokhlova TD, Wang Y-N, D'Andrea S, Starr F, Hwang JH (2014), "In vivo cavitation enhanced delivery of doxorubicin in mouse pancreatic tumors",14th International Symposium on Therapeutic Ultrasound, Las Vegas, NV.

treatments *in vivo* [8]. However, the quantitative difference in the cavitation nucleation threshold and cavitation activity metrics between *in vivo* and *ex vivo* conditions in the same tissue type has been a subject of long-term debate. Commonly, the cavitation threshold is believed to be lower for *ex vivo* tissues, primarily due to the absence of circulation *ex vivo*, and the presence of higher dissolved gas concentrations resulting from tissue decomposition, outgassing and potential exposure to air during tissue sample preparation [30], [31]. Cavitation activity and the threshold for cavitation nucleation also depend significantly on tissue composition [5]; therefore, the results obtained for a single tissue type may not be uniformly applicable to other tissues. Thus, the second goal of this chapter was to compare the different metrics of cavitation activity in *ex vivo* and *in vivo* pancreatic tumor tissue, and to compare these metrics among different types of *ex vivo* tissues.

To effectively deliver chemotherapeutic drugs into tumors, such as pancreatic tumors, it is important to monitor the site and extent of cavitation activity during HIFU treatment, and find the pressure level necessary to reliably induce that activity in a given tissue. Multiple techniques are available and have been shown useful for characterizing cavitation activity during HIFU exposures [9], but passive cavitation detection (PCD) of broadband noise, produced by collapsing bubbles during inertial cavitation, is by far the most widely used technique [10], [11]. Several different ways to interpret the signals acquired by PCD, i.e. cavitation activity metrics, are currently in use. Inertial cavitation dose - the root-mean-square (RMS) amplitude, in the frequency domain, of the broadband noise within a frequency window located between the harmonic peaks - was introduced and correlated to endothelial cell damage and hemolysis *in vivo* in several studies [11], [12], it was also validated to monitor *in vitro* drug release from liposomes [32]. Probability of cavitation occurrence is another metric, which indicates the likelihood of observing a cavitation event at a given HIFU peak negative pressure level and pulse duration and was used to study cavitation thresholds in different *ex vivo* tissues and gel phantoms [5], [13], [33]. A third metric – cavitation persistence - should be introduced to describe how long cavitation lasts when pHIFU is consistently delivered at a single treatment location. This indicator is useful for optimization of the treatment duration. Cavitation noise level relates to the intensity of bubble collapse, the cavitation probablity applies to the presence of cavitation nuclei

while the cavitation persistence pertians to the replenishement of nuclei. If one considers these three metrics with respect to the design of exposures for cavitation-mediated drug delivery, all of them appear equally important and complementary for the following reasons. Inertial cavitation noise level is an measure of the extent of the cavitation activity, and does not allow differentiation between multiple subtle emissions and infrequent powerful emissions, which can occur throughout the pulsed HIFU exposure. Neither probability, nor persistence of cavitation occurrence are sufficient for proper treatment planning: probability of cavitation nucleation may be high, but the collapses not violent enough to perturb the tissue and facilitate drug transport. In in *vivo* conditions where multiple pHIFU pulses are delivered, neither probabiliy nor noise level reflects how long cavitation persists because cavitation nuclei could be both replenished or carried away by *in vivo* circulation and used up by pHIFU treatment. A cavitation occurrence with the same probability and noise level but high persistence could result in a higher cavitation dose than one with low persistence. In this study, all three metrics were employed for a better understanding of cavitation activity patterns in different media - gel phantoms, *ex vivo* tissues and *in vivo* murine pancreatic tumors).

2.2 Methods

2.2.1 Experimental Setup

A customized pre-clinical focused ultrasound system (VIFU 2000, Alpinion US Inc, Kirkland, WA), was used for pHIFU exposures and cavitation monitoring. The system included a 1.1-MHz HIFU transducer (64 mm aperture and radius of curvature) with a circular central opening, into which a focused ring-shaped PCD transducer and a B-mode imaging probe (P4-12 phased array) were built (Fig. 2.1a,b). The signals received by the PCD were amplified (Panametrics PR5072, Waltham, MA, USA) and recorded by a digital oscilloscope (Picoscope 4424, Pico Technology, St. Netos, Cambridgeshire, UK) at the sampling frequency of 50 MHz. The PCD (outer diameter 38 mm, inner diameter 33 mm, radius of curvature 64 mm) was made of 70 μm PVDF film and had a frequency bandwidth of 2.3 – 8.8 MHz at the –6 dB level. The geometric foci of the PCD and the HIFU transducers were aligned in the axial direction, so that the overlap of the focal areas was maximized. The dimensions of the focal areas for both transducers were

simulated numerically using Field II [34], and confirmed using hydrophone measurements to be 19 mm x 0.5 mm and 16 mm x 1.5 mm at the –6 dB level for the PCD and HIFU transducers, respectively. The samples undergoing HIFU exposures (gel phantoms, *ex vivo* tissue or tumor-bearing mice *in vivo*) were positioned at the HIFU focus using a computer-controlled 3D positioning system. The position of the HIFU focus within the sample was controlled using B-mode imaging. All of the exposures were performed in a water tank, which was connected to a degassing system and a heating unit.

The HIFU exposures used in this study had the same pulsing protocol (1 ms pulse duration, 1 Hz pulse repetition frequency, 60 s exposure duration), and differed only in the focal pressure levels. The pulse duration choice was based on the fact that millisecond-long pulses are commonly used in drug delivery treatments [35], and the low duty factor (0.001) avoided substantial thermal effects. The focal waveforms produced by the HIFU transducer in water at different power levels were measured by a fiber optic probe hydrophone (FOPH 2000; RP Acoustics, Leutenbach, Germany) and are presented in Fig. 2.1c. The peak negative focal pressure ranged from 1.6-12.4 MPa, and the peak positive pressure ranged from 1.9-77 MPa, which corresponded to 15-800 W of pulse average electrical output power. Note, that at the medium output levels, the focal waveform is significantly nonlinearly distorted, and at the higher output levels (over 500 W or 10 MPa peak negative pressure) contains a shock front.

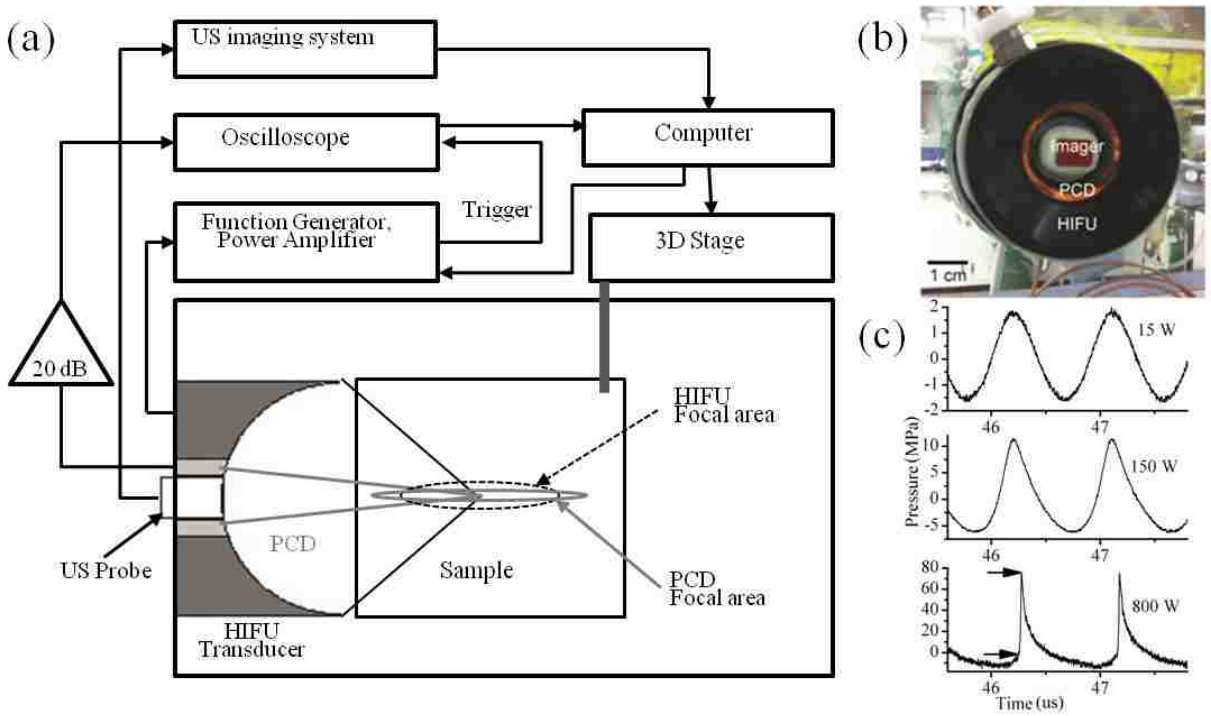

Figure 2.1: (a) Schematic illustration of the HIFU treatment system (VIFU, Alpinion US, Bellevue, WA). The 1.1 MHz HIFU transducer, ring-shaped PCD transducer and an ultrasound imaging probe (P4-12) were aligned confocally and coaxially and built into the side of the acrylic water tank. The focal areas of the PCD and HIFU at –6 dB level are shown in gray and black, respectively. (b) Photograph of the HIFU transducer, PCD transducer, and the ultrasound imaging probe arrangement. (c) Focal HIFU waveforms measured in water using fiber-optic probe hydrophone (FOPH) at different electric power levels (15, 150 and 800 Watts). The arrows indicate the shock front that forms at the focal region at high output powers.

2.2.2 Pressure Estimation

In order to estimate the *in situ* focal pressures from the measurements in water, we used a modified derating procedure developed in previous work [36], that accounts for not only tissue attenuation, but also for the higher coefficient of nonlinearity in tissue compared to water. Briefly, in that method the focal HIFU waveforms are first measured in water at each output electric power setting, W_{el}. The *in-situ* focal pressure waveform at a depth l in tissue, at the power level W_{el} is then calculated as follows: 1) Take the focal waveform measured in water at lower source excitation power, W'_{el}, defined as:

$$W'_{el} = W_{el} \cdot \beta_{water} / \beta \cdot \exp(-2\alpha l) \quad (1)$$

2) Multiply the corresponding waveform by the ratio β/β_{water} .

Here β_{water} =3.5, the values for attenuation for different tissues and gel phantoms were taken from the literature (Lafon *et al.* 2005; Duck 1990; Kyriakou *et al.* 2011; Normand *et al*. 2000) as follows: for bovine liver $\alpha = 0.05$ Np cm^{-1}, for porcine kidney $\alpha = 0.11$ Np cm^{-1}, for bovine tongue $\alpha = 0.15$ Np cm^{-1}, for porcine adipose tissue $\alpha = 0.25$ Np cm^{-1}, for agarose gel $\alpha = 0.011$ Np cm^{-1}, for polyacrylamide gel $\alpha = 0.016$ Np cm^{-1}. The nonlinear parameter was considered as β = 4 for all the investigated tissues, which is equivalent to our previous measurement in bovine cardiac tissue and liver tissue [36]. The nonlinear parameter in gel phantoms was considered equivalent to that of water (β = 3.5).

Although tissue temperature elevation in tissues was assumed to be small, at the highest output levels used in this study the waveforms contain a shock front, which leads to an efficient heat deposition. Therefore, even a 1-ms pulse could cause a noticeable temperature elevation within the super-focused area where the shocks are present. Tissue temperature elevation ΔT , caused by the absorption of shocks within a short pulse with duration Δt can be estimated using weak shock theory:

$$\Delta T = \frac{\beta f_0 A_s^3}{6\rho^2 c^4 c_p} \Delta t \quad (2)$$

where A_s is the shock amplitude, f_0 is the fundamental HIFU frequency, ρ is the tissue density, c is the sound velocity in tissue, and c_p is the specific heat capacity of tissue. In the case of the highest output setting used in this study, the peak temperature elevation in tissues resulting from a single HIFU pulse was 17^{o}C. We followed the cylindrical Gaussian beam approximation introduced by Parker [37] to account for heat diffusion between HIFU pulses and evaluate the focal temperature elevation throughout the 60-second pulsed exposure. The necessary tissue properties (density, sound speed, heat capacity, thermal diffusivity) were taken from literature [38]. The resulting mean steady-state temperature increase was 6.5^{o}C. However, this calculation is only valid for shocked waveforms. At the lower transducer output levels, when the waveform

is nonlinearly distorted, but not shocked, the peak temperature is dominated by the absorption of the main harmonic. The highest calculated temperature elevation in that case in adipose tissue (which has the highest absorption coefficient of all the tissues tested) per pulse and averaged over the exposure are 1°C and 2°C correspondingly.

2.2.3 PCD signal processing and analysis

During the HIFU exposures, a series of 1 ms duration broadband signals were acquired by the PCD transducer and processed using a custom-made program using MATLAB (MATLAB 2010b, The MathWorks, Natick, MA, USA) as follows. First, each signal was band-pass filtered in the frequency domain (MATLAB function fir1), with the filter band of 2.3-8.8 MHz, which corresponds to the sensitive band of the PCD, in order to eliminate the main HIFU harmonic backscattered from the sample as well as high-frequency noise. Since the majority of the focal HIFU waveforms used in this study were significantly nonlinearly distorted, the backscattered harmonics of the HIFU wave dominated the band-pass filtered PCD signal (Fig. 2.2c, e). To eliminate the harmonic, ultraharmonic and superharmonic content in the PCD signal, a notch-shaped comb filter (MATLAB function iirnotch, notch bandwidth 100 kHz) was applied (Fig. 2.2a). The bandwidth of 100 kHz is the half-maximum width of the spectral peak at each harmonic, so the comb filter removes the contribution from each harmonic and ultraharmonic. The resulting frequency spectrum was only associated with inertially collapsing bubbles (Fig. 2.2f). The filtered PCD signal in the time domain is shown in Fig. 2.2d. The notch filter was used here because it introduces minimal artifacts into the signal in the time domain as compared to a rectangular shaped comb filter that has been widely used for extracting broadband noise [39]. Figure 2.2b demonstrates the difference in the level of artifacts introduced by the notch and the rectangular filters when filtering a short broadband unipolar pulse).

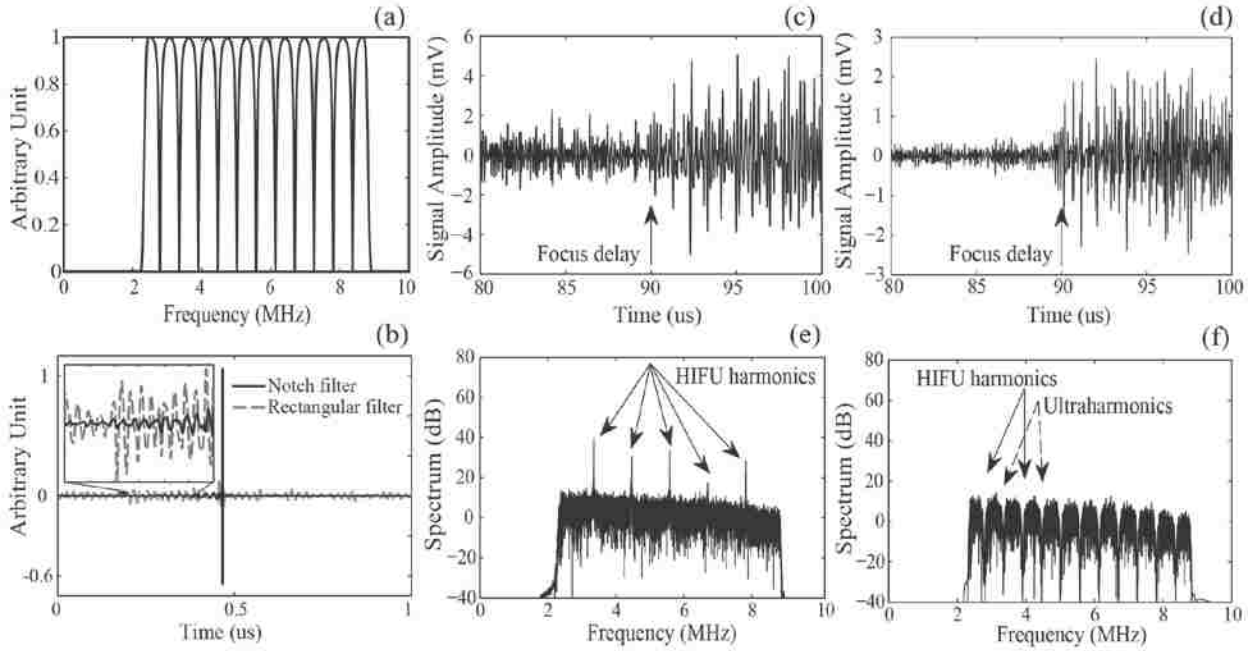

Figure 2.2: (a) A combination of a band-pass filter (2.3 - 8.8MHz) and a notch shaped comb filter with a notch bandwidth of 100 kHz applied to the PCD signals in the frequency domain to suppress the harmonics of HIFU backscattered by tissue and the ultraharmonics generated by stably oscillating bubbles. (b) A short unipolar signal, modeling the acoustic signal produced by an inertial bubble collapse, after filtering by a band-pass and notch filter combination used in the current study (solid line) and a rectangular band-pass and comb filter combination (dashed line). As seen, the filtering procedure used in this study introduces fewer artifacts to the signal in the time domain compared to the rectangular comb filter. An example of a band-pass filtered signal detected by the PCD transducer before (c) and after (d) notch filtering. The corresponding frequency spectra are shown in (e) and (f). The signal was recorded during HIFU exposure of a polyacrylamide gel phantom at peak negative focal pressure of 5 MPa.

The filtered PCD signal was further analyzed to obtain two metrics: a binary evaluation of whether a cavitation event took place within the 1 ms interval and, if a cavitation event was observed, a measure of the cavitation activity in the form of the broadband noise amplitude. The binary measure relied on the assumption that the signals from collapsing bubbles within a sample were expected to arrive with a certain time delay corresponding to the double distance to the sample surface. The signals arriving before that timepoint were considered as background noise. The cavitation event was considered observed if its arrival time exceeded the aforementioned time delay, and if the signal amplitude exceeded the maximum amplitude of the background

noise by $\sqrt{5}$ – the Rose criterion. This criterion ensures that the signal is distinguishable from a simple statistical variation of the background noise with a 98% confidence level [40]. The measure of cavitation activity was obtained by integration over the broadband noise components in the frequency domain. This metric is similar to that used by Hwang *et al.* [11].

It is known that the surface of tissue samples, and the animal skin in the case of *in vivo* exposures, often harbors many more small air bubbles and cavitation nuclei than the bulk tissue. Cavitation events at a given peak negative pressure level are therefore more likely to occur at the sample surface rather than within the sample. In all the *ex vivo* tissue and gel phantom exposures, HIFU focus was intentionally placed no less than 1 cm deep within the tissue to avoid cavitation at the surface. However, since the axial size of the focal regions of HIFU transducers are rather large, cavitation at the sample surface could still occur at the highest power outputs. Furthermore, in the case of *in vivo* experiments, the depth of tumor location in some cases was less than 1 cm, which made cavitation at the skin surface more probable. To address that problem, if the cavitation events occurred at the sample surface (according to the arrival time of the signal to the PCD transducer) and did not occur at the focus, the corresponding PCD signal was excluded from the study. Therefore, surface cavitation was monitored and excluded from the analysis.

2.2.4 Gel phantoms and Ex Vivo Tissue Samples

Two types of tissue mimicking phantoms were used in this study – 5% polyacrylamide and 6% agarose gels. We chose these two types of gels because they were acoustically similar but very different in the polymertization process, and hence gas content and the distribution of gas cavitation nuclei were also likely to differ. Polyacrylamide (PA) gel is optically transparent, which makes it very convenient for optical observation of the cavitation bubbles, and multiple studies on bubble dynamics were performed in PA phantoms [36], [41], [42]. The additional advantage of PA gel phantoms is that polymerization takes place at room temperature; therefore, proteins like egg white or bovine serum albumin (BSA) can be added to the gel to serve as indicators for thermal denaturation induced by HIFU. Note, however, that in the present study no protein constituents were added to the gel to avoid the introduction of additional cavitation nuclei.

To prepare the samples, the liquid mixture of gel constituents was degassed for 1 h in a desiccant chamber, then poured into a custom mold and polymerized.

Agarose gel is another popular tissue-mimicking material, which is non-toxic and can therefore be used in cell seeding experiments [43], [44]. Relevant to the current study, the agarose gel is likely to be different from PA gel in terms of gas content, because of the difference in the polymerization and degassing procedures. Agarose powder (agarose type VII, Sigma-Aldrich) was added to distilled water at 5% concentration, and the solution was placed into an autoclave and allowed to boil for 20 minutes to displace any dissolved gas. The solution was then poured into a custom mold and rapidly cooled down for fast polymerization.

The bovine and porcine *ex vivo* tissue - porcine adipose tissue, bovine tongue, porcine kidney and bovine liver - was obtained from an abattoir on the same day as experiments and stored in phosphate buffered saline and on ice until experiments were performed. The four types of tissues were selected due to their difference in structure and composition. The tissue was cut into samples to fit in a custom-designed tissue holder (8 cm wide by 8 cm tall by 2.7 cm deep) and was brought to room temperature and degassed for 1 h in a desiccant chamber immediately prior to experiments.

In the *in vivo* experiments, a transgenic mouse model of pancreatic ductal adenocarcinoma was used. The KrasLSL.G12D/+; p53R172H/+; PdxCretg/+ (or KPC) model closely recapitulates the genetic mutations, clinical symptoms and histopathology found in human pancreatic cancer, unlike xenograft or orthotopic models [20]. The tumors generally have a moderately differentiated ductal morphology with extensive dense stromal matrix that, together with poorly developed vasculature presents a major obstacle to chemotherapeutic drug penetration. The KPC mouse model is thus the most relevant in the studies on ultrasound-induced chemotherapeutic drug delivery in pancreatic cancer. All of the animal experimental procedures were approved by the Institutional Animal Care and Use Committee at the University of Washington. KPC mice were used for the study when their tumor size reached 1 cm according to diagnostic ultrasound examination. The animal was anesthetized by inhalation of isoflurane, and the abdomen was

depilated and washed. The animal was then placed into a specially designed holder and submerged into the heated water tank (at 36°C) for the HIFU exposure.

2.2.5 Experimental Procedures and Measurements

In the experiments with gel phantoms and *ex vivo* tissue, the samples were positioned so that the HIFU focus was 10 mm below the sample surface. Pulsed HIFU exposures were delivered, with peak negative pressures varying within the 1.5-12.5 MPa range in increments of 0.5-1 MPa. After each exposure, the HIFU focus was moved by 3 mm to another spot within the sample to account for the sample heterogeneity. At each peak negative pressure level, 5-10 spots were sonicated. In the *in vivo* experiments, the total number of exposure spots was limited by the tumor size and the number of animals. Therefore, only five different HIFU output levels were used, 4-12 treatment spots per level, and the distance between the treatment spots was reduced to 2 mm. The HIFU focus was placed within the tumor, 8-12mm below the animal skin depending on the depth of the tumor location. In a separate set of experiments, the pancreatic tumor was removed after the animal was sacrificed and used for the cavitation activity measurements similar to those described for *ex vivo* tissue. Four treatment spots per pressure level were used in that experiment.

A PCD transducer signal was recorded during the delivery of each HIFU pulse using a digital oscilloscope and was stored to a host PC. The PCD signals were then filtered as described in the section “PCD signal processing and analysis”, and batch-processed to extract the following metrics of cavitation activity in a certain tissue type or phantom: probability of cavitation occurrence, cavitation persistence and broadband noise amplitude.

Probability of cavitation occurrence at a certain HIFU output level is defined here as the ratio (expressed in percent) of the number of HIFU focus locations, at which at least one cavitation event was observed throughout the exposure, to the total number of spots treated at this HIFU output level.

Cavitation persistence is defined as the percentage of the HIFU pulses that induced a cavitation event among the pulses delivered at a single treatment spot. Cavitation persistence at each HIFU output level was averaged among the different HIFU focus locations.

Broadband noise amplitude was the integral of the absolute value of the filtered PCD signal, representing the broadband noise emitted by collapsing bubbles, in the time domain. The integration was performed starting from the time delay corresponding to the HIFU focus, and over the HIFU pulse duration. Note that this metric was only applied to the signals in which a cavitation event was observed. The broadband noise amplitude at each pulse was averaged over all 60 HIFU pulses delivered to the different HIFU focus locations.

The mean and standard deviation values of cavitation persistence and broadband noise amplitude were calculated in a certain tissue type, at a certain HIFU output level.

2.3 Results

2.3.1 Cavitation Activity in Water and Gel Phantoms

Figure 2.3 shows the three metrics – cavitation probability, cavitation persistence and cavitation noise level - at different HIFU peak negative focal pressures, measured in agarose and polyacrylamide gels and degassed, deionized water. The probability of cavitation occurrence is similar in the gel phantoms at lower pressure levels: the 50% probability is reached at p^{-}=4-5 MPa. The probability of 100%, however, is reached at a lower pressure level in the agarose gel (7 MPa) than in the PA gel (10 MPa). This is most probably due to the difference in the degassing procedures used for the two gel phantoms. PA gel was degassed using a dessicant chamber, whereas the agarose gel was degassed by boiling, which seems to be a more efficient procedure for removing the cavitation nuclei. The probability of cavitation in degassed, deionized water was lower than in both gels, and did not reach 50% within the peak negative pressure limits of the study. This result is consistent with findings by others, that pure water has a very high cavitation threshold [5], [45]. Since HIFU causes streaming in water, each HIFU pulse was assumed to be incident at a different volume of water, therefore, the cavitation

persistence (that, according to the definition, is calculated for a single HIFU focal spot location) was not calculated for water.

In both gel phantoms, cavitation persistence (Fig. 2.3b) grows steadily with the increase of peak negative focal pressure. An important observation, also reported previously by our group [36], is that cavitation activity, if any, always occurs within the first several pulses of HIFU, and then stops, and the following HIFU pulses, delivered at the same spot, do not induce cavitation. According to the high-speed camera observations from our previous studies, this is likely due to the fact that the available cavitation nuclei present within the focal volume are used within the first pulses, and the remnants of the cavitating bubbles are pushed away from the focus into the post-focal region by acoustic radiation force. Another possible mechanism is the fragmentation of the cavitation bubbles into small-sized voids that are more likely to dissolve quickly or less likely to cavitate, before the arrival of the next HIFU pulse [46]. In the agarose gel phantom, the cavitation persistence is consistently lower, at all pressure levels, than that in the PA gel. We speculate that this is due to a lower number of cavitation nuclei within the HIFU focal area, which results from different dissolution and polymerization processes in between agarose gel and PA gel. Another potential explanation is higher levels of streaming within the focal area that result in displacing the bubbles towards the postfocal region.

The average amplitude of the broadband noise (Fig. 2.3c) emitted by collapsing bubbles is very similar for both of the gel phantoms and water at most peak negative pressure levels. Therefore, the intensity of bubble collapses is similar in all three media, but cavitation is much less likely to occur in water than in gel phantoms.

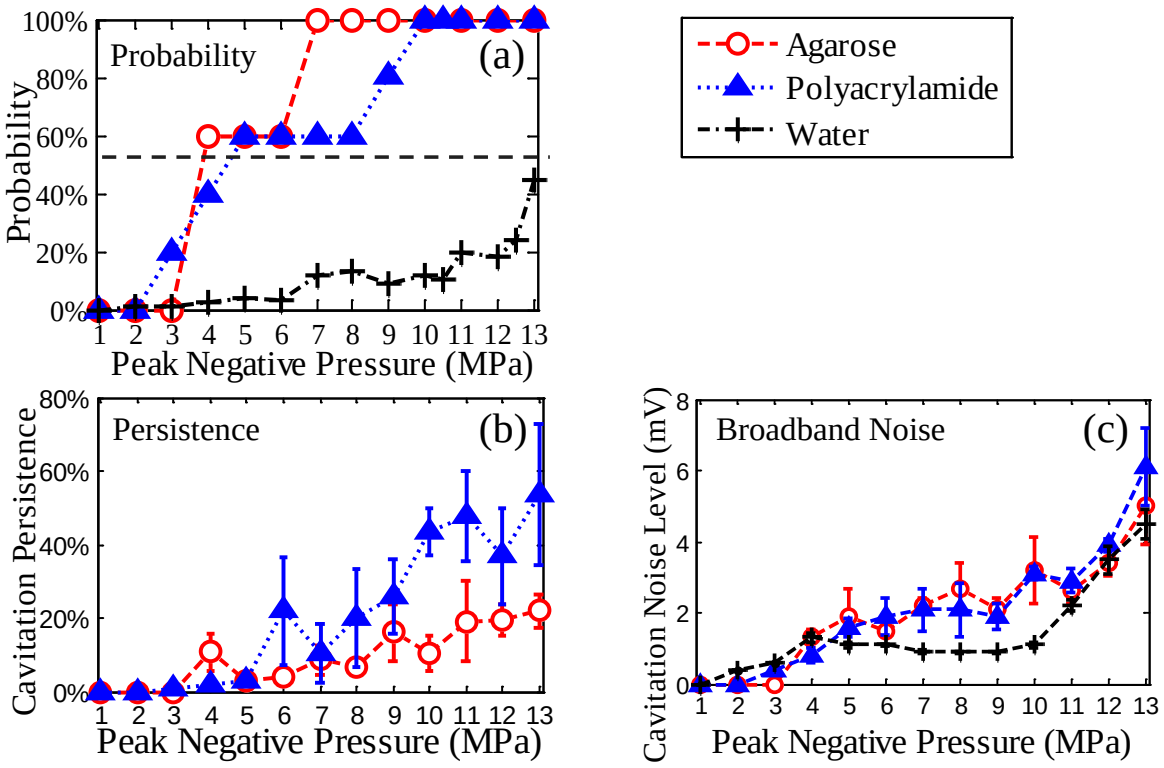

Figure 2.3: Dependence of the metrics of cavitation activity on the HIFU peak focal negative pressure in deionized water and in water-based tissue phantoms - polyacrylamide and agarose gels: (a) the probability of cavitation occurrence, calculated over 5-10 HIFU focus locations in the phantom for each peak negative pressure level, the dash line indicates where the probablity equals to 50% of cavitation occurrence (b) cavitation persistence, calculated over 60 HIFU pulses delivered to a single HIFU focus location, and averaged over 5-10 focus locations, and (c) broadband cavitation noise level, averaged over all recorded PCD signals, that contained a cavitation event, at each HIFU pressure level. In the case of water, the probability is calculated over 100 HIFU pulses delivered to the water volume of the tank at each pressure level. As seen, the probability of cavitation occurrence is similar in both gel phantoms, and is significantly lower in water. The persistence of cavitaiton in polyacrylamide is, however, considerably larger, which is most probably because it has more pre-existing nuclei compared to agarose gel or water. Cavitation noise level for all three media is within the experimental error, and increases steadily with peak pressure, which indicates that bubble collapses become more violent and/or a larger number of cavitation bubbles form in the focal region.

2.3.2 Cavitation activity in Ex Vivo Tissue

Comparison of the metrics of cavitation activity in the four *ex vivo* tissue types – porcine adipose tissue, bovine tongue, porcine kidney and bovine liver – are presented in Figure 2.4. The

probability of cavitation occurrence (Fig. 2.4a) is highest in porcine adipose tissue, which contains 65% fat [47], and is somewhat lower in bovine tongue, which contains 15-24% fat [48]. In adipose tissue, fat is distributed rather uniformly, whereas in the tongue tissue, areas of fat are located in between muscle bundles. Although the multiple interfaces between water-based and fatty tissue in the tongue may be considered as efficient cavitation nuclei, the data suggest that cavitation is easier to induce in the more homogenous fatty tissue. The probability of cavitation in kidney is bifurcated, changing abruptly from 0 to 100% between peak negative pressures of 7 and 9 MPa. This is likely an indication of high homogeneity in the distribution of cavitation nuclei throughout the tissue. In liver tissue, the increase of probability with pressure was slower, and at higher pressure levels (over 7 MPa) the probability of cavitation was lower than in all other tissues.

The pattern of cavitation occurrence in all tissues throughout the 60-pulse exposure was similar to that in the gel phantoms: at lower pressure levels cavitation activity was only observed following the first few HIFU pulses. The cavitation persistence (Fig. 2.4b) was highest in the adipose tissue, lower in tongue and kidney and lowest in liver, at all pressure levels. Since adipose tissue is very cohesive, consisting of loose connective tissue holding clusters of adipocytes and is also very viscous, both effects that may increase cavitation persistence - streaming and dissolution of the bubble remnants - are expected to be less pronounced than in water-based tissues.

Similar to other metrics, the cavitation noise level (Fig. 2.4c) is highest in adipose tissue. Cavitation noise in tongue is lower, and very similar to that in kidney, despite the differences in tissue structure and composition. In liver, cavitation noise level is the lowest.

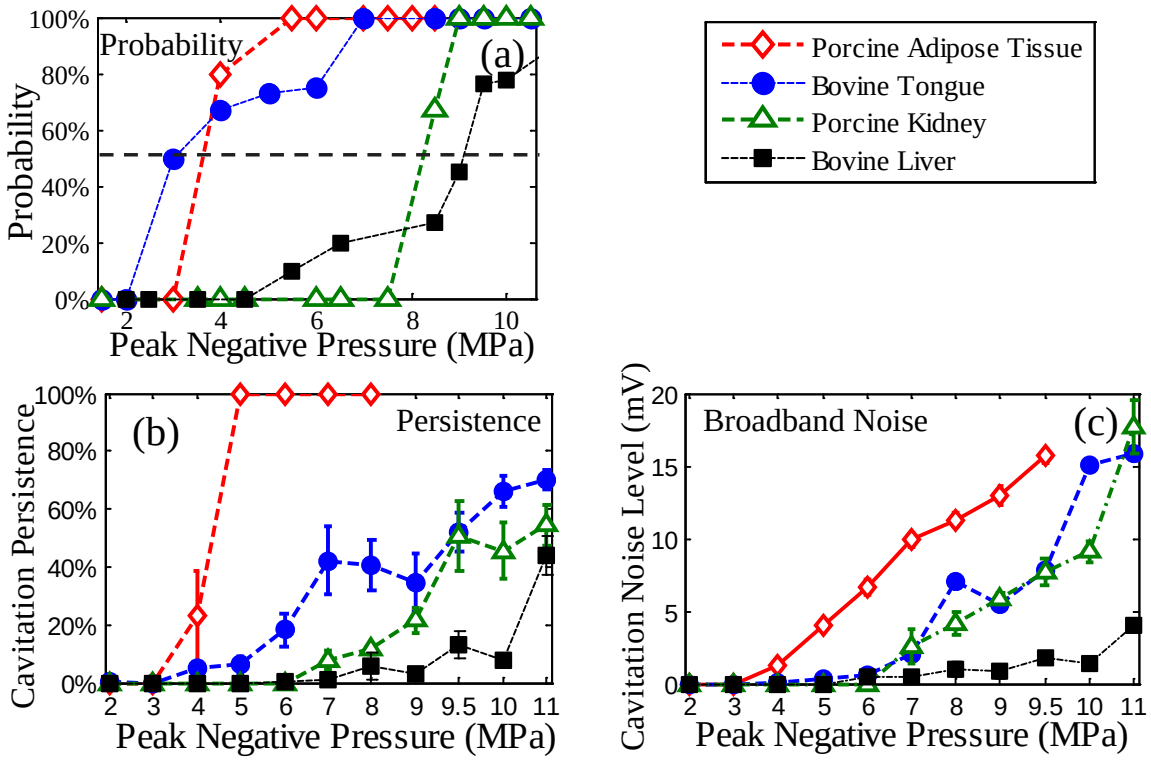

Figure 2.4: Dependence of the metrics of cavitation activity on the HIFU peak focal negative pressure in *ex vivo* tissues: bovine tongue and liver and porcine subcutaneous adipose tissue and kidney: (a) the probability of cavitation occurrence, calculated over 5-10 HIFU focus locations in tissue for each peak negative pressure level, the dash line indicates where the probablity equals to 50% of cavitation occurrence (b) cavitation persistence, caluclated over 60 HIFU pulses delivered at a single focus location, and averaged over 5-10 focus locations, and (c) cavitation noise level, averaged over each HIFU pulse delivered at a certain pressure level. As seen, all three metrics are highest in adipose tissue at most HIFU pressure levels. In tongue, which contains 15-24% lipid and 60-74% water, the probability and persistence of cavitation are considerably higher than in water-based tissues (liver and kidney), but the cavitation noise level is comparable to that in kidney. All three metrics are lowest in liver.

2.3.3 Cavitation Activity in Mouse Pancreatic Tumors In Vivo and Ex Vivo

Cavitation activity metrics obtained from the pancreatic tumors of KPC mice *in vivo* and *ex vivo* are presented in Figure 2.5. Surprisingly, the cavitation probability (Fig. 2.5a) was 100% for the *in-vivo* tissue, at the entire range of peak negative pressures used (5-11 MPa), and reached 100% in the *ex vivo* tissue at the same peak negative pressure level as that of fat ($P^- = 4$ MPa). An

important difference in the pattern of cavitation occurrence throughout a single 60-pulse exposure is shown in Fig. 2.6. In the *ex vivo* tissue, the cavitation occurs following the first few pulses of HIFU, similarly to other *ex vivo* tissues and gel phantoms, whereas *in vivo*, cavitation events are distributed sporadically throughout the exposure (Fig. 2.6a). The cavitation noise level (Fig. 2.6b) in the *ex vivo* case declines over the course of the exposure, whereas in the *in vivo* case it stays nearly constant. We speculate that this is likely due to the replenishment of the nuclei within the HIFU focal area by the circulation. The cavitation persistence was consistently lower in the *in vivo* case compared to *ex vivo* within the 60s exposure, and only reached 100% at the highest peak negative pressure level tested (11 MPa). The cavitation noise level, indicating the intensity of cavitation bubble collapses, was mostly similar (within the standard deviation) in the *in vivo* and *ex vivo* setting.

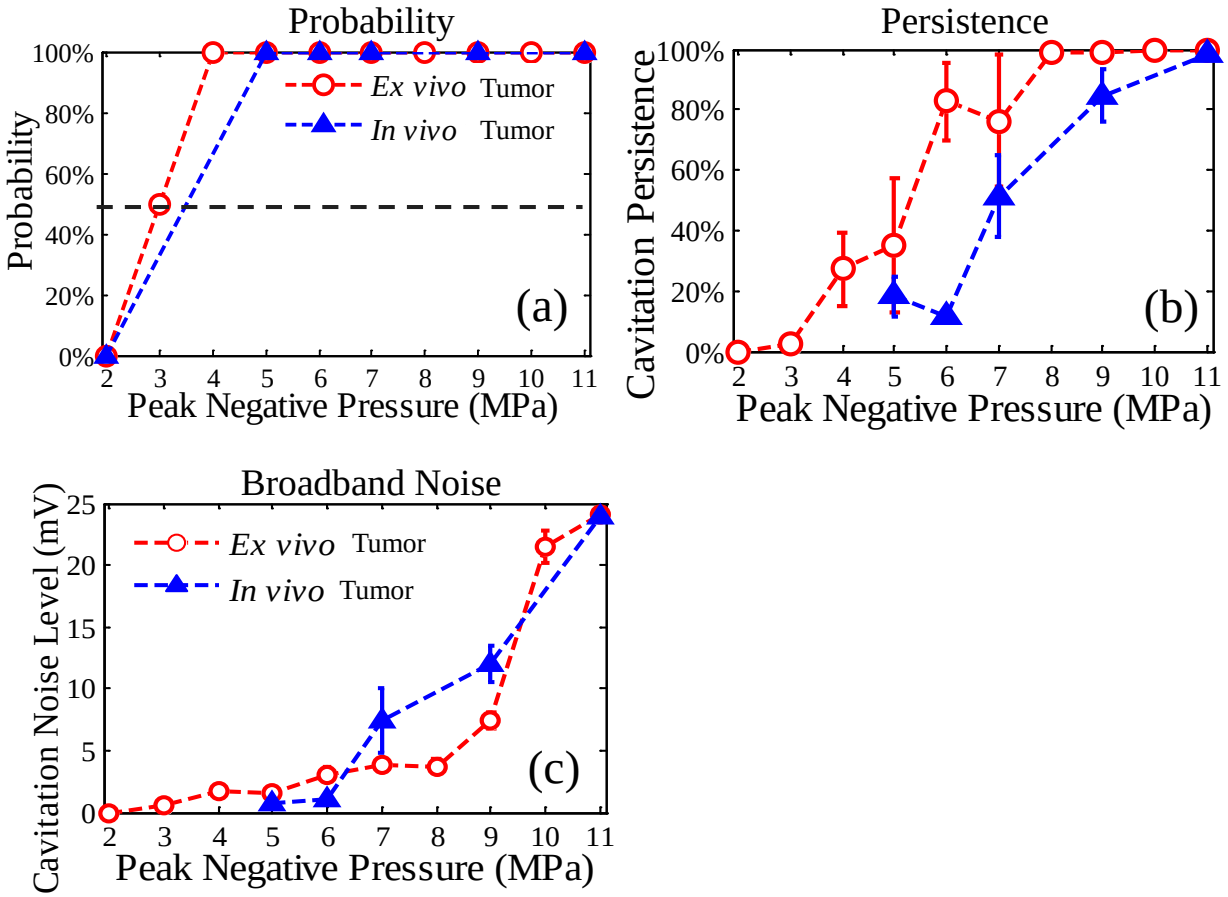

Figure 2.5: Dependence of the metrics of cavitation activity on the HIFU peak focal negative pressure in the pancreatic tumor of a KPC mouse *in vivo* (blue solid symbol) and *ex vivo* (red

open symbols).(a) The probability of cavitation occurrence, calculated over 4-12 HIFU focus locations in the *in vivo* tumor tissue and 4 focus locations in the *ex-vivo* tumor tissue for each peak negative pressure level, the dash line indicates where the probablity equals to 50% of cavitation occurrence (b) cavitation persistence, caluclated over 60 HIFU pulses delivered at a single focus location, and averaged over the different focus locations, and (c) cavitation noise level, averaged over each HIFU pulse delivered at a certain pressure level. Both *in vivo* and *ex vivo*, the pressure sufficient to achieve 100% probability and persistence lies around 11 MPa. Cavitation noise level gradually increases when peak negative pressure increases, in both *ex vivo* and *in vivo* case.

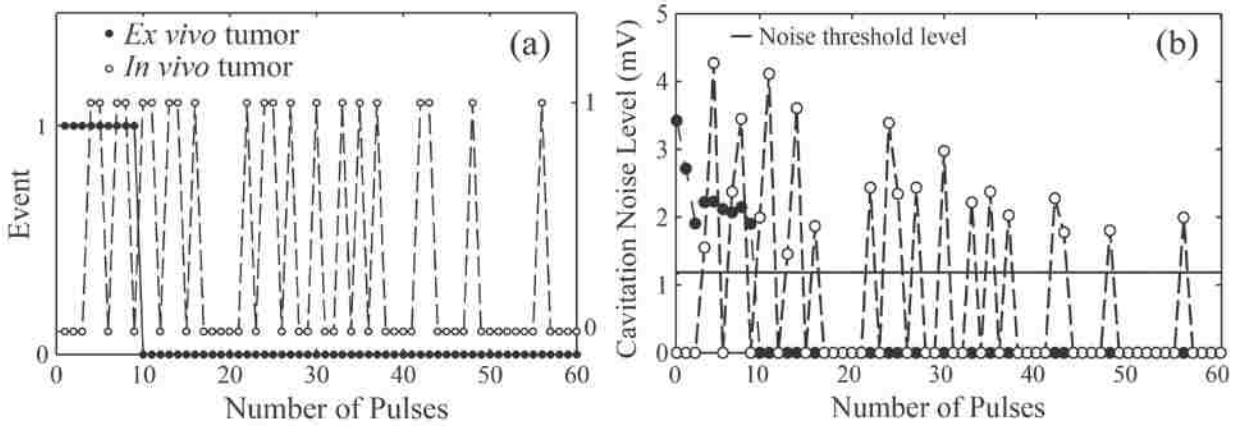

Figure 2.6: A representative illustration of the behavior of cavitation activity metrics throughout pulsed HIFU exposure of an *ex vivo* (solid symbols) and *in vivo* (open symbols) pancreatic tumor of KPC mice. HIFU peak negative focal pressure was 5 MPa in both cases. (a) Binary metric of cavitation occurrence within each HIFU pulse: "1" indicates that a cavitation event was observed, "0" indicates no cavitation events. In the *ex vivo* tumor tissue, the cavitation events only occur within the first few HIFU pulses, whereas in the *in vivo* case they occur sporadically throughout the exposure. (b) Cavitation noise level recorded during each HIFU pulse. In the *ex vivo* tumor tissue, the cavitation noise gradually declines over the first few HIFU pulses, which is typical for other *ex vivo* tissues and gel phantoms. In the *in vivo* tumor, the noise level fluctuates randomly throughout the exposure.

2.4 Discussion

In this chapter, we compared the metrics of cavitation activity induced by pulsed 1.1 MHz HIFU exposures in different *ex vivo* tissues, *in vivo* pancreatic tumor tissue and different tissue-mimicking phantoms, within the range of peak negative focal pressures of 1.5 – 12 MPa. Three different metrics of cavitation activity were used: cavitation probability, persistence and

broadband noise level, and their dependence on the HIFU focal peak negative pressure was investigated.

The probability of cavitation as a function of peak negative pressure generally followed a sigmoid curve for all tested media, with the probability equal to zero at the low peak negative pressures (below 2 MPa) and approaching or reaching 100% at the higher pressures. The width of the transition region of the sigmoid curve (where the probability has any value other than 0 or 100%) may be associated with the degree of tissue heterogeneity at the macroscopic level, i.e. the heterogeneity of the spatial distribution of the cavitation nuclei. Our data supports this assumption: tissues with a lower degree of heterogeneity – adipose tissue, kidney cortex and pancreatic tumors in KPC mice – had a much narrower transition region (2 MPa) compared to more heterogenous tissues – liver and skeletal muscle (over 5 MPa). Liver is composed of mm-scale lobules, separated by connective tissue, and organized around biliary structures; tongue muscle is composed of muscle fiber bundles with adipose tissue inclusions. The adipose tissue (pork belly) is highly homogenous, and so is kidney cortex, which is composed of micron-scale channels. Pancreatic tumors, which form spontaneously in KPC mice, have a very homogenous structure and are very rarely necrotic [20]. The blood vessels present in the tumor are often nearly collapsed due to high pressure within the tumor.

Following this line of thought, one would expect a high degree of homogeneity and hence a narrow transition region in the gel phantoms. However, a broad transition region was observed in the case of agarose gel (4 MPa), and even broader – for the PA gel. This may be explained by the difference in crosslinking polymer of the gels, mechanical structure and, therefore, the number of gas nuclei distributed within the two types of gel.

The peak negative pressure, which corresponds to 50% or 100% cavitation probability level, is often referred to as the cavitation threshold [5], [13]. Of all the media, tested in this work, the lowest cavitation threshold, defined at the level of 50% probability, was observed in porcine adipose tissue, bovine tongue and murine pancreatic tumor tissue (2.5-3 MPa). In both of the gel phantoms a somewhat higher cavitation threshold (3.5-4.5 MPa) was found, and it was the highest in bovine liver and porcine kidney (9 MPa and 8 MPa, respectively). Probability of

cavitation in deionized water did not reach 50% within the peak negative pressure range that was tested here. Comparison of these results to the threshold values reported by others at the same HIFU frequency is difficult and not always relevant due to the differences in the sonication regime and the associated tissue temperature elevation. For example, the cavitation threshold reported by McLaughlan *et al.*[9] for *ex vivo* bovine liver tissue sonicated continuously at 1.1 MHz for 4 s was much lower (~2 MPa) than that observed here. In that study, the thermal effects were readily visible, and tissue denaturation was observed. Tissue heating and denaturation may considerably alter the cavitation bubble behavior. In other studies, the cavitation threshold was measured in sheep brain *in vivo* [45] and in different *ex vivo* tissues [5] in the opposite extreme case of very short, microsecond-duration pulses. The reported threshold values were much larger than the peak negative pressure range used in this study: 30 MPa in kidney, 27 MPa in deionized, degassed water, 15 MPa in adipose tissue (at 1 MHz) and 18 MPa in sheep brain *in vivo* at 0.66 MHz. This discrepancy may be due to pulse duration, a 50% threshold for 1-cycle and 1000-cycle pulses are different, or the likely lower sensitivity of the bubble detection method employed in these studies: the authors used HIFU backscattered signals from the bubbles as the indication of cavitation, and the bubble has to grow to a relatively large size to be detectable in such a way [5]. However, the results are similar to our data in that the threshold in adipose tissue or tissue with high fat content is substantially lower than in water based tissue, such as kidney. In a study by Kyriakou *et al.* [49] cavitation detection method was similar to that used here, and the cavitation threshold for adipose tissue was reported as 0.82 MPa at 0.5 MHz and over 2.1 MPa for 1.1 MHz, which is in agreement with our results.

Commonly, the cavitation threshold is assumed to be larger *in vivo* than *ex vivo* in the same tissue type. *Ex vivo* tissue is likely to have higher gas content after it is removed from the living organism, mostly due to tissue outgassing, exposure of the tissue to air and tissue decomposition over time. We have found the thresholds and the cavitation noise levels to be remarkably similar for murine pancreatic tumor tissue *ex vivo* and *in vivo*, and close to these for porcine adipose tissue and bovine tongue. This may be, in part, due to the fact that KPC tumors are enclosed in a dense stromal matrix that prevents the penetration of air into the tissue after the tumor is removed. The measurements on the *ex vivo* tumor were performed within two hours after the

tumor was excised, so that tissue decomposition processes were unlikely to occur. The other differences – the presence of circulation *in vivo* and the difference in tissue temperature (20ºC *ex vivo* and 36ºC *in vivo*) did not appear to have influenced the cavitation threshold and the cavitation noise level.

The largest difference between the *in vivo* and the *ex vivo* pancreatic tumor tissue was in the pattern of cavitation occurrence throughout the pulsed HIFU exposure. In the cases of all of the tested *ex vivo* tissues (including the pancreatic tumor) and phantoms, cavitation only occurred during the first few HIFU pulses of the exposure, and the cavitation noise level quickly declined with the number of HIFU pulses delivered, as illustrated in Figure 2.6. In the *in vivo* case, cavitation events occurred sporadically throughout the exposure, and the cavitation noise level fluctuated in a random manner from one HIFU pulse to the next. We speculate that this is due to the presence of circulation in the *in vivo* case. The blood flow speed in murine pancreatic tissue can be estimated as 0.5 mm/s [50], therefore, the blood volume within the 1.5 mm-wide HIFU focal area is at least partially renewed between the subsequent HIFU pulses (one HIFU pulse per second). Note, that this renewal of the cavitation nuclei by the circulation was significant even in the present case of very poorly vascularized pancreatic tumors [20]. The interplay between the destruction of cavitation bubbles by HIFU pulses and replenishment of cavitation nuclei by blood perfusion is likely to influence the cavitation persistence in *in vivo* conditions.

The cavitation persistence, as measured over 60 HIFU pulses, was higher *ex vivo* than *in vivo*. In the *in vivo* case, cavitation persistence reached 100% only at the highest peak negative pressure level (11 MPa). This, again, may be attributable to the presence of circulation *in vivo*, which not only supplies the nuclei, but also carries them and the cavitation bubble remnants away from the HIFU focal area. In the *ex vivo* case, cavitation nuclei are contained in the tumor tissue and are not diminished unless they result in cavitation bubbles and are pushed away from the focal region by radiation force or broken into daughter bubbles and dissolved.

The next goal following this chapter was to identify the optimal pressure levels for pHIFU exposures aimed at drug delivery to pancreatic tumors. Clearly, all three metrics of cavitation introduced here are important for this optimization, and we have observed a difference in the

behavior of cavitation probability/persistence and the cavitation noise level with an increase of pressure level. The probability of cavitation reached 100% at 5 MPa, and the persistence exceeded 50 % at 7 MPa in both *ex vivo* and *in vivo* pancreatic tumors. However, the broadband noise level continued to increase steadily as the peak negative pressure was further increased (6-11 MPa). It is not clear yet whether reaching high levels of probability and persistence alone are enough for efficient drug delivery or whether the intensity of bubble collapses (characterized by broadband emissions) has to reach a certain threshold. This question will be addressed in chapter 3 on pHIFU-aided drug delivery to pancreatic tumors. The cavitation metrics will be correlated with the drug uptake in tumor tissues.

2.5 Summary and Conclusions

In this chapter, the metrics of cavitation activity (probability, persistence and broadband noise level) induced by pulsed HIFU exposures were studied in tissue-mimicking gel phantoms, different *ex vivo* tissues and murine pancreatic tumors *in vivo*, using passive cavitation detection. Cavitation thresholds in these different media were identified at the HIFU frequency of 1.1 MHz and varied within 2.5 – 10 MPa, depending mostly on the relative concentration of water and lipid in tissue. The results demonstrated an important difference in the pattern of cavitation occurrence *in vivo* and *ex vivo*: cavitation activity ceased after only a few HIFU pulses in *ex vivo* tissue, but occurred sporadically throughout the HIFU exposure *in vivo*. Pulsed HIFU exposures used in this study were designed to introduce minimal tissue heating (short pulses, low duty cycle), but to enhance mechanical tissue damage introduced by cavitating bubbles and/or acoustic radiation force. Such exposures are most commonly needed in HIFU-aided drug and gene delivery, and the conclusions drawn in this study would be relevant in these applications, but likely not in the ablative applications, where tissue temperature is considerably elevated.

Chapter 3

Correlation between Cavitation Activity and the Degree of Chemotherapeutic Drug Uptake in *In Vivo* Pancreatic Tumors

3.1 Introduction

Pancreatic ductal adenocarcinoma (PDA) is the fourth leading cause of cancer-related mortality in the United States [19], [51]. In 2013, more than 45,000 Americans are diagnosed with cancer of the pancreas [19]. Unlike many other cancers, the survival rate for the disease has not improved substantially. Since 1975, the five-year relative survival rate for pancreatic cancer has increased from 2 % to only 6 %. Gemcitabine, a deoxycytosine analog, is the current standard chemotherapy for advanced disease. Gemcitabine has been shown to be effective in inducing apoptosis in pancreatic cancer cells *in vitro* and in arresting tumor growth in xenograft [52] and syngeneic mouse models [53], [54]. However, it has offered only modest, survival benefit when translated into clinical use [55], [56]. There is a number of characteristics of pancreatic cancer that make it resistant to chemotherapy; most importantly, it is the formation of a dense stroma termed a desmoplastic reaction that separates cancer cells from the blood vessels and significantly decreases tissue permeability [57], [58]. High interstitial pressures within pancreatic tumors as well as poor vascularization contribute to insufficient diffusion of drug molecules through the interstitium to the targeted cancer cells. The main reason for the discrepancy in gemcitabine efficiency between human trials and preclinical animal studies is the absence of desmoplastic reaction in xenograft and syngenic autograft models. Only recently a transgenic mouse model of PDA, termed KPC mouse, was developed that closely recapitulates the genetic mutations, clinical symptoms and histopathology found in human pancreatic cancer [20]. Lately, it has become the only accepted mouse model for studying drug delivery in pancreatic cancer, because it provides much more realistic data to evaluate the potential for clinical translation [59].

Work published part in:

Li T., Khokhlova TD, Wang Y-N, D'Andrea S, Starr F, Hwang JH (2014), "In vivo cavitation enhanced delivery of doxorubicin in mouse pancreatic tumors",14th International Symposium o Therapeutic Ultrasound, Las Vegas, NV.

Studies in this KPC mouse model have demonstrated that breaking down the stromal matrix by the administration of smoothened inhibitor, IPI-926, increases delivery of gemcitabine into the tumors [20], [60]. It also results in a transient increase in intratumoral vascular density and intratumoral concentration of gemcitabine, leading to transient stabilization of disease and a modest benefit in survival. In spite of these promising results, IPI-926 performed poorly in pancreatic cancer clinical trials, making the tumors more aggressive, with heightened proliferation, indicating that stromal elements may also restrain tumor growth [61]. Thus, the development of efficient strategy for chemotherapeutic drug delivery to pancreatic tumors remains an unmet challenge.

High intensity focused ultrasound (HIFU) therapy is a non-invasive modality for thermal ablation of diseased tissue. In HIFU, powerful ultrasound waves from an extracorporeal source are focused inside the human body to induce thermal or mechanical damage to the tissue at the focus without affecting surrounding tissues. Most HIFU treatments utilize the thermal effect resulting from absorption of continuous ultrasound waves by tissue and have been used to ablate various solid tumors, including pancreatic neoplasms [62]. Alternatively, pulsed HIFU (pHIFU) treatments may be used to minimize the thermal effect on tissue and promote the mechanical effects, primarily acoustic cavitation – formation and ultrasound-driven activity of micron-sized bubbles in tissue. Although live tissue does not initially contain gas bubbles, tiny gas bodies dispersed in cells may serve as cavitation nuclei that grow into bubbles when subjected to sufficiently large rarefactional pressure, i.e. a certain cavitation threshold, that “tears” the tissue apart at the site of a nucleus [63]. The violent collapses of the cavitation bubbles, termed inertial cavitation, can disrupt tissue due to the accompanying high shear forces that are generated and thus increase tissue and/or vascular permeability [64]. In recent years, there has been an increasing interest in using pHIFU alone or in combination with microbubbles to enhance drug/gene delivery to solid tumors by permeabilizing the tissue through cavitation [18], [65].

In a recent study by Tinkov [66], ultrasound-induced targeted destruction of Dox loaded microbubbles was used to enhance localized drug delivery in a rat model with subcutaneously grafted pancreatic carcinoma. The results showed a 12-fold higher tissue concentration of Dox

and a significantly lower tumor growth in the targeted tumor compared to the contralateral control tumor. However, animal model used in the study is not ideal for evaluating clinical translation due to the absence of the desmoplastic reaction. The major goal of this work was to demonstrate that pHIFU-induced cavitation can improve Dox penetration in the pancreatic tumor using the realistic KPC mouse model (16).

Unlike most other works on cavitation-enhanced drug and gene delivery, this study was based on nucleating and sustaining cavitation in the tumor tissue itself, without systemic administration of ultrasound contrast agents (UCAs). This choice was dictated by the characteristics of pancreatic cancer – poor vascularization and high interstitial pressure, which made it unlikely for the UCAs to be circulating through the tumor in large enough numbers. Moreover, main obstacle to drug delivery is the stromal matrix, and its disruption is the desirable outcome, whereas the UCAs are confined to vasculature and may not cause sufficient permeabilization of the interstitium. As cavitation is a stochastic phenomenon, the cavitation threshold, as well as the correlation between drug penetration and the cavitation activity metrics is difficult to establish and is still controversial [35], [65], [67]. In our previous studies, we developed a methodology for quantification of cavitation activity in pancreatic tumors during pHIFU using passive cavitation detection (PCD) [68]. Here, we aimed to correlate the corresponding cavitation metrics to the enhancement of the drug uptake by the tumor.

The third goal of this study was to compare the efficiency of HIFU-aided drug delivery in two different treatment protocols: when the drug is administered during pHIFU exposure, both its active diffusion is facilitated by bubble activity and passive diffusion due to permeabilized tissue by bubble collapsing, and when the drug is administered immediately after pHIFU exposure, the only mechanism is passive diffusion through previously permeabilized tissue by bubble collpsing.

3.2 Materials and Methods

3.2.1 Experimental Setup

pHIFU system

A customized pre-clinical focused ultrasound system (VIFU 2000, Alpinion Medical Systems, Bothell, WA), was used for pHIFU exposures, treatment planning and cavitation monitoring. The system, shown in Fig. 1a, was used with either of the two alternative HIFU transducers - a 1.1-MHz transducer (64 mm aperture and radius of curvature) and a 1.5-MHz transducer (64 mm aperture and 45 mm radius of curvature). Both transducers had a circular central opening of 38 mm diameter, which was fitted with a focused ring-shaped PCD transducer and an ultrasound imaging probe (C4-12 phased array, center frequency: 7MHz, Alpinion Medical Systems, Seoul, Korea). The geometric foci of the PCD and the HIFU transducers were aligned in the axial direction, so that the overlap of the focal areas was maximized. The dimensions of the focal areas for both transducers were simulated numerically using Field II (Jensen 1992), and confirmed using hydrophone measurements to be 19 mm x 0.5 mm, 5.5mm x 0.5mm and 16 mm x 1.5 mm at the –6 dB level for the PCD, the 1.5MHz and 1.1MHz HIFU transducers, respectively. The PCD had a frequency band of 2.5 - 17 MHz at -6 dB level. The HIFU focus location was preregistered with the imaging system (E-CUBE series, Alpinion, Seoul, Korea) and was indicated by a white cross sign on the screen (Fig. 1b) for convenient in-line targeting of the tumor.

The peak electric power available to the pHIFU transducer could be varied within 25 – 1000 W. The corresponding focal pressure waveforms were measured in water by the fiber optic probe hydrophone to determine the range of achievable peak-rarefactional pressures: 1.6 - 12.4 MPa and 2.2-17 MPa for the 1.1 MHz and 1.5 MHz transducers, correspondingly. The transducers were mounted in an acrylic water tank attached to a water conditioning system for continuous degassing, heating and filtering.

The signals received by the PCD were amplified and recorded exactly the same way as our previous publication [69]. The geometric foci of the PCD and the HIFU transducers were aligned

in the axial direction, so that the overlap of the focal areas was maximized. The dimensions of the focal areas for both transducers were simulated numerically using Field II [34], and confirmed using hydrophone measurements to be 19 mm x 0.5 mm, 5.5mm x 0.5mm and 16 mm x 1.5 mm at the –6 dB level for the PCD, the 1.5MHz and 1.1MHz HIFU transducers, respectively. The PCD had a frequency band of 2.5 - 17 MHz at -6 dB.

The HIFU focus location was preregistered with the imaging system (E-CUBE series, Alpinion, Korea) and was confirmed by a fiber optic probe hydrophone (FOPH 2000; RP Acoustics, Leutenbach, Germany) measurement through acoustic field mapping. Therefore, the HIFU focus was conveniently positioned within the tumor of the mouse using B-mode image guidance, indicated by a white cross sign on the screen.

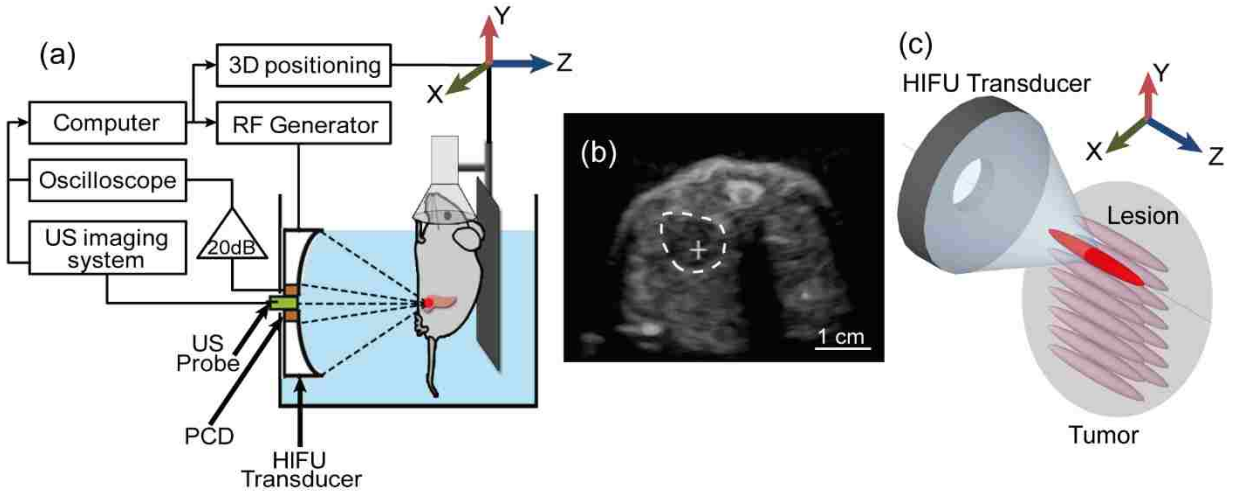

Figure 3.1 Schematic illustration of the HIFU treatment system. The HIFU transducer, ring-shaped passive cavitation detector (PCD) transducer and an ultrasound imaging probe were aligned confocally and coaxially and built into the side of the acrylic water tank. The water was continuously degassed and heated to 37 ^{o}C. The KPC mouse was attached to a custom holder and was anesthetized by inhalation of isoflurane through a cone. The mouse was positioned by a 3D positioning system to align the tumor targeting region with HIFU focus under the guidance of B-mode imaging (b). Both the positioning and HIFU delivery were planned and controlled by computer. The mouse was positioned so that the pHIFU focus was at least 10 mm below the skin surface to avoid cavitation damage to the skin. The pHIFU treatment grid in the two transverse dimensions was then generated to cover the tumor region (c) accessible through the previously identified acoustic window (white dashed line).

Animal Model

A transgenic mouse model of PDA was used. The KrasLSL.G12D/+; p53R172H/+; PdxCretg/+ (KPC) model closely recapitulates the genetic mutations, clinical symptoms and histopathology found in human pancreatic cancer, unlike xenograft or orthotopic models [20]. The tumors have a moderately differentiated ductal morphology with extensive dense stromal matrix that, together with poorly developed vasculature presents a major obstacle to chemotherapeutic drug penetration. All of the animal experimental procedures were approved by the Institutional Animal Care and Use Committee at the University of Washington. They were kept under pathogen-free conditions and received food and water ad libitum. The general status and body weight of each animal were assessed at the start and at the end of experiments. KPC mice were used for the study when their tumor size reached 1 cm according to diagnostic ultrasound examination.

Experimental Procedures

The animal was first anesthetized by inhalation of isoflurane, and the abdomen was depilated. It was examined by ultrasound imaging to measure the dimensions of pancreatic tumor in length, width, and depth. Then treatment window was identified to avoid gas tissue interface in the HIFU pathway. To decrease the chance of cavitation on the skin surface, the mice were washed several times in a warm water bath and then wiped by ethanol. Lastly, the animal was immobilized into the custom-made holder and submerged into the heated water tank (at 37°C) for treatment planning.

The treatment planning was performed as follows (using the software package from VIFU system): The center of the tumor was aligned at the HIFU focus (the cross sign on B-mode) using a computer-controlled 3D positioning system as shown in Fig. 3.1a and Fig. 3.2.

Figure 3.2 An example of user interface on aligning HIFU focus with the center of the pancreatic tumor. The mouse was positioned and tumor boundary was identified (white dashed line). A 3D positioner (along x, y, z axes) was used to move the animal holder, which was attached to positioning system, so that the HIFU focus (red cross) was aligned with the center of the tumor.

The tumor region along the longitudinal axis on sagittal plane of the mouse was defined from the top slice to the bottom slice of the tumor by an experienced sonographer (Fig. 3.2). The positions of the top and the bottom of the tumor were memorized by the treatment planning program. Then a number of slices were generated between top and bottom at a separation of 1 mm. Lastly, each slice was defined individually with a specific width so that only the tumor region with appropriate acoustic windows were treated, the chance of collateral damage to bowel or other organs were minimized.

Figure 3.3 An example of user interface on defining treatment width on each the transverse slice of the tumor. The mouse was moved up and down at a step size of 1 mm along the vertical axis (head to tail direction). The positions of top slice and the bottom slice were determined by experienced sonographer and were recorded by the treatment planning program. The length between top and bottom slices was divided into a number of slices at a separation of 1 mm. The widths of the each slice can be individually determined to avoid collateral damage to other organs.

After the tumor region in 3D was defined, the pHIFU treatment grid was generated within the tumor region across the mouse coronal plane (the x,y plane) and the focal depth is fixed to about 7-10 mm below the mouse skin. As the focal region is 2.5mm long by 0.5mm wide, the distance between two neighboring spots was 1 mm for a 1.5 MHz HIFU system to reduce the chance of interference among spots. Figure 3.1b showed an example of the selected treatment area on transverse plane of the mouse with the HIFU focus located at the center of the tumor. The white dash line indicated the boundary of the tumor. The pHIFU parameters for each spot can be independently defined (Fig. 3.4). During the treatment, the mouse was moved such that the treatment spots were scanned in a raster pattern.

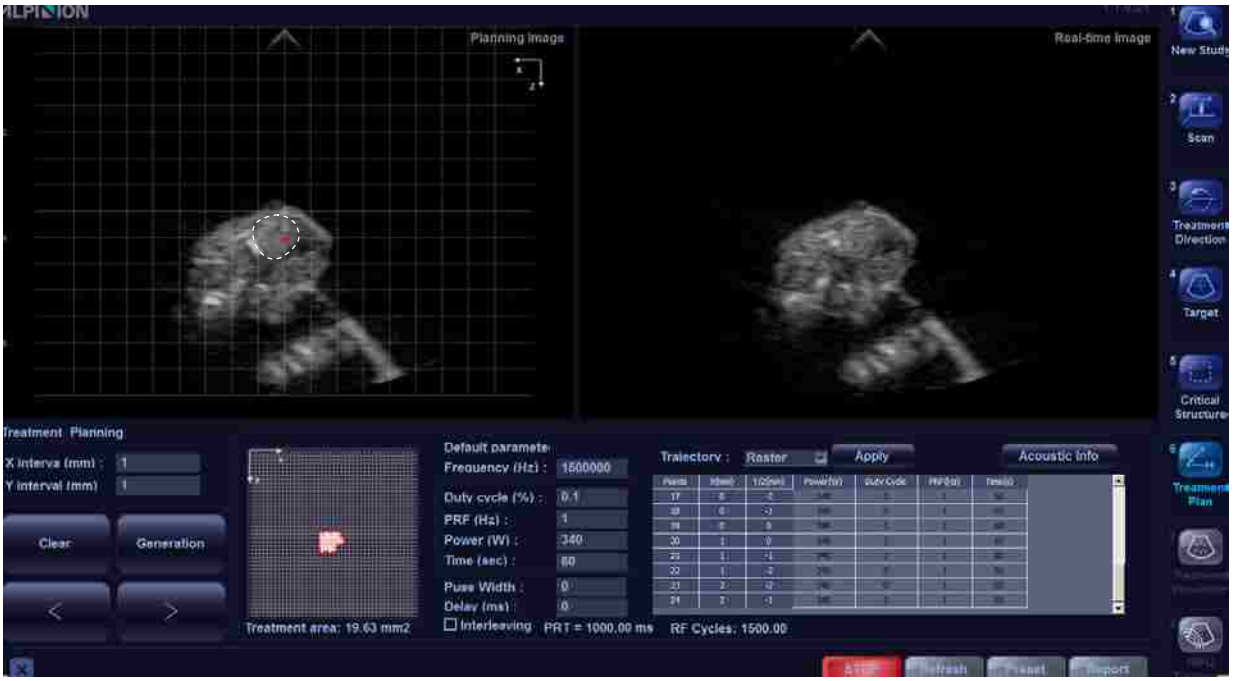

Figure 3.4 An example of user interface on treatment pattern generated across coronal plane of pancreatic tumor. After a separation distance is determined between two neighboring locations, a treatment grid was generated and parameters of duty cycle, pulse repetition frequency, electrical power and time duration for each spot were determined. The mouse was moved such that the treatment was performed in a raster pattern both laterally and vertically across the x, y plane.

Intravenous administration of Dox was performed either before or after pHIFU treatment. Dox was used as proxy of gemcitabine as it is fluorescent. Each mouse received an intravenous injection of 9 mg/kg doxorubicin via the tail vein. The mouse was moved such that the treatment was performed in a raster pattern both laterally and vertically. At each treatment spot, the same pulse protocols were used: a series of 60 1ms HIFU pulses were delivered at a pulse repetition frequency of 1Hz. The focal pressure levels were varied for different degree of cavitation activity. Millisecond-long pulses were used in drug delivery treatments [35]; however, in most studies longer pulse durations were used (10-100 ms). In this study, 1 ms pulse duration was chosen to avoid substantial thermal effects, especially at the higher focal pressure levels. A duty factor of 0.1 % prevented heat accumulation. A PCD signal was acquired during the delivery of each HIFU pulse using a digital oscilloscope and was stored at the host PC. Signal processing is performed as described in the previous chapter. Cavitation metrics of cavitation probability, cavitation persistence, and cavitation noise level were calculated from the signals. An average

surface projection of tumor area is 1 cm^2, which takes about 30 mins total treatment time per mouse. Immediately after treatment with high-intensity focused ultrasound, mice were removed from the water bath. The abdomen of the animal was surgically opened and the pancreatic tumor was collected.

3.2.2 Multispectral Imaging

Within 30 minutes of harvesting the tumor, it was examined with a fluorescent imaging system (Maestro *in vivo* Imaging System, CRi, Woburn, MA) to obtain the overall distribution of the fluorescent drug. The imaging system had an automated multispectral acquisition with excitation wavelengths in 500 - 950 nm range. In this study, a blue excitation (500 – 720 nm)/green emission filter (550 – 800 nm) set was used. Images from the front side and back side of each tumor were acquired. Then, the tumor was cut along the perpendicular plane of the HIFU incident wave, and an image of the cut tumor was acquired. In order to account for tissue autofluorescence, a non-treated region of the tumor was selected as control and spectral unmixing was applied. The resulting distribution of volumetric fluorescent intensity directly showed the distribution of Dox (yellow color) in the targeted area versus control area shown in purple color.

However, this measurement was only qualitative. For the qualitative assessment, small (2 mm in diameter) segments of the tumor in the treated and the control area were collected using a biopsy punch (Miltex Inc., York, PA) to be analyzed for volumetric Dox concentration quantification by high pressure liquid chromatography (HPLC).

3.2.3 Fluorescent Microscopy and Histology Examination

After multispectral imaging, the samples were immediately embedded in optimum cutting temperature medium (O.C.T) and frozen in isopentane cooled on dry ice. Embedded tissue was stored at -80°C until sectioning. Sections of 8 um thickness were taken at various locations throughout the tumor mass using a Leica CM 1950 Cryostat (Leica Biosystems, Nussloch, Germany) and allowed to air dry while protected from light. In the sets of four sequential histological sections, the first section was investigated by fluorescent microscopy to characterize

the distribution of Dox at the microscopic level. The second section was stained with Hematoxylin and Eosin (H&E) for visualization of cellular structure [70]. The third section was stained with Masson's trichrome stain for fibrosis evaluation, which was used before for analyzing pancreatic tumor sections [71]. It this work, Masson's trichrome stain was used to characterize the potential damage caused by pHIFU to the collagenous matrix.

3.2.4 High-Pressure Liquid Chromatography (HPLC) Analysis

The concentration of Dox was measured in tumor samples using high-pressure liquid chromatography (HPLC). HPLC is a chromatographic technique used to separate the components in a mixture, to identify each component, and to quantify each component. In order to quantify doxorubicin from murine tumor, specific sample preparation for HPLC was carried out following a previously developed protocol [72].

As described in previous section, following treatment with HIFU and Doxorubicin, the pancreas of each mouse was surgically removed and the mouse was euthanized. Subsequently, the tissue concentration of Doxorubicin was quantified within the targeted area of the tumor as well as the within an area not targeted by HIFU. The ratio of the tissue concentration of Doxorubicin from the treated area relative to that of the untreated area constituted the primary response measure of interest.

Briefly, a 0.2 mg specimen of the pancreatic tumor tissue was collected from the pHIFU treated area, which were facing the direction of the incident pHIFU wave. Another 0.2 mg specimen was collected from the non-treated area. The Dox concentrations from both specimens were later normalized into a ratio as an outcome of the Dox uptake. The specimens were first homogenized with KH_2PO_4 (20 mM, pH 3.8) using a homogenizing kit (OMNI International, Kennesaw, GA) and stored at -20C until analysis. Before the analysis, the sample was incubated at 37°C for protein biding equilibrium. The samples were then mixed with 250 µL acetone and 100 µL $ZnSO_4$ solutions (saturated) and re-incubated at 37°C for another 15 min to precipitate the proteins. Subsequently, the samples were centrifuged and subjected to evaporation under a weak

stream of nitrogen gas at room temperature. The dried residue was completely dissolved in 200 µL HPLC mobile phase and introduced into the HPLC system for analysis.

Since the drug uptake in tumor varies drastically from one mouse to another due to the differences in vasculature density, homogeneity and intratumoral pressure, the HPLC results were normalized by the ratio of Dox concentration in the specimen of treated area to the concentration in the specimen of non-treated area from the same tumor. In this way, the baseline variances across difference mice were justified. The normalized uptake was then correlated with cavitation activities measured during pHIFU exposures.

3.2.5 Statistical Analysis

In this study, a number of mice were applied with both treatments cases (5 out of 30 mice). But most of the mice (25 out of 30 mice) were subjected to only one of the treatment cases (i.e. they either received Dox injection during HIFU treatment or Dox injection following HIFU treatment), while the remaining five were observed under both treatment cases.

Performing both treatments on a mouse required the tumor to have a large enough acoustic widow to allow for HIFU targeting of the tumor in two different areas of the tumor. Therefore, only mice with relatively large tumors were subjected to both treatment protocols. Besides this anatomical restriction (which was factored in whether a mouse was treated under one or both treatment protocols), treatment assignment was random. Specifically, the intensity of HIFU that was chosen to treat a mouse was also random.

Given that the outcome variables are ratios of Dox concentrations in the treated areas relative to the untreated areas, the response is recorded on a multiplicative scale. First, cavitation persistence was tested in relation with Dox uptake. As cavitation persistence maximum value is at 100%. In other words once cavitation persistence reaches 100%, any additional mechanical impact of HIFU will not be quantified by cavitation persistence and therefore, at higher values of cavitation persistence more variation around the mean could be expected. Based on these, the natural logarithm of the response variable was considered in studying the association of interest using the following equations:

$$\mathbb{E}\left[\log(relative\ concentration)|CP, Trt\right] = \beta_0 + \beta_1 CP + \beta_2 Trt + \beta_3\, CP * Trt$$

Where CP is the cavitation persistence, and Trt is an indicator variable that equal 1 when HIFU treatment and Dox injection are delivered simultaneously and is zero when HIFU treatment was followed by Dox injection. In this model β_3 captures how the rate of Dox as a function of cavitation persistence changes between the two treatment types, while β_1 characterizes the association between changes in cavitation persistence and the Dox uptake.

Similarly, cavitation noise level was tested in relation with the Dox uptake. As cavitation noise level doesn't reach a specific maximum number, the response itself was considered as the outcome using the following equation:

$$\mathbb{E}\left[relative\ concentration|CN, Trt\right] = \beta_0 + \beta_1 CN + \beta_2 Trt + \beta_3\, CN * Trt$$

Where CN is the cavitation noise level, and the other parameters are the same corresponding to the Dox uptake.

The method that can properly estimate the effect of cavitation persistence or cavitation noise level as well as two different treatment protocols on Dox uptake is by using generalized estimating equation (GEE). Using GEE package geepack in R version 3.1[73], the regression specified in both equations was performed.

3.3 Results

3.3.1 Preliminary Experiment

A mouse bearing subcutaneous injected pancreatic tumor were used as an animal model for a pilot study of the dependence of Dox uptake on cavitation activities. The Dox uptake distribution corresponded to the treatment plan (9 by 2 treatment locations), shown as red colored circles with black lines in Fig. 3.5a. The intensity of the red color indicated increased peak-rarefactional pressure ranged from 5 to 11 MPa, as shown in the color bar (Fig. 3.5a). Cavitation noise levels, averaged over all recorded PCD signals at each HIFU pressure level, increased with the HIFU peak-rarefactional pressure, indicating that Dox uptake was enhanced when pHIFU induced

bubble collapse became more violent (Fig. 3.5b). Cavitation persistence increased with peak-rarefactional pressure. From the Dox uptake distribution (Fig. 3.5a), the yellow color corresponding to drug uptake started to appear when peak-rarefactional pressure became greater than 8 MPa. The color became intense and consistence when pressure became greater than 9.5 MPa. The cavitation persistence was less than 25% when the peak-rarefactional pressure was below 8 MPa, 25% to 75% between 8 MPa and 9.5 MPa and over 75% when pressure increased from 9.5 MPa to 11 MPa (Fig. 3.5c). In the subsequent experiments, the cavitation persistence and cavitation noise level were correlated with Dox uptake.

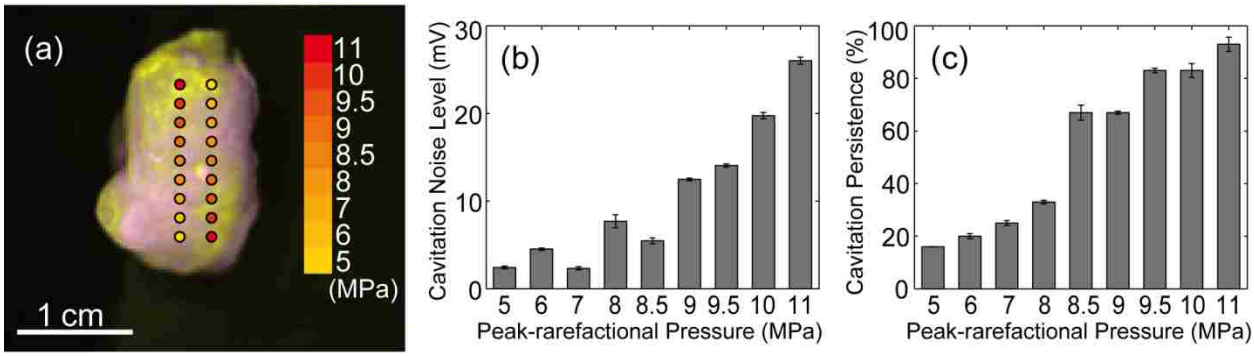

Figure 3.5 The fluorescence emission distribution of Dox uptake in an *in vivo* murine subcutaneous pancreatic tumor was shown in yellow color after spectral unmixing from autofluorescence (purple color). The Dox enhancement corresponded to treatment planning (9 by 2 treatment locations), shown as gradient red colored circles (a). The intensity of red color indicated increased peak-rarefactional pressure ranged from 5 to 11 MPa, shown in the color bar (a). Cavitation noise levels, averaged over all recorded PCD signals at each HIFU pressure level, increased with the HIFU peak-rarefactional pressure, indicating that Dox uptake was enhanced when pHIFU induced bubble collapse becomes more violent (b). Cavitation persistence increased with peak-rarefactional pressure. From the Dox uptake profile (a), the Dox uptake started to appear when peak-rarefactional pressure became larger than 8 MPa. The color became intense and consistent when pressure became larger than 9.5 MPa. The cavitation persistence was less than 25% when peak-rarefactional pressure was below 8 MPa, 25% to 75% between 8 MPa and 9.5 MPa and over 75% when pressure increased from 9.5 MPa to 11 MPa.

3.3.2 Multispectral Imaging

The multispectral images of treated tumor showed the distribution of drug uptake matched well the targeted treatment area. After the spectral unmixing, the multispectral imaging revealed that

locations that were treated with pHIFU during or before Dox injection had a significant increase of fluorescent intensity. Figures 3.6a, 3.6b, 3.6c and 3.6d were the camera image, multispectral images of front, back and middle views of a KPC tumor from the control group which did not receive HIFU treatment but was injected with Dox. The camera image did not show any regions of hemorrhage. The multispectral images showed no significant Dox uptake. Figure 3.7a, 3.7b, 3.7c were the corresponding camera and multispectral images of a KPC tumor from the treatment group that were applied with pHIFU treatment first and then injected with Dox. The camera image showed significant hemorrhage area corresponding to the treatment region (white dashed line). Both the front side and the back side of the tumor showed enhanced fluorescent intensity in the treated region compared to the non-treated region.

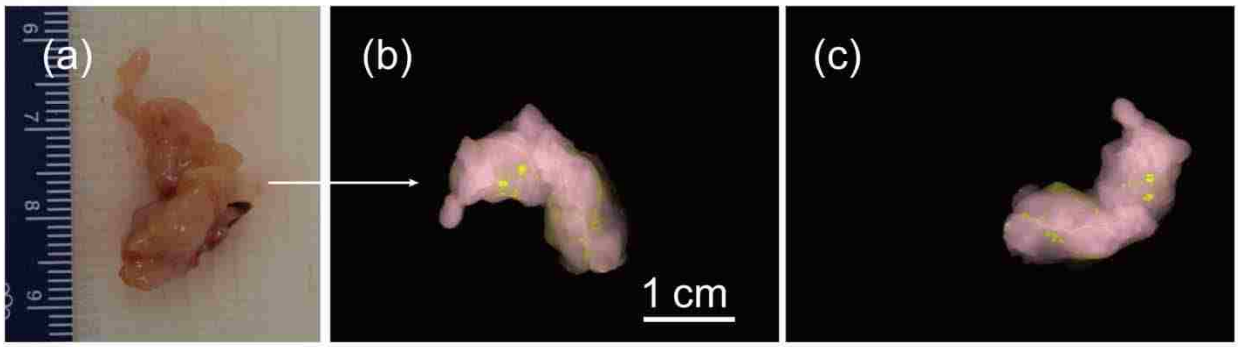

Figure 3.6 A multispectral image of an *in vivo* KPC tumor from the control group, in which only Dox was administered to the mouse without any pHIFU treatment. The front (b) and back (c) sides of the tumor showed no significant Dox uptake.

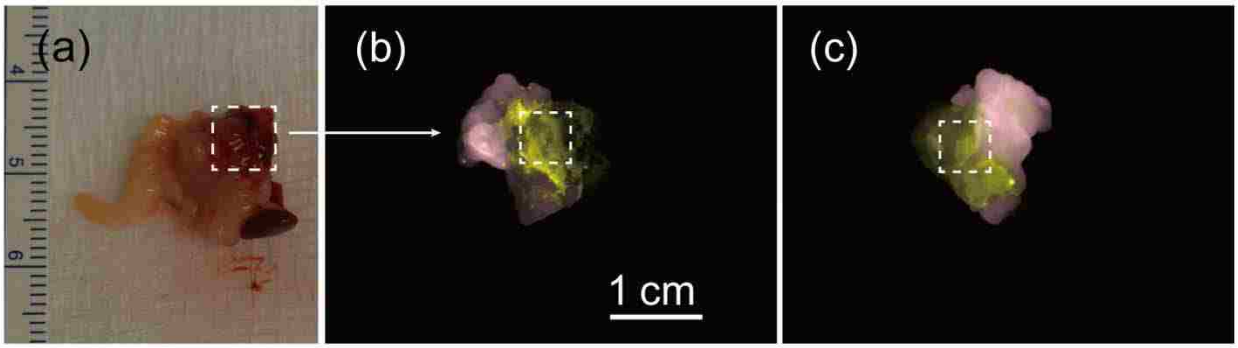

Figure 3.7 A multispectral image of an *in vivo* KPC tumor excised from the experiment when Dox was administered immediately after pHIFU treatement. The mouse was flushed with saline right after euthanasia and the tumor was clear of superficial blood clots (a). The direction of HIFU incident wave was perpendicular of the plane of the image. The targeted region (white dashed line) showed significant hemorrhage area. All fluorescent signals came from the integrated volume of tumor. The fluorescent spectrum of Dox (yellow color) was unmixed from autofluorescence (purple color). The front of the tumor showed enhanced uptake (b) corresponded to the targeted area (white dashed line). After flipping over the tumor horizontally, the back of the tumor also showed strong Dox uptake (c) in the treated area (white dashed line). Tumor was cut along the plane perpendicular to the HIFU incident wave.

When the tumor was cut into two halves perpendicular to the HIFU incident direction, blood vessel damage was observed in the middle of the treated area (Fig. 3.8a, b, c). As the mouse circulation was flushed by saline thoroughly, all the blood in the vasculature should be flushed away by circulation. If no damage existed in the tumor, there shouldn't be any blood left after flush. Therefore, the remained redness area shown in the examples below suggested the vessels were disrupted and blood leakage was resulted due to pHIFU treatment.

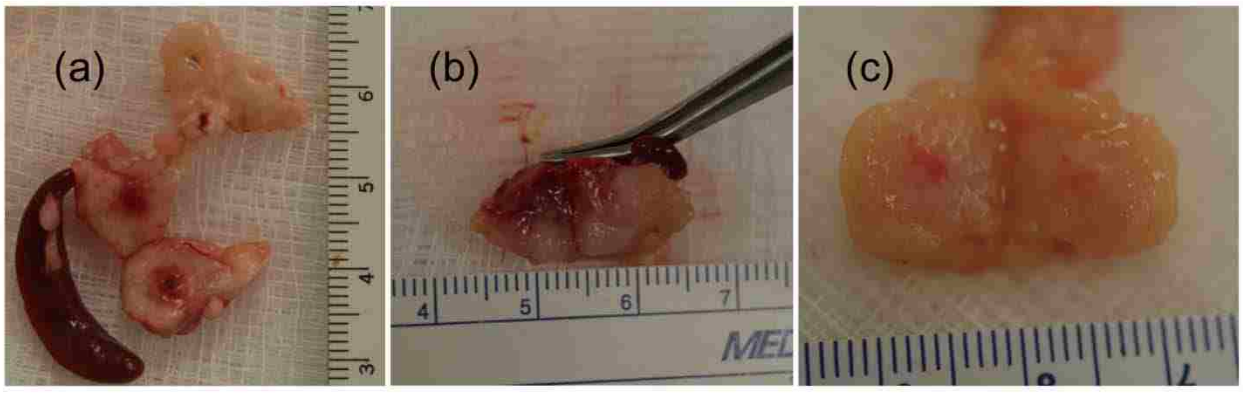

Figure 3.8 Photographs of treated tumor examples (a, b, c) showed an obvious hemorrhage area corresponding to the HIFU treatment area. For example (a) and (c), the direction of HIFU incident wave was perpendicular of the plane of the image. For example (b), the direction of HIFU wave was from top to bottom of the tumor shown in the photograph.

3.3.3 Fluorescent Microscopy

Examples of fluorescent microscopy images of tumor slices from non-treated group (Figs. 3.9, 3.10) and the treated group (Figs. 3.11, 3.12) were shown. All of the sliced were compared with

their neighboring slices which were stained by H&E and Masson's trichrome staining to correspond to the actual cellular structure, yellow dashed line outlined some feature of the sliced to make sure they correspond to the same location. In the examples of non-treated tumor slice, tumor didn't show successful uptake from the fluorescent image either at the boundary (Fig. 3.9) or at the inner part of the non-treated tumor (Fig. 3.10). On the other hand, in the examples of the treated group, enhanced Dox uptake was observed in not only the border of the tumor (Fig. 3.11), where more vasculature was expected, but also the inner part of the tumor (Fig. 3.12). The fluorescent image showed that Dox was uniformly distributed, shown as bright dots (Fig. 3.11b, 3.12b). It implied that cell nucleus has successfully bond with the Dox. H&E stained slices showed the cellular structure was loosely distributed in the treated group (Fig. 3.11a, 3.12a), whereas the non-treated group the cellular structure was more uniform (Fig. 3.9a, 3.10a). Masson's trichrome stain showed the collagen was disrupted (Fig. 3.11c, 3.12c), indicating that pHIFU pulses have damaged collagen and disrupted fibrosis matrix through mechanical effects. The non-treated group didn't show any damage (Fig. 3.9c, 3.10c).

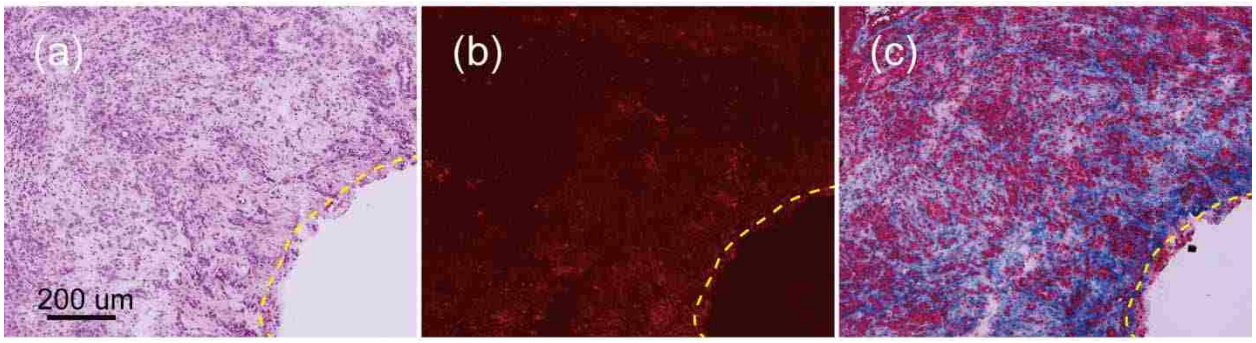

Figure 3.9 H&E staining (a), fluorescent microscopy image (b), and Masson's trichrome staining (c) of consecutive slices a treated KPC tumor were shown. No significant Dox uptake was observed. Masson's trichrome image showed a dense collagen area at the border of the tissue, which may prevent drug diffusing into the tissue.

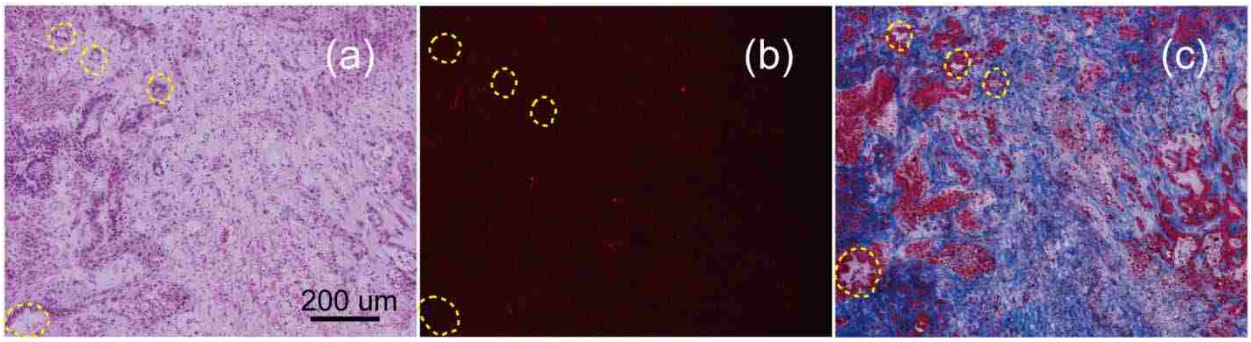

Figure 3.10 H&E staining (a), fluorescent microscopy image (b), and Masson's trichrome staining (c) of consecutive slices a non-treated KPC tumor were shown. No significant Dox uptake was observed. Masson's trichrome image showed a dense collagen area at the inner part of the tumor tissue.

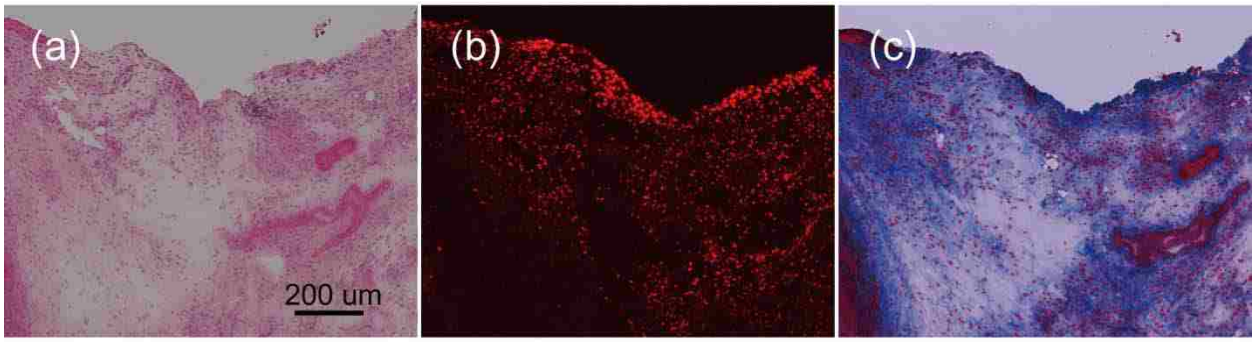

Figure 3.11 H&E staining (a), fluorescent microscopy image (b), and Masson's trichrome staining (c) of consecutive slices a treated KPC tumor were shown. Significant Dox uptake was shown toward the boundary of the tumor but also penetrated into the inner part of the slice. Masson's trichrome image showed that although collagen (blue color) was abundant in this area, the cells close to the collagen successfully bond due to disrupted collagen.

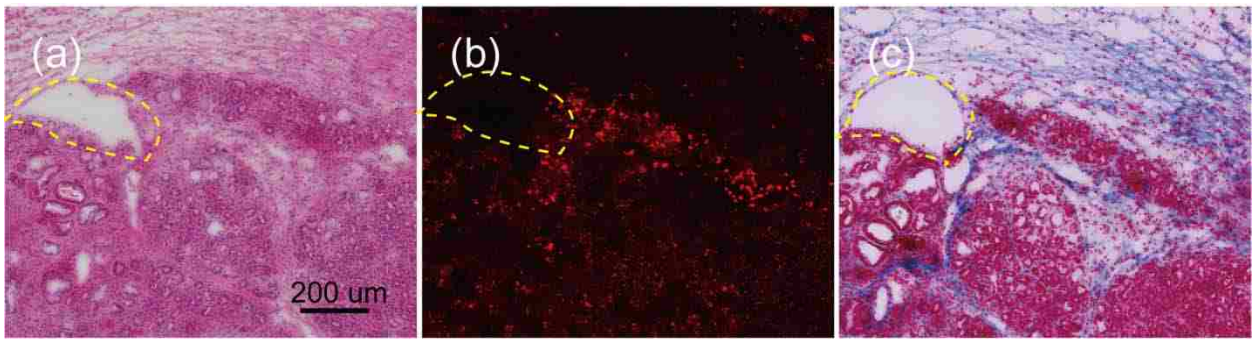

Figure 3.12 H&E staining (a), fluorescent microscopy image (b), and Masson's trichrome staining (c) of consecutive slices a treated KPC tumor were shown. Significant Dox uptake was observed on the lower portion of the image. (c) Masson's trichrome image show that collagen

(blue color) was fraying, likely due to cavitation. The tissue adjacent to the collagen had significant Dox uptake suggesting Dox leaked through matrix and perfused to tumor cells.

3.3.4 High-Pressure Liquid Chromatography Analysis

The dependence of normalized HPLC results on cavitation persistence and on cavitation noise level in different treatment groups were shown in scatter plots Figs. 3.13 and 3.14 respectively. The results showed as cavitation persistence increased from low to 100% and the noise level gradually increased, the Dox uptake was almost linearly enhanced. Therefore, A linear regression fit was applied. As mentioned in the methods section, there existed a larger variation when cavitation persistence approaches 100%, a natual logorithm was applied to the normalized Dox concentration to account for equal variance across the range of cavitation persistence. As for the cavitatio noise level metric, there was no maximum, therefore no natural logorithm was applied. In both cases, the distribution of the data was generally linear.

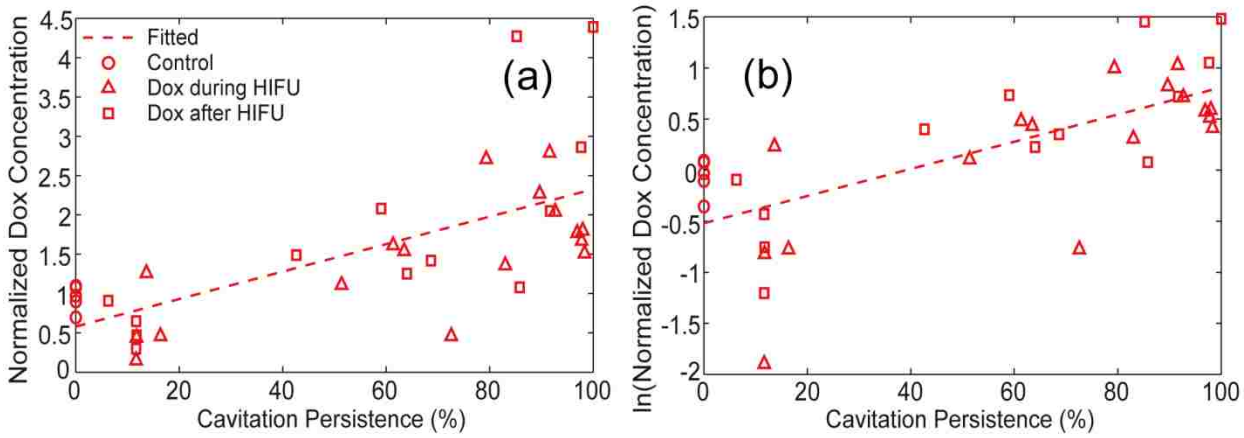

Figure 3.13 Scatter plot of normalized Dox concentration (the outcome) versus cavitation persistence (a). The outcome was generally in a linear relationship with the persistence. When approaching 100% persistence, the response had a larger variance. Therefore, the natural logarithm of the response was used in the statistical analysis, which also showed a linear relationship (b). The fitted relation (dashed line), outcomes from control group (circles), outcomes from the simultaneous HIFU treatment and Dox injection group (triangles) as well as from Dox injection after HIFU treatment group (squares) were shown.

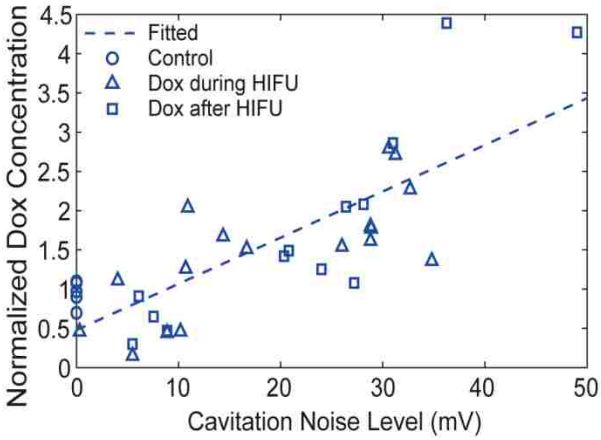

Figure 3.14 Scatter plot of normalized Dox concentration versus cavitation noise level. The fitted relation (dashed line), outcomes from control group (circles), outcomes from the simultaneous HIFU treatment and Dox injection group (triangles) as well as from Dox injection after HIFU treatment group (squares) were shown.

The table below showed the statistical test results by the GEE method. In average every 1% increase in cavitation persistence is associated with a 1.02 fold larger geometric mean of the normalized Dox concentration (or alternatively a 10% increase in cavitation persistence is associated with a 1.23 fold greater geometric mean of the normalized Dox concentration). This estimate is significant (p value < 0.01) suggesting that cavitation persistence was significantly associated with the Dox uptake. However, in average, the outcome is not statistically different between different treatment cases (p value 0.75), meaning that treatment protocol of pHIFU during Dox infusion doesn't increase drug uptake more than the treatment protocol of pHIFU followed by Dox infusion.

A)

	Value	Std. err	Wald stat	Pr(>|W|)
$\hat{\beta}_0$	-0.65	0.29	4.91	0.03
$\hat{\boldsymbol{\beta}}_{\mathbf{1}}$	0.02	0.01	15.68	<0.01
$\hat{\beta}_2$	-0.51	0.41	1.49	0.22
$\hat{\boldsymbol{\beta}}_{\mathbf{3}}$	<0.01	0.01	0.10	0.75

B)

Intercept	% Cavitation Persistence	Treatment type = 1	Cavitation Persistence * Treatment Type

$e^{\hat{\beta}_0} = 0.52$	$\boldsymbol{e^{\hat{\beta}_1} = 1.02}$	$e^{\hat{\beta}_2} = 0.60$	$\boldsymbol{e^{\hat{\beta}_3} = 1.00}$

Table 3.1: A) Estimated value of the coefficient for relationship between cavitation persistence and Dox uptake. B) Exponentiated coefficient estimates for each parameter

Similar results were generated for testing the relationship between cavitation noise level and normalized Dox concentration. On average every 1 mV increase in cavitation noise level is associated with an increase in the concentration of Dox of 0.09 higher (or alternatively a 10 mV increase in noise level is associated with an increase in the normalized concentration of Dox of 0.9 higher). This estimate is significant at the 0.05 level (p value <0.01) suggesting that cavitation noise level was significantly associated with the Dox uptake. Additionally, the per 'cavitation noise level' rate of Dox uptake is on average 0.04 lower in the case when Dox was injected during pHIFU treatment compare to the case that Dox was injected after pHIFU treatment.

	Value	Std. err	Wald stat	Pr(>|W|)
$\hat{\beta}_0$	-0.22	0.23	0.88	0.35
$\boldsymbol{\hat{\beta}_1}$	0.09	0.01	61.67	< 0.01
$\hat{\beta}_2$	0.69	0.33	4.49	0.03
$\boldsymbol{\hat{\beta}_3}$	-0.04	0.02	6.21	0.01

Table 3.2: Estimated value of the coefficient for relationship between cavitation noise level and Dox uptake.

3.4 Discussion

We studied the efficacy of pulsed high-intensity focused ultrasound for enhancing drug delivery in *in vivo* pancreatic tumor by using a realistic animal model - KPC mouse model. In the first treatment protocol, which is the case when doxorubicin was infused through the tail vein during the pHIFU treatment, there were two mechanisms that could have improved drug penetration. First, the cavitation effect from pHIFU directly disrupted the highly fibrotic stromal matrix and blood vasculature. So drug molecules leaked out from the vessels and were passively diffused

into the disrupted area. Second, radiation force from pHIFU resulted in localized fluid streaming, which could actively diffuse drug molecules from leaky blood vessels into the disrupted stroma, and further into the cancer cells.

The results from pHIFU treatment followed by drug administration and the results from pHIFU treatment during drug administration showed no statistical difference. In the first case, cavitation was the dominant mechanism during pHIFU treatment. Therefore, it's likely that when cavitation disrupted the highly fibrotic stromal matrix, and permeability increased instantly, and passive drug diffusion was enhanced. Recent publication reported that dense stromal matrix in the tumor squeezes tumor vessels and thus crush blood flow, preventing chemotherapy drug from reaching malignant cells [21], [22]. Therefore, we speculate that pHIFU induced cavitation reduced the solid stress surrounding the tumor vessels by disrupting the stromal matrix. So the blood vessels are no longer compressed and drug can penetrate further into cancer cells which formerly received no blood flow. In the second case, when pHIFU treatment was accompanied by the Dox injection, both cavitation and streaming, i.e., the rapid movement of fluid away from transducer due to radiation force, were resulted. It both actively enhanced drug diffusion from vasculature to stromal tissue and disrupted the stromal matrix. The results from both treatment cases demonstrated that the potential active diffusion by streaming didn't results in additional uptake. Therefore, cavitation was the dominant effect for drug delivery. Intense and reliable cavitation was correlated with drug uptake.

In this work, the combination of multispectral imaging, microscopy and HPLC gives a complementary perspective of the drug delivery mechanism by pHIFU on pancreatic tumor. The multispectral imaging detected an overall distribution of Dox uptake. Multispectral imaging is a quick imaging method to detect drug uptake right after the mouse is sacrificed and confirm if the drug distribution corresponded to pHIFU targeted region. In all the treated tumors, enhanced fluorescent intensity corresponding to Dox spectrum was observed in the planned treated region. The fluorescent microscopy located Dox uptake in the microstructure level. The microscopy results suggested dense fibrotic matrix was disrupted and drug uptake was found in cell nucleus. The HPLC results accurately quantified Dox concentration. The normalized Dox concentration

was linearly related to both cavitation persistence and cavitation noise level. It suggests that cavitation must happen strong and consistently to cause significant penetration in pancreatic tumor.

The photograph of the cut-open treated tumor showing hemorrhage region showed blood vessel damage in the middle of the tumor tissue. Histological analysis with H&E staining showed the cellular structure of differentiated pancreatic tumor tissue was disrupted. Masson's trichrome stain showed that stromal matrix, which consisted of collagen, was disrupted and permeabilized during pHIFU treatment. The Dox uptake observed in the fluorescent imaging was close to the disrupted structure suggesting that Dox perfused from leaky blood vessels into tumor cells. Dox uptake was observed both at the border of the tumor and the center.

Comparing of two different operating frequency systems, the 1.1MHz HIFU transducer has a focal region of 16 mm x 1.5 mm, which is relatively long compare to the size of the pancreatic tumor in mouse. Several complication resulted, including skin burn, bleeding from other organs surround the tumor, and spine heating when tumors are close to the spine. The mouse under such situation were often not able to be flushed well, results were not taken in such cases. Therefore, a 1.5MHz HIFU system (focal region of 5.5mm by 0.5mm) with a smaller focal region but even higher energy at the focus had an improved Dox uptake.

3.5 Summary and Conclusions

In this chapter, we demonstrated an improved Dox penetration by pHIFU-induced cavitation disrupting the stromal matrix, thereby increasing local delivery of chemotherapeutic agents in a targeted fashion. Results show that cavitation was the dominant effect for drug delivery. The potential mechanism is due to cavitation disrupting blood vessels and permeabilizing the stromal matrix so that blood vessels become leaky and are no longer compressed. Passive drug diffusion was enhanced instantly. The long term effect will be evaluated in future studies to compare with the effect of using a stroma depleting drug. In the clinical setting, the treatment protocol of pHIFU treatment prior to chemotherapy injection will be more convenient clinically since it's

easier to administer either HIFU or chemotherapy separately than administering both simultaneously.

In summary, ultrasound exposures resulting in cavitation with high probability, high persistence, and high noise level warrant further investigation for HIFU-enhanced drug delivery. We demonstrated for the first time the relationship between cavitation activity metrics versus the chemotherapeutic drug penetration. *In vivo* study results have clearly shown that penetration is enhanced from pHIFU exposure using the KPC mouse model of pancreas cancer. The study also showed cavitation was the dominant effect in pHIFU enhanced drug delivery.

Chapter 4.

Spatial Monitoring of Cavitation Occurrence in pHIFU-aided Drug Delivery Treatments

4.1 Introduction

In this chapter, a new active cavitation mapping technique for pulsed high-intensity focused ultrasound (pHIFU) applications termed bubble Doppler is proposed and its feasibility tested in tissue-mimicking gel phantoms. pHIFU therapy uses short pulses, delivered at low pulse repetition frequency, to cause transient bubble activity that has been shown to enhance drug and gene delivery to tissues. The current gold standard for detecting and monitoring cavitation activity during pHIFU treatments is passive cavitation detection (PCD), which provides minimal information on the spatial distribution of the bubbles. B-mode imaging can detect hyperecho formation, but has very limited sensitivity, especially to small, transient microbubbles. The bubble Doppler method proposed here is based on a fusion of the adaptations of three Doppler

Work published part in:

Li T, Khokhlova TD, Spozhnikov OA, O'Donnell M, Hwang JH. Bubble Doppler on monitoring cavitation in tissue during high-intensity focused ultrasound therapy. IEEE-UFFC. 2014

Li T., Khokhlova TD, Sapozhnikov OA, Hwang JH (2013), "Twinkling artifact of Doppler imaging for cavitation detection during high-intensity focused ultrasound therapy: sensitivity and resolution", 166th Meeting of Acoustic Society of America, San Francisco, CA.

Sapozhnikov OA, **Li T**, Khokhlova TD, Hwang JH (2013), "The use of twinkling artifact of Doppler imaging to monitor cavitation in tissue during HIFU therapy", The 13th International Symposium on Therapeutic Ultrasound, Shanghai, China.

Sapozhnikov OA, **Li T,** Khokhlova TD, O'Donnell M, Khokhlova VA, Hwang JH(2014), "A new active cavitation mapping technique for pulsed HIFU applications – Bubble Doppler ", The 14th International Symposium on Therapeutic Ultrasound, Las Vegas, NV.

Khokhlova TD, **Li T,** Sapozhnikov OA and Hwang JH (2013), "The use of twinkling artifact of Doppler imaging to monitor cavitation in tissue during high intensity focused ultrasound therapy", Proceedings of meetings on Acoustics, Acoustical Society of America.

techniques that had been previously developed for imaging of ultrasound contrast agents – color Doppler, pulse inversion Doppler, and decorrelation Doppler. Doppler ensemble pulses were interleaved with therapeutic pHIFU pulses using three different pulse sequences and standard Doppler processing was applied to the received echoes. The information yielded by each of the techniques on the distribution and characteristics of pHIFU-induced cavitation bubbles was evaluated separately, and found to be complementary. The unified approach - bubble Doppler – was then proposed to both spatially map the presence of transient bubbles and to estimate their sizes and the degree of nonlinearity.

Pulsed high-intensity focused ultrasound (pHIFU) therapy is a modality used in such clinical applications as drug and gene delivery, where mild mechanical disruption of tissue by bubbles is desired, and thermal effects are to be avoided. Therefore, pHIFU treatment protocols consist of short pulses, delivered at low pulse repetition frequency, to cause transient cavitation bubble activity. pHIFU exposures have been extensively used to enhance drug/gene delivery to tumors with and without the assistance of microbubbles [1], [74], [75]. In addition, low to moderate intensity ultrasound treatments, such as low intensity pulsed ultrasound (LIPUS) for orthopedic applications, or brain stimulation have recently gained momentum, and cavitation has often been suggested as one of the mechanisms of action; however, the existing methods of cavitation detection are not sensitive enough to prove this claim [76].

Passive cavitation detection (PCD) is considered to be the most reliable, cost-effective and sensitive means of real-time cavitation detection methods [77]. In that method, broadband emissions resulting from bubble collapses are detected by a single-element focused hydrophone, aligned confocally with the HIFU transducer. The amplitude of detected broadband noise was shown to correlate with the observed bioeffects at the cellular level [12], [25], [78]. Unfortunately, this technique does not monitor the spatial distribution of bubbles with respect to the tissue being treated.

Recently, a passive method to map broadband cavitation emissions with multi-element ultrasound arrays has been proposed [27]. However, the image reconstruction technique requires

a large aperture transducer to achieve reasonable image quality that is not always acceptable in clinical applications.

One of the earlier active cavitation detection methods is B-mode imaging that utilizes the fact that cavitation bubbles are highly reflective and may appear as a hyperechoic region on the image [79]–[81]. This method has subsequently been shown to only be sensitive to large bubbles or bubble clouds that are reflective enough to be distinguishable from the tissue speckle pattern on the B-mode image [80]–[82].

Different Doppler ultrasound methods have been used to image blood vessels [83], [84], and ultrasound contrast agents (UCAs) in diagnostic applications for a long time [85], [86]. Recently, color Doppler, a method normally used to image moving scatterers in tissue, such as red blood cells, was also found to be sensitive to bubbles trapped in the cracks and crevices of solid concretions in soft tissues (e.g. kidney stones, calcifications or edges of medical instruments) [17]. Crevice bubbles have been shown to give rise to the so-called twinkling artifact (TA) - a dynamic color mosaic on the image of a hard concretion in the color Doppler ultrasound display (Fig. 4.1a) [87]. Experimental evidence suggests that irregular scattering of Doppler ensemble pulses from the submicron-size fluctuating crevice microbubbles leads to the random amplitude and phase changes in received signals, which in turn causes the random color display (Fig. 4.1b). Based on this evidence, we hypothesized that color Doppler imaging may be a sensitive means to detect small-size transient bubbles induced by pHIFU.

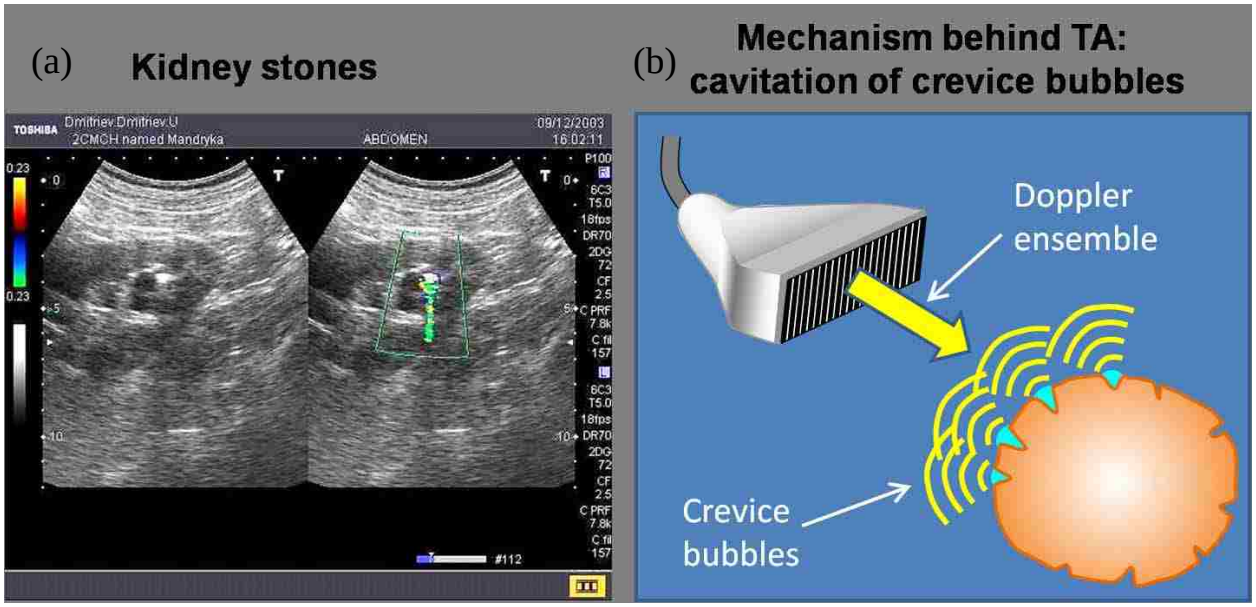

Figure 4.1 An example of TA on kidney stone (a) and proposed mechanism behind TA (b). The TA was defined as a collection of brightly colored spot that appear when color Doppler imaging is used to image hard concretions in tissue such as kidney stones. The left figure is an example of TA below kidney stone, shown as a white bright spot. The color looks as if there are scatters that move in all directions at once with all speed at once, which of course cannot be real, that's why it's called an artifact. As recently shown, the mechanism is hypothesized as cavitation of crevice bubbles trapped in stones.

Pulse inversion Doppler is a widespread method to image nonlinear scattering objects such as UCAs using a conventional color Doppler sequence modified by inverting every other transmit pulse [88]. Harmonic Doppler processing is then performed on the received echoes, so that only signals from moving nonlinear scatterers remain. The method provides superior contrast and sensitivity compared to other UCA imaging techniques, and may therefore be useful for detecting and characterizing pHIFU-induced bubbles.

Another Doppler-based approach to detection of UCAs is based on correlating Doppler ensemble pulses transmitted before and after destruction of the UCAs by a longer, higher amplitude ultrasound pulse [89], [90]. The change in echo signal associated with disruption of the UCAs and the release of free gas bubbles is construed as motion in color Doppler imaging and, similar to TA, is displayed as bright color mosaic. Since the distributions of cavitation bubbles induced

by each pulse of pHIFU treatment are likely to be different, this decorrelation Doppler approach was hypothesized to be very sensitive to the presence of pHIFU-induced bubbles.

Although the Doppler imaging methods described above provide high sensitivity and spatial resolution in imaging UCAs, they may not be immediately applicable to mapping pHIFU-induced bubbles. Unlike UCAs, the size of these bubbles is not known in advance, and the bubbles are transient, i.e., disappear very quickly after HIFU has been turned off. Imaging bubbles during the HIFU pulse, however, is not always possible due to the strong HIFU backscatter which may saturate the imaging probe electronics. The goal of this chapter was to evaluate the feasibility of bubble imaging using Doppler ensembles transmitted between HIFU pulses. The experiments were performed in transparent polyacrylamide (PA) gel phantoms to enable visual observation of pHIFU-induced cavitation activity. The three Doppler methods – color Doppler, pulse inversion Doppler, and decorrelation Doppler - were assessed separately and their sensitivities were compared to that of PCD.

4.2 Materials and Methods

4.2.1 Experimental Setup of Bubble Doppler Technique

The experimental setup used in this study is shown in Fig. 4.2. The pHIFU exposures were performed in an acrylic water tank filled with purified water degassed to 20-24% oxygen saturation, as measured by a dissolved oxygen meter (WTW Oxi 330i, Weilheim, Germany). All pHIFU exposures were performed with a 1.27-MHz spherically focused transducer (Sonic Concepts, Bothell, WA) with 64 mm aperture and 64 mm radius of curvature, and a central circular opening of 22 mm in diameter. The HIFU transducer was powered by a computer-controlled combination of an RF amplifier (ENI 400B; ENI, Rochester, NY) and a function generator (AFG 3022B; Tektronix, Beaverton, Oregon). Before the experiments, focal pressure waveforms produced by the transducer in water at different power levels were measured by a fiber optic probe hydrophone (FOPH 2000; RP Acoustics, Leutenbach, Germany). To vary the amounts of induced cavitation activity and to determine cavitation thresholds, the focal peak negative HIFU pressure was varied within the range of 0.9 – 11 MPa, with a step of 0.5 MPa. A

focused 5 MHz PCD transducer with 19 mm diameter and 49.5 mm focal length (Olympus NDT, Inc, Waltham, MA) was fitted into the circular opening of the HIFU transducer and aligned confocally with the HIFU transducer (Fig. 4.2). The dimensions of the focal areas for HIFU and PCD were 12 mm X 1.6 mm and 55 mm X 2 mm at -6dB level, respectively.

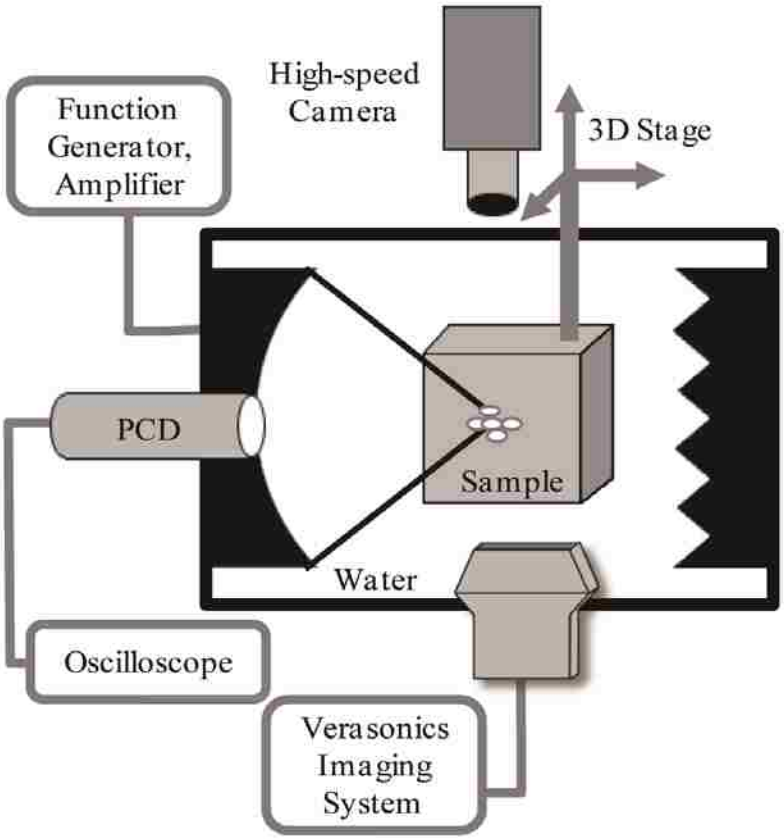

Figure 4.2 Schematic of the experimental setup. All pulsed HIFU exposures of the transparent polyacrylamide gel phantoms were performed in a large water tank with a 1.27 MHz transducer. Cavitation activity in the sample was monitored by three separate techniques simultaneously: passive cavitation detection (PCD) using a single element focused transducer, aligned confocally and coaxially with the HIFU transducer; active cavitation detection using the linear ultrasound imaging probe ATL L7-4 connected to a Verasonics imaging system; and visual observation of bubble activity using a high-speed camera. Acoustic absorbers were positioned behind the sample to avoid reverberations inside the tank.

For ultrasound imaging of the HIFU exposures, the Verasonics Ultrasound Engine (VUE, Verasonics, Redmond, WA) was used, with a clinical linear imaging probe ATL/Philips HDI L7-4 (Bothell, WA) consisting of 128 elements. The probe was aligned perpendicular to the HIFU transducer axis (Fig. 4.2). On the opposite side of the clinical probe, a Photron APX-RS high-speed camera (monochrome, Photron, San Diego, CA) was placed to visually observe and record bubble activity at the HIFU focus. The high-speed camera was set to a frame rate of 30 000 frames/s and a resolution of 256x512 pixels.

4.2.2 Gel Phantoms Preparation

To optically monitor bubble activity, all studies were performed in transparent PA (7% w/v) phantoms [36], [41], [42]. The gel was combined with 7% w/v bovine serum albumin (BSA) to serve as an indicator for thermal denaturation. To prepare the samples, a liquid mixture of PA gel constituents was degassed for 1 hour in a desiccant chamber by a vacuum pump (VTE8, Thomas, Sheboygan, WI). The degassed mixture was poured into a custom mold (5 cm wide by 5 cm tall by 8 cm deep). Polymerization was then initiated by the addition of a 10 % (w/v) ammonium persulfate solution (APS, Sigma) and N,N,N',N'-tetra-methylethylene/diamine (TEMED, Sigma). After the PA gel phantom was set, it was placed into a custom designed holder. It had four side openings to provide both acoustic and optical windows for observation. The acoustic absorber was attached to the wall of the water tank opposite the HIFU transducer to reduce reverberation. The gel phantom was positioned so that the HIFU focus was 15 mm deep below the gel proximal surface.

4.2.3 PCD Signal Processing

During HIFU exposures, a series of 1 ms duration broadband signals were acquired by the PCD transducer and processed using a custom-made digital filter using MATLAB (MATLAB 2010b, The MathWorks, Natick, MA, USA) as described in our previous study [69]. Since the majority of focal HIFU waveforms used in this study were nonlinearly distorted (Fig. 4.3a), the backscattered harmonics of the HIFU wave dominated the band-pass filtered PCD signal. Fig. 4.3b shows an example of the frequency spectrum of the signal recorded by the PCD. A

combination of a band-pass filter (Matlab function *fir1*) and a notch-shaped comb filter (Matlab function *iirnotch*) was used to separate frequency components associated with broadband noise emissions from inertially collapsing bubbles (Fig. 4.3c).

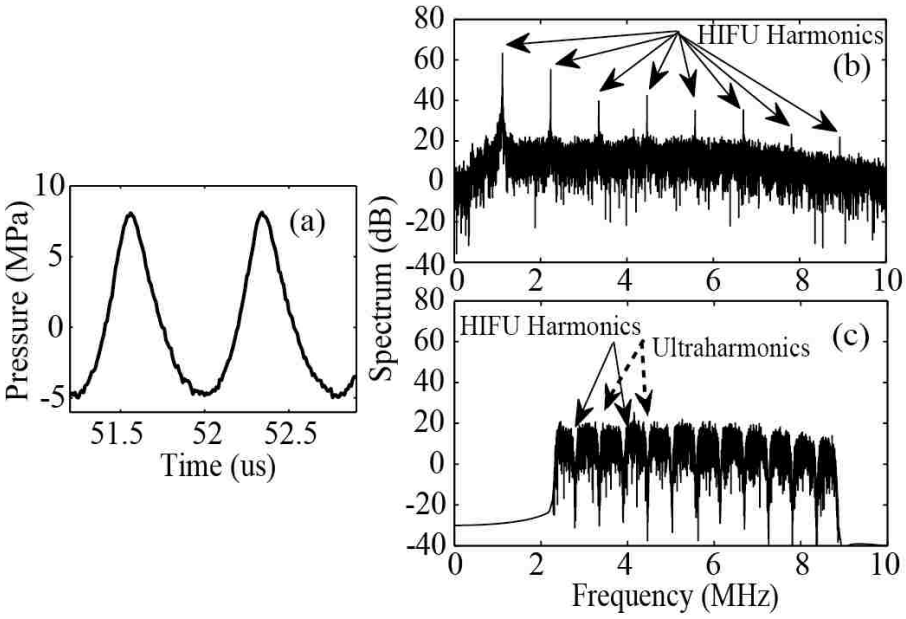

Figure 4.3 (a) An example of a nonlinearly distorted HIFU waveform. Frequency spectrum of a signal detected by the PCD transducer in polyacrylamide gel phantom before (b) and after (c) filtering. A combination of a band-pass filter (2.3 - 8.8MHz) and a notch shaped comb filter with a notch bandwidth of 100 kHz was applied to PCD signals in the frequency domain to suppress backscattered harmonics of the HIFU pulse and the ultraharmonics generated by stably oscillating bubbles.

The filtered PCD signal was further analyzed in the time domain to obtain a binary evaluation metric of whether a cavitation event took place within the HIFU pulse duration. The cavitation event was considered observed if the signal amplitude exceeded the maximum amplitude of the background noise by a factor of $\sqrt{5}$ – the Rose criterion, which ensures the signal is distinguishable from a simple statistical variation of the background noise with a 98% confidence level [40]. This binary measure was obtained for pHIFU exposures at each of the peak negative pressure levels.

At each level, 20 different spots in the gel phantom were treated. We then calculated cavitation probability at each level as the ratio (expressed in percent) of the number of pHIFU focus locations, at which at least one cavitation event was observed throughout the exposure, to the total number of spots treated. Similar to our previous work, the cavitation threshold [69] was defined as the peak negative pressure level corresponding to a 50% probability of cavitation.

4.2.4 Ultrasound Imaging

Imaging was performed in a "flash" transmitting mode in which all array elements were excited simultaneously to emit a quasi-plane wave in the direction orthogonal to the radiating surface, i.e., a zero degree incident angle. Color Doppler imaging was followed by B-mode imaging. In Doppler mode, the central 64 elements were excited by a series of 14 Doppler ensemble pulses (the default number of pulses for VUE) emitted with a pulse repetition frequency (PRF) set through VUE flash mode color Doppler programmable script [91]. The event sequence of the VUE script was modified so that Doppler pulses were transmitted following HIFU pulses. Each Doppler pulse was a 3-cycle tone burst with 5 MHz central frequency. In B mode, all 128 elements were excited by a single-cycle 5 MHz pulse. Received signals in both Doppler and B-mode regimes were sampled at 20 MHz with a 12-bit analog-to-digital convertor (ADC) and saved in the receive buffer of VUE. Saved radio-frequency (RF) signals were later used for Doppler processing and image reconstruction.

It was important to note that, of the 14 Doppler ensemble pulses, the first two pulses were omitted to avoid possible unrepeatable tissue reverberation. The later 12 pulses were used in further Doppler processing and image reconstruction. Therefore, further in the text the third transmitted Doppler pulse would be referred to as the first Doppler pulse.

Three different pulse sequences were used here to synchronize HIFU pulses with the Doppler ensemble, as illustrated in Fig. 4.4. The first was referred to as color Doppler sequence (Fig. 4.4a). A series of twenty 1-ms HIFU pulses were delivered at a PRF of 1 Hz to a single treatment location. This HIFU pulsing scheme was chosen to match our previous work on the cavitation

threshold in tissues and phantoms and chemotherapeutic drug delivery to pancreatic tumors [69], [92].

After each HIFU pulse, a series of 14 Doppler ensemble pulses were transmitted and received by the imaging probe in flash mode with a PRF of 3 kHz. This PRF was chosen because it should properly sample the range of expected velocities and was typical for the Doppler regimes in clinical ultrasound machines. Each Doppler pulse was transmitted with a 700 μs delay after the corresponding HIFU pulse to avoid interference between HIFU pulse reverberations in the tank and Doppler pulses. Received Doppler ensemble pulses were then stored for off-line processing and also used in real time to form a color Doppler image.

Immediately after transmitting and receiving Doppler pulses, a 1-cycle 5 MHz pulse was transmitted in flash mode and received by the imaging probe to form a B-mode image, which was then combined with the color Doppler image. After 20 sets of pulses (consisting of one HIFU pulse, 14 Doppler pulses and one B mode pulse) were transmitted, the focus was moved to a different location in the phantom.

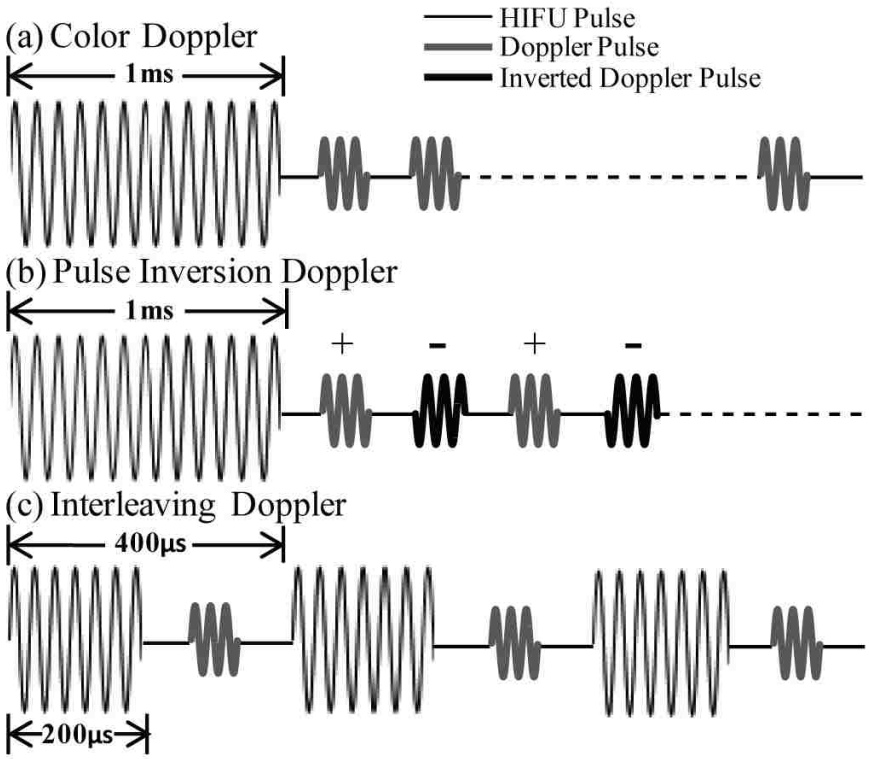

Figure 4.4 Pulse sequences of the different modes of the active cavitation technique employed here - "bubble Doppler". In all cases, Doppler ensemble pulses were transmitted in a flash mode, in which all array elements were excited simultaneously to emit a quasi-plane wave. (a) Color Doppler: one 1-ms HIFU pulse (thin line) was followed by fourteen 3-cycle Doppler pulses (thick grey line). (b) Pulse inversion Doppler: one 1-ms HIFU pulse was followed by fourteen Doppler pulses, and every other pulse was inverted (thick and black lines). (c) Interleaving Doppler: each of the fourteen 200-μs HIFU pulses were followed by a single Doppler pulse. The HIFU-Doppler pulse pair was repeated with a period of 400 μs.

The second pulse sequence - pulse inversion Doppler – was identical to color Doppler, with one modification: every other pulse in the Doppler ensemble following the HIFU pulse was inverted, as shown in Fig. 4.4b. This sequence can separate those components of the Doppler signal arising from nonlinear scattering, in particular – the second harmonic of the transmit signal [88]. Since the frequency band of the imaging probe was 4 – 7 MHz, the transmit frequency was set to 3 MHz so that the second harmonic (6 MHz) would be within the frequency band of the transducer.

The third pulse sequence was referred to as "interleaving Doppler" and is illustrated in Fig. 4.4c. Twenty sets of pulses, each consisting of 14 HIFU pulses interleaved with 14 Doppler ensemble pulses, were delivered to a single treatment spot at a PRF of 1 Hz. Each HIFU pulse was reduced in duration to 200 μs compared to the first two pulse sequences to keep the Doppler pulse PRF nearly the same - 2.5 kHz. Each Doppler pulse was transmitted well after the corresponding HIFU pulse to avoid interference. Similar to color Doppler and interleaving Doppler sequences, one Doppler image was reconstructed from the later 12 Doppler pulses. Immediately after each set of interleaved HIFU and Doppler pulses were delivered, a single 1-cycle 5 MHz signal was transmitted and received to form a B-mode image.

4.2.5 Signal Processing

All RF signals were analyzed in Matlab (MATLAB 2010b, The MathWorks, Natick, MA, USA) to reconstruct Doppler images according to the algorithm illustrated in Fig. 4.5. Consider a Doppler ensemble consisting of N = 12 pulses. The time from one transducer firing to the next was defined as "slow time", and was denoted as the number of the pulse within the Doppler

ensemble, *i*. The time elapsed during reception of each pulse was defined as "fast time", *t*, and was determined by the round-trip time of flight of a Doppler pulse and measured in millimeters: $l = ct/2$, where c is the speed of sound. Received RF signals were first beamformed using conventional "delay-and-sum" processing. Then the signal was transformed to obtain the in-phase and quadrature (I/Q) components. In this study, Hilbert transform was used to perform I/Q processing. The received beamformed signal can be then represented as a complex (analytic) discrete signal $Z(n)$, the real and imaginary parts of which are the I and Q components.

Next, wall filtering (first order regression filter) was applied to the complex, beamformed signals along slow time to remove signals from stationary or slowly moving scatterers and separate only Doppler residuals [93]. For pulse inversion Doppler, an additional low pass filter along slow time was applied to remove signals associated with linear scatterers [88]. The cut-off frequency of the filter was PRF/4 (Matlab function *sgolayfilt*).

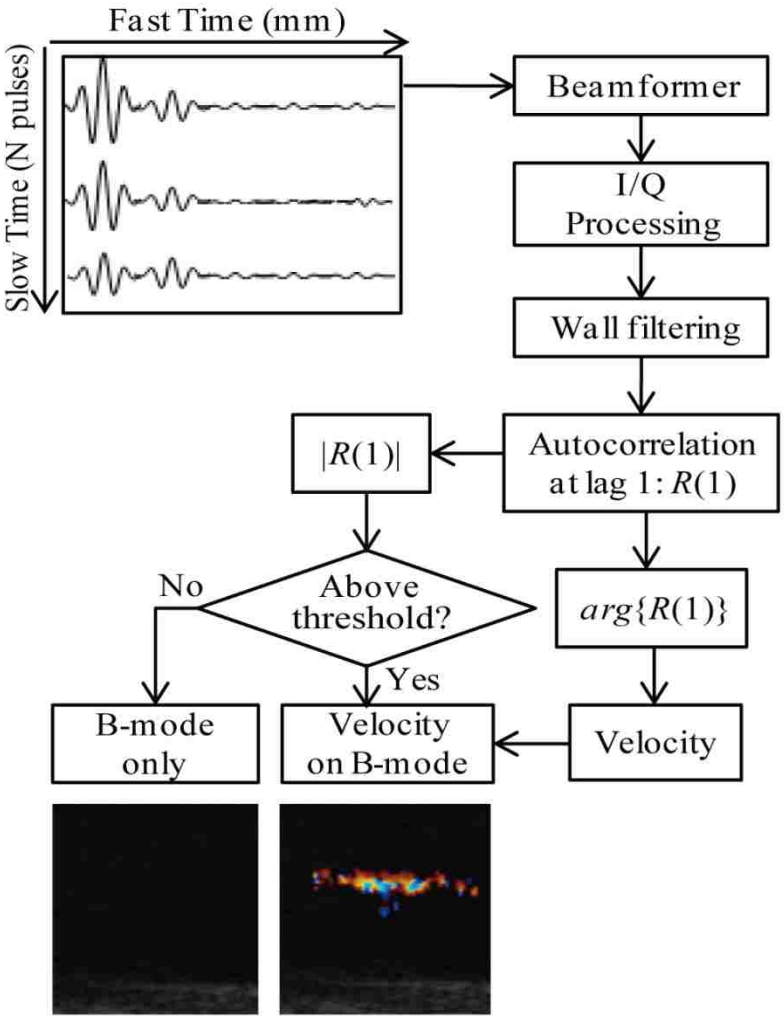

Figure 4.5 Flow diagram of Doppler signal processing employed in this study. Each of the twelve received pulses of the Doppler ensemble were first beamformed and then Hilbert transformed to obtain in-phase and quadrature components (IQ). They were then wall filtered along slow time to remove slow motions. For the color Doppler case, wall filtering is performed with a linear regression filter. For the pulse inversion case, wall filtering is performed with an additional low pass filtering at a cutoff frequency of PRF/4 so that only the signal associated with nonlinear scattering processes is retained. After wall filtering, the autocorrelation function of the complex signal along slow time at a lag of one Doppler pulse, $R(1)$, was computed at each depth, i.e., for each fast time sample. If the amplitude of the autocorrelation function, $|R(1)|$, was lower than a threshold of 6 dB above the background noise level, the B-mode image was displayed in corresponding pixels. If $|R(1)|$ was higher than the threshold, the corresponding pixels displayed color, which was determined by the phase of $R(1)$. Arg$\{R(1)\}$ corresponds to the derivative of the autocorrelation phase along slow time and can be converted to the velocity of moving scatterers.

After wall filtering, we used the most common method for velocity and Doppler power estimation in modern systems, the autocorrelation algorithm [94].

Let $R(k)$ be the Doppler autocorrelation function along slow time at a lag of k pulse repetition periods:

$$R(k) = \sum_{i=1}^{N} Z(i)Z^*(i+k)$$

where N is the total number of Doppler pulses along slow time and i is the pulse number in the Doppler ensemble. According to Kasai *et al.* [94], the mean Doppler frequency shift $\bar{\omega}$ canbe calculated as the phase of the autocorrelation function at a lag of one Doppler pulse repetition period, $\arg\{R(1)\}$:

$$\bar{\omega} = \arg\{R(1)\} = \arg\{\sum_{i=1}^{N-1} Z(i)Z^*(i+1)\}$$

Doppler power can be calculated as $|R(1)|$. The mean velocity can be also derived from $\bar{\omega}$ as follows:

$$\bar{v} = \frac{\bar{\omega}c}{\omega_0 2\cos\theta}$$

where ω_0 is the angular frequency of the carrier signal, θ is the angle between the sound beam and the direction of the flow. Thus, both Doppler frequency shift and Doppler power at each fast time sampling point were calculated using this approach. At the final step, the Doppler power at each pixel of the image was compared to a threshold, and if it exceeded the threshold, color Doppler information, i.e., the phase of $R(1)$, was displayed on top of B-mode pixels. The threshold was defined the same way as in Lu *et al.*[17]: the background noise level, defined as the average of the Doppler powers over all pixels in the image, multiplied by a factor of two.

4.2.6 Pilot Doppler Imaging on *In Vivo* Mouse Pancreatic Model

Following the gel phantom studies, the ultrasound imaging method using the three pulse sequences described above were perform in an *in vivo* mouse model bearing subcutaneous pancreatic tumor. The animal was anesthetized by inhalation of isoflurane, and the abdomen was

thoroughly shaved and depilated. It was tied by two thin Velcro tapes to a customized holder so the legs wouldn't interfere with the HIFU wave. The holder could be moved by a 3D positioning system to position the HIFU focus at different locations of the tumor. Similar to the gel phantoms study, a PCD was used to record cavitation activities and a linear imaging probe (L7-4) was perpendicular aligned with HIFU incident direction for active cavitation imaging (Fig. 4.6a). A focus pointer, which was previous designed to align with HIFU focus, was capped onto HIFU transducer. The imaging probe was first operated in B-mode to record the location of the HIFU focus and was positioned so that the HIFU focus was at the center of the B-mode image. The focus pointer was then removed and the pancreatic tumor was moved to the HIFU focus by B-mode guidance (Fig. 4.6b).

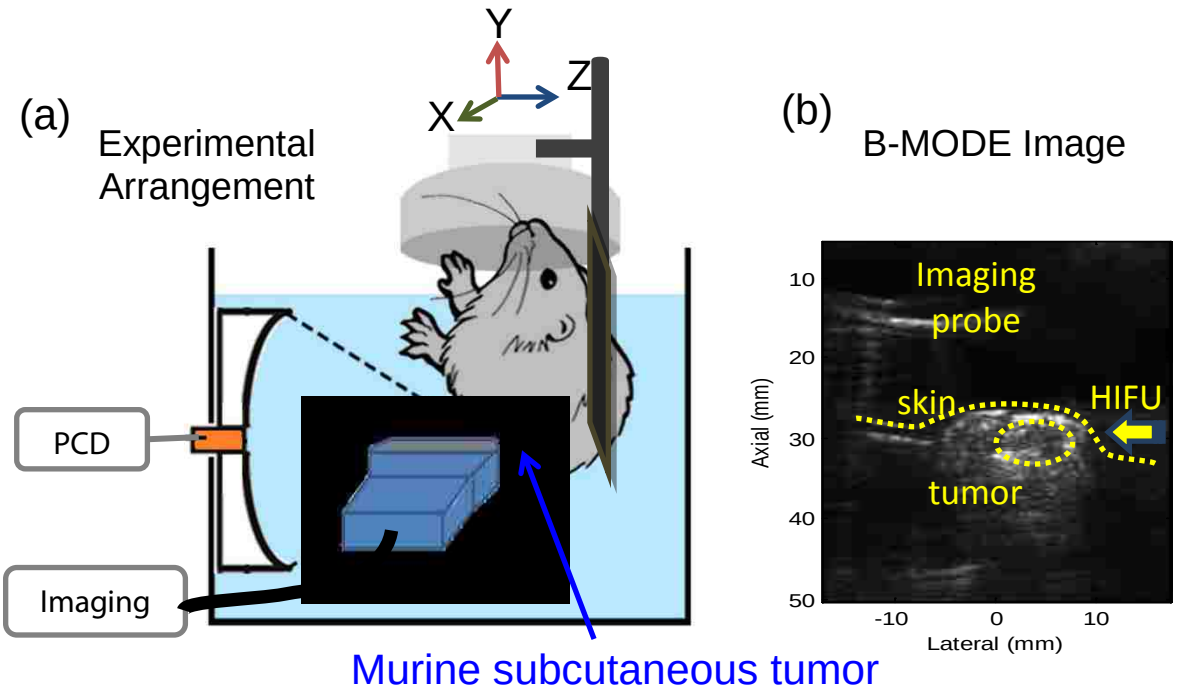

Figure 4.6 Schematic illustration of the setup of using ultrasound Doppler imaging to perform active cavitation imaging on an *in vivo* mouse. The animal was attached to a custom holder and was anesthetized by inhalation of isoflurane through a cone (a). The animal could be positioned by a 3D positioning system to align the tumor region with HIFU focus. The transverse plane of the tumor was shown (yellow dashed line) in B-mode image (b). The HIFU wave was delivered from the right of the tumor and focused to the center.

4.3 Results

4.3.1 Pilot Observations with High-Speed Camera and Color Doppler Ultrasound Imaging

In the first series of experiments, simultaneous observation of pHIFU-induced bubble activity in the gel phantom was performed by high-speed camera and Doppler ultrasound using two different pulse sequences – color Doppler and interleaving Doppler. The pHIFU focal peak negative pressure in this case was 5.1 MPa. The VUE ultrasound system was used to display color Doppler images in real time, without any further signal processing. The obtained color Doppler images of the HIFU transducer focal area are presented side-by-side with the corresponding high-speed camera images in Fig. 4.7 for both pulse sequences. Cavitation bubbles distributed throughout the transducer's oval-shaped focal area were clearly visible in both high-speed camera images as dark spots (Figs. 4.7a, c). The bubbles were somewhat smaller in the interleaving Doppler pulse sequence (Fig. 4.7c) due to the smaller duration of the HIFU pulse in this case. Across the whole exposure, no thermal denaturation was observed in the gel phantoms. The size and position of the colored region in Doppler ultrasound corresponded well to the size and position of the bubble distribution seen on the high-speed camera images, providing one confirmation that the color region originates from cavitation bubbles. In both cases, the color region grew in size with increasing HIFU focal peak negative pressure, and disappeared as the peak negative pressure fell below a certain threshold (3.1 MPa for color Doppler and 1.9 MPa for interleaving Doppler).

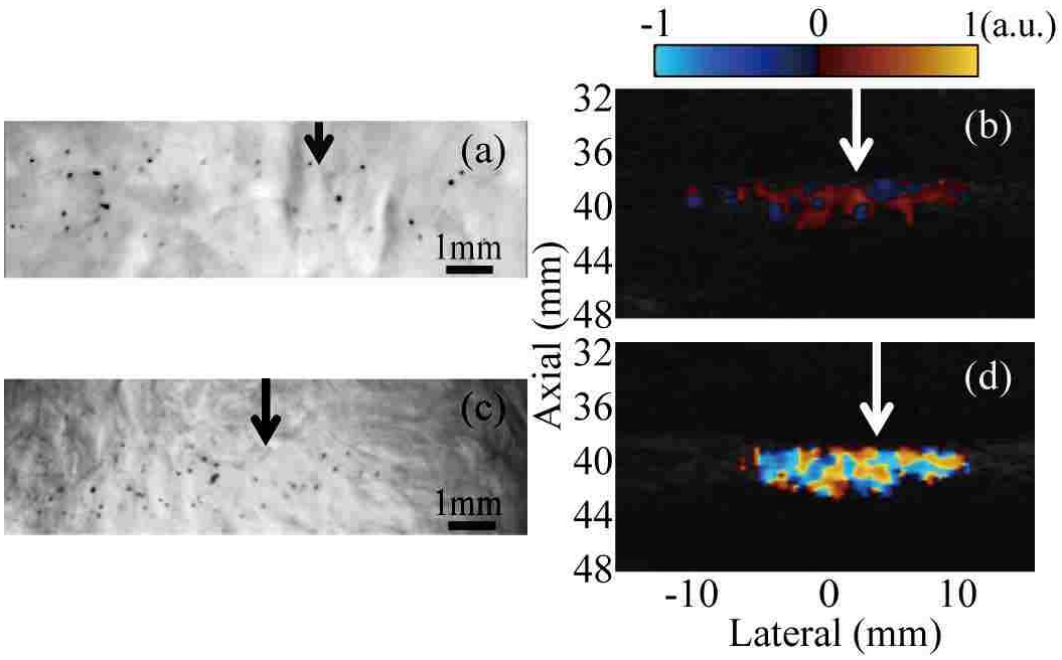

Figure 4.7 Simultaneous observation of HIFU-induced cavitation bubble activity performed with the high-speed camera and Doppler ultrasound for two pulse sequences: color Doppler ((a) and (b)) and interleaving Doppler ((c) and (d)). The HIFU transducer (focal region size 16 mm x 1.5 mm at the –6 dB level) is located to the left of all images; arrows indicate the lateral position of the focus. Cavitation bubbles were readily observed in both high-speed camera images, (a) and (c), as small black dots scattered throughout the focal region. The sizes and positions of these bubble distributions corresponded to the regions of alternating dark red and blue color in color Doppler regime (b), and to the bright color mosaic in the interleaving Doppler regime (d).

Doppler images for the two pulse sequences looked qualitatively different. In the color Doppler sequence, regions displaying color contained alternating dark red and blue areas that, in Doppler processing, would be interpreted as very slowly, chaotically moving scatterers (Fig. 4.7b). In interleaving Doppler, the color region contained a color mosaic characteristic of the TA typically seen on hard concretions in tissue (Fig. 4.7d), and would be interpreted as scatterers having the entire range of speeds and moving in all directions at once. These qualitative characteristics were the same across the whole range of pHIFU focal pressures.

4.3.2 Interpretation of Pilot Results

To explain the origin of the different color displays in color Doppler and interleaving Doppler, non-beamformed RF signals from the middle element of the ultrasound array were considered. Figure 4.8a presents the first two waveforms from the ensemble of Doppler pulses from the depth corresponding to the HIFU focus. As seen, the amplitude of the first pulse was larger than that of the second pulse, but there was no visible phase shift between pulses. Figure 4.8b shows the received signal amplitude plotted along slow time and fast time for the entire Doppler ensemble. At all of the fast time sampling points, the signal amplitude gradually declined across slow time, suggesting the presence of a scatterer with decreasing reflectance. The amplitude (Fig. 4.8c) of the autocorrelation function at lag one peaked in fast time at the point with the fastest decrease in signal amplitude over slow time (40.2 mm). The fast time range in which the amplitude of the autocorrelation exceeded the threshold for color display (39.4 – 41 mm) corresponded to the autocorrelation phase (Fig. 4.8d) that fluctuated around zero, within a narrow range of -0.3 - 0.3 radians.

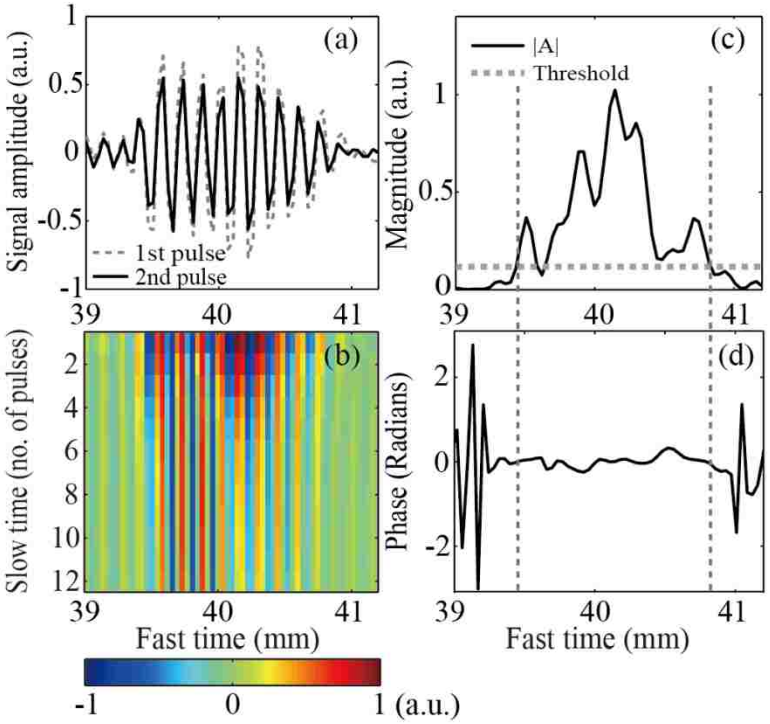

Figure 4.8 (a) Examples of the first two RF signals of the color Doppler ensemble received by the middle element of the imaging array, from the depth corresponding to the HIFU focus. The second pulse (solid line) had lower amplitude than the first (dashed line), but no phase shift. (b) All 12 received RF signals from the Doppler ensemble plotted along fast time (distance from the array element) and slow time (pulse number). The amplitude of the signals declined gradually across slow time, but the waveform remained unchanged and was not shifted in time. This suggested the presence of a stationary scatterer with declining reflectance, e.g. a shrinking bubble. (c) The magnitude and (d) the phase of the autocorrelation function at lag 1, calculated using the entire Doppler ensemble and plotted along fast time. The phase change was close to zero over the fast time segment (vertical dashed lines) in which the autocorrelation function amplitude exceeded the threshold (horizontal dashed line). Therefore, in the ultrasound image this region was displayed in color, corresponding to a very slowly moving scatterer (dark blue and red).

These observations suggested the following mechanism for the appearance of the dark red and blue area in the color Doppler image: pHIFU induced cavitation bubbles that gradually dissolved after the HIFU pulse was delivered. The amplitude of backscattered Doppler pulses was strongly affected by the change in the bubble size, and therefore the amplitude of the autocorrelation at lag 1 was high, and the bubble was displayed as color. However, the signal phase did not change from one Doppler pulse to the next, because bubbles were not moving, and the displayed speed was close to zero, as shown by the dark red and dark blue regions in the reconstructed color image (Fig. 4.8b).

For the interleaving Doppler pulse sequence, the overall levels of the first two signals of the Doppler ensemble were similar (Fig. 4.9a); however, noticeable phase shifts and amplitude fluctuations were present. As seen in Fig.7b, these fluctuations continued across slow time, suggesting that the backscattered signal from pHIFU-generated bubbles changed sporadically from one Doppler pulse to the next. Figs. 7c and 7d show that the fast time segment, at which the autocorrelation amplitude was above the threshold (39.8 - 41.2 mm), corresponds to phase fluctuations over a wide range ($-\pi - \pi$). This suggested that the distribution of bubbles resulting from each HIFU pulse differed in bubble size, number, and positions. These changes induced by different HIFU pulses resulted in large autocorrelation amplitude and random phase changes which manifested themselves as the color mosaic in the color Doppler image.

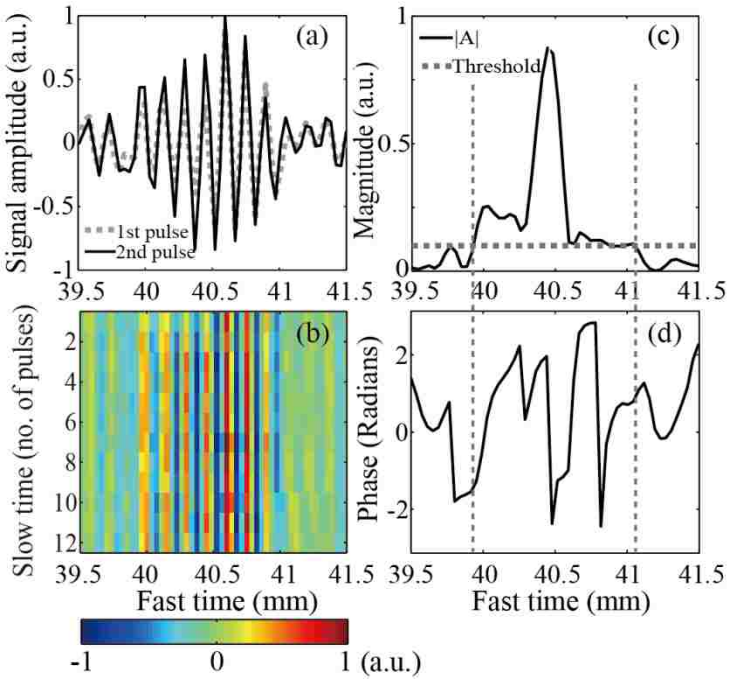

Figure 4.9 (a) Examples of the first two RF signals of the interleaving Doppler ensemble received by the middle element of the imaging array, from the depth corresponding to the HIFU focus. The overall level of the first pulse (dashed line) was similar to that of the second pulse (solid line), but there were substantial differences between the two signals: noticeable temporal shift and relative fluctuations. (b) All 12 received RF signals from the Doppler ensemble plotted along fast time (distance from the array element) and slow time (pulse number). The signal amplitude changed sporadically across slow time. (c) The amplitude and (d) phase of the autocorrelation function at lag 1, calculated using the entire Doppler ensemble and plotted along fast time. The range of autocorrelation magnitude (vertical dashed lines) which was higher than the threshold (horizontal dashed line) corresponded to a randomly changing phase over a wide range, which produced the color mosaic in the Doppler image.

In pulse inversion Doppler, the sum of inverted and non-inverted subsequent Doppler pulses only contained the second harmonic of the transmitted signal, i.e., the signal associated with nonlinear scatterers. An example of the first two received RF signals from a pulse inversion Doppler ensemble is shown in Fig. 4.10a. The spectrum of both signals (Fig. 4.10c) contained harmonics of the center transmit frequency of 3 MHz. When the pulses were summed (Fig. 4.10b), only the

second harmonic signal at 6MHz was left in the spectrum (Fig. 4.10d). This suggested that residual bubbles induced by the HIFU pulse produced a strong enough nonlinear response to be detectable by pulse inversion Doppler. In this particular example, the peak negative focal pressure of the HIFU pulse was 4.6 MPa.

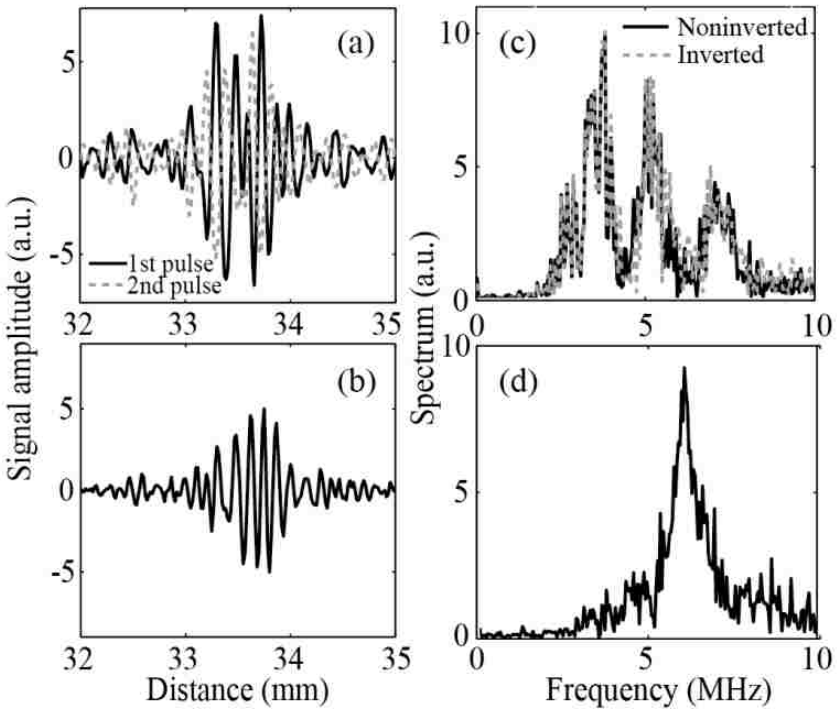

Figure 4.10 (a) An example of two consecutive RF signals from the pulse inversion Doppler ensemble received by the middle element of the array. The carrier frequency of the imaging pulses was set to 3 MHz. (b) The signal resulting from summation of the two received signals is shown in (a). (c) The frequency spectrum corresponding to the received signals and (d) summed signal in the range of 0-10MHz. After the signals were summed, only the second harmonic at 6 MHz was left in the spectrum.

The fast time range in which the amplitude of autocorrelation function (Fig. 4.11a) exceeded the threshold for color display (33 - 33.8 mm) had an autocorrelation phase (Fig. 4.11b) that fluctuated around zero, suggesting that bubbles did not move from one pulse to the next but did produce a nonlinear response.

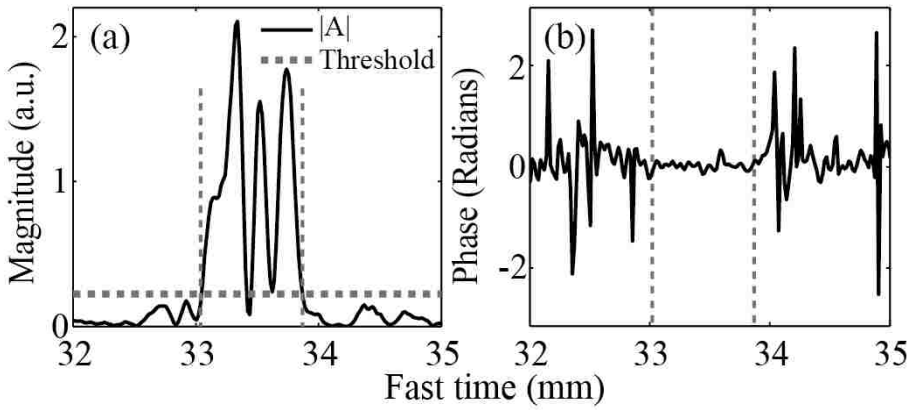

Figure 4.11 (a) The amplitude and (b) phase of autocorrelation function at lag 1 calculated using the entire pulse inversion Doppler ensemble, plotted along fast time. Similar to the color Doppler case, the phase was close to zero at the fast time segment (vertical dashed lines) that corresponded to the autocorrelation amplitude exceeding threshold (horizontal dashed line).

4.3.3 Investigation of the Doppler Techniques Sensitivity

Pilot experiments with all three pulse sequences indicated that in all cases the increased magnitude of the Doppler signal originated from changes in the pHIFU-induced bubble distribution across slow time, or from the nonlinearity of the bubbles. However, the Doppler signal phase did not correspond to true motion of the bubbles or reflect any of the bubble characteristics. Therefore, phase information was discarded in the future studies, and instead Doppler signal magnitude was displayed on top of the B-mode images, i.e., power Doppler regime, rather than color Doppler, was implemented. The corresponding images, reconstructed offline, for all three pulse sequences at two different pHIFU power levels are shown in Fig. 4.12.

Based on the pilot experimental results, the three Doppler techniques reflected different characteristics of the residual bubble distribution: bubble size and rate of dissolution (color Doppler), the degree of change in bubble distribution from one HIFU pulse to the next (interleaving Doppler) and the magnitude of the bubble nonlinear response (pulse inversion Doppler). Therefore, the sensitivities of the three techniques were likely to be different and were measured, similarly to PCD, in terms of the threshold for 50% probability of observation of a cavitation event (see Section II B). A cavitation event was considered observed if color was displayed on top of the B-mode image.

In the color Doppler sequence, color images were not displayed until HIFU focal peak negative pressure reached 3.1 MPa (Figs. 4.12a and 4.12b). The interleaving Doppler sequence appeared to have the lowest threshold of all techniques - 1.9 MPa (Figs. 4.12c and 4.12d), and the displayed distribution was larger in size than in the other sequences at the same HIFU power level. The threshold in the pulse inversion Doppler sequence was similar to that in the color Doppler sequence: 3.1 MPa (Figs. 4.12e and 4.12f).

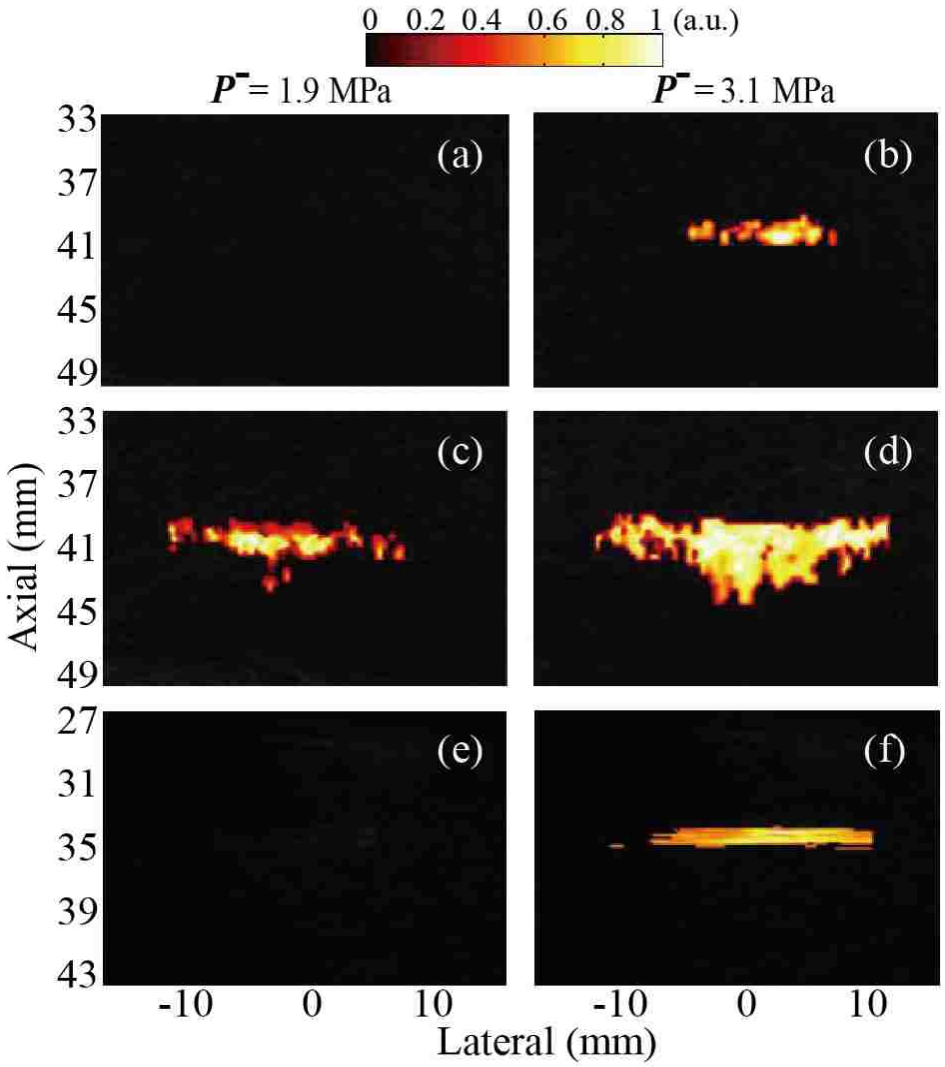

Figure 4.12 Reconstructed maps of normalized Doppler power representing cavitation activity induced by pHIFU with peak-rarefactional focal pressure of 1.9 MPa (left column) and 3.1 MPa (right column) using the following pulse sequences: (a), (b) color Doppler, (c), (d) interleaving Doppler, and (e), (f) pulse inversion Doppler. The interleaving Doppler sequence appeared to be

the most sensitive to the onset of cavitation, and the color region was displayed when HIFU focal peak rarefactional pressure exceeded 1.9 MPa. Both color Doppler and pulse inversion Doppler sequences had the same sensitivity to cavitation and color was displayed only at 3.1 MPa pressure.

The sensitivities of all Doppler techniques were compared to those of PCD and high-speed photography, as summarized in Table 1. The comparison was performed separately for interleaving Doppler to account for the smaller HIFU pulse duration used in this technique. The accuracy of the thresholds was mostly determined by the step size in changing peak negative focal HIFU pressure – 0.5 MPa. As seen, all of the Doppler techniques appeared substantially more sensitive than other methods.

TABLE 4.1 Sensitivity Thresholds For Cavitation Detection Techniques

	Techniques						
	Single 1-ms HIFU pulse				***Twelve 200-us HIFU pulses***		
	PCD	***High Speed photography***	***Color Doppler***	***Pulse Inversion Doppler***	***PCD***	***High Speed photography***	***Interleaving Doppler***
pHIFU peak-rarefractional pressure at 50% probability of cavitation event (MPa)	4.6	5.1	3.1	3.1	5.1	5.6	1.9

4.3.4 Doppler Imaging during pHIFU Exposures in *In Vivo* Mouse Pancreatic Tumor

Finally, the reconstructed images from *in vivo* mouse study were shown in figure 4.13. The interleaving Doppler image (orange) was overlaid on B-mode image shown in figure 4.13b. The interleaving Doppler image showed the decorrelation of the received Doppler pulse to the next between pHIFU pulses. The pulse inversion Doppler image was overlaid on both the interleaving Doppler image and B-mode image. The pulse inversion Doppler image showed the backscatter signals that not only changed from pulse to pulse but also were nonlinear.

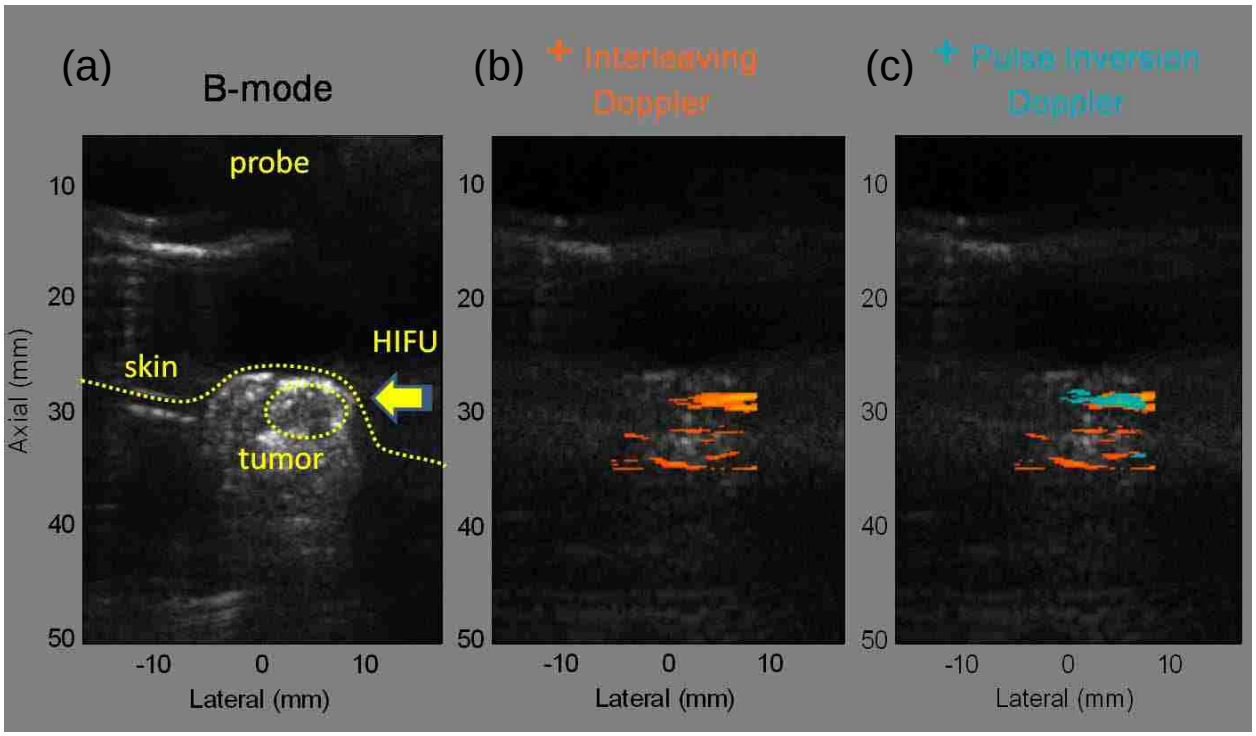

Figure 4.13 The B-mode image of the transverse plane of *in vivo* mouse bearing subcutaneous pancreatic tumor (a). The interleaving Doppler image was overlaid on flash mode B-mode image (b). The orange color region corresponded to the location of the HIFU focus inside the tumor region. The color at the bottom of the tumor is likely to be caused by the movement of other organs. The pulse inversion Doppler image was further overlaid onto the interleaving Doppler image and B-mode image (c). The blue color region corresponded to the reflected signals that were both changing from pulse to pulse and nonlinear.

4.4 Discussion

In this work, we investigated the feasibility and sensitivity of three different Doppler techniques in detection of pHIFU induced cavitation bubbles: color Doppler, pulse inversion Doppler and interleaving Doppler. These techniques were found to be not only more sensitive than conventional PCD or high-speed photography, but also complementary to each other, i.e., providing different information about the bubble distribution.

For interleaving Doppler, the Doppler signal fluctuated over slow time (i.e., from one HIFU pulse to the next) because each HIFU pulse produced a different bubble distribution. It could

therefore be interpreted as sensitive to the mere presence of bubbles, not necessarily bubble activity, and was found to be the most sensitive among the considered techniques. In concept, interleaving Doppler is similar to Doppler decorrelation algorithms [89], [95], which measure the decorrelation of backscattered signals from UCAs before and after they are disrupted by a more intense pulse. The difference in our case was that the intense pulse was the bubble-producing HIFU pulse, and more than two Doppler pulses were used.

The Doppler signal in the color Doppler mode originated from the change in the size of the bubbles as they dissolved rapidly after HIFU was turned off. The signal was therefore representative primarily of bubble size, but also of the elastic properties of the medium around the bubble, because it would influence dissolution speed. Pulse inversion Doppler was found to have similar sensitivity to color Doppler, and was an indicator of the strength of the bubble's nonlinear response to Doppler ensemble pulses. This response was, in turn, dictated by bubble size and medium properties. However, pulse inversion Doppler has an important advantage over color Doppler for *in vivo* implementation – it is only sensitive to nonlinear scatterers, and is not cluttered by the linear signal component reflecting body motion or blood circulation.

In all the pulsing sequences used in this work, 12 Doppler pulses per ensemble were used, primarily because this is the default number for many clinical ultrasound machines. However, this number may potentially be reduced to increase imaging speed, depending on the bubble dissolution time (for color Doppler and pulse inversion Doppler) and the degree of change in bubble distribution between HIFU pulses. To determine the optimal number of pulses in the Doppler ensemble, the amplitude of the autocorrelation function between two consecutive RF pulses was plotted along slow time and compared between different pulse sequences (Fig. 4.14). As seen, the autocorrelation amplitude dropped very rapidly in the color Doppler case and hardly changed after the 6^{th} pulse of the ensemble. Therefore, the number of pulses can be reduced in this case without loss of signal strength. For interleaving Doppler, the autocorrelation amplitude changes randomly across pulse pairs; therefore, the more pulses delivered, the stronger the Doppler signal. The number of pulses in the ensemble can thus be adjusted based on the needs in a particular situation.

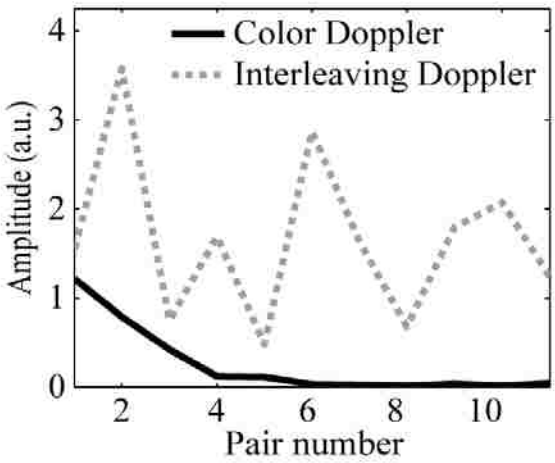

Figure 4.14 The amplitude of autocorrelation function at lag 1 calculated using a consecutive pair of Doppler pulses along slow time. The amplitude declines gradually with increasing pair number for color Doppler (solid line), but not for interleaving Doppler (dashed line).

In this work, all Doppler methods were implemented in flash mode, because cavitation bubbles are very transient, and transmitting multiple beams or waves at multiple angles would not be rapid enough to capture these bubbles. Flash mode is known to provide relatively poor spatial resolution in the transverse direction [96], [97] that was not critical in this pilot study, but would certainly be unacceptable in a clinical setting. However, since the number of pulses in a Doppler ensemble can be substantially reduced, it is potentially feasible to utilize multiple transmit beams or incident angles within the same imaging time, and enhance image resolution through coherent spatial compounding.

As interleaving Doppler and pulse inversion Doppler provided complementary information about cavitation bubbles, they can be combined into a single method using more complex pulse sequences with multiple HIFU pulses, followed by multiple Doppler ensemble pulses with interchanging polarities. This method, that we term “bubble Doppler” quantifies the bubble nonlinearity and map bubble presence at the same time. It should be able to provide superior sensitivity compared to PCD methods. It would also be readily translatable for clinical use, because it uses a commercially available imaging probe, which can be incorporated into a HIFU system. Future work of this chapter will test bubble Doppler for cavitation mapping during pHIFU exposures in *ex vivo* and *in vivo* tissues. In particular, pHIFU insonations to enhance drug

delivery to pancreatic tumors through cavitation activity has been our recent research focus, and a transgenic mouse model has been used in these experiments [69]. The cavitation threshold in murine pancreatic tumors *in vivo* was identified previously using PCD (3.1 MPa) and was similar to that in PA gel phantoms. Therefore, color Doppler and pulse inversion Doppler methods are expected to have similar or slightly lower sensitivity thresholds *in vivo*. We expect that bubble Doppler images could be displayed when HIFU reaches a similar peak-rarefactional level in *in vivo* pancreas as in PA gel phantoms - 3.1 MPa, due to their similar cavitation thresholds characterized by PCD [69]. Interleaving Doppler technique, however, is likely to be even more sensitive *in vivo*, because the bubble population and cavitation nuclei distribution are constantly changing not only by HIFU, but also by the circulation and tissue motion.

4.5 Conclusions

In this chapter, the methods for pHIFU-induced microbubble detection were studied. Color Doppler imaging showed the decrease in bubble size after the HIFU pulse. Pulse inversion could capture the nonlinearity of the bubbles. Interleaving Doppler was most sensitive to the presence of bubbles among all techniques. The combination of these techniques is likely to be beneficial for imaging bubble location and characterizing bubble nonlinearity. In summary, a new ultrasound imaging protocol was proposed to detect microbubbles induced by pHIFU using a modification of Doppler pulse sequences. This imaging modality was shown to provide sensitivity superior to that of existing cavitation detection methods, and at the same time can spatially resolve bubble location, similarly to conventional Doppler imaging.

Chapter 5

Conclusions and Future Directions

5.1 Conclusions

The work presented in this dissertation addressed the challenges in using pHIFU induced cavitation to enhance drug delivery. Here is a summary of the key achievements in this thesis work.

In the first part of this study, the metrics of cavitation activity such as cavitation probability, cavitation persistence and cavitation noise level were established to quantify the likelyhood of a, the longevity, and the strength of cavitation occurrence. The metrics were studied in various medium such as tissue-mimicking gel phantoms, different *ex vivo* tissues and murine pancreatic tumors *in vivo*, using passive cavitation detection. Cavitation thresholds in these different media were identified at the HIFU frequency of 1.1 MHz and varied within 2.5 – 10 MPa, as well as at the HIFU frequency of 1.5MHz and varied within 10.3 – 16.5 MPa, depending mostly on the relative concentration of water and lipid in tissue. The pressure levels for consistently inducing cavitation in pancreatic tumor were determined to be 11 MPa at 1.1 MHz and 16 MPa at 1.5 MHz. Results also showed the difference of cavitation pattern between *in vivo* and *ex vivo*: cavitation activity ceased after only a few HIFU pulses in *ex vivo* tissue, but occurred sporadically throughout the HIFU exposure *in vivo*. It's shown that pulse mode HIFU of 1.1MHz and 1.5MHz induced cavitation are fully characterized and are strongly relevant for the application of pHIFU enhanced drug delivery treatment planning and monitoring.

After cavitation thresholds are determined and compared between *ex vivo* and *in vivo* pancreatic tumors, the correlation of between chemotherapeutic drug uptake and pHIFU induced cavitation were studied in an *in vivo* mouse model of pancreatic tumor. With 1.5MHz HIFU, the transgenic mice had a drug enhancement correlated with cavitaion. The drug uptake was higher when HIFU treatment was applied before drug injection comparing to the results when HIFU treatment was applied during drug injection. It indicates drug diffusion from enhanced tissue permeability as well as reduced interstitial pressure by inertial cavitation (drug injection after HIFU treatment

case) is more effective for improving drug delivery than drug diffusion by radiation force (drug injection during HIFU treatment case). The drug uptake with 1.5MHz system had a larger drug enhancement than the uptake with 1.1MHz system when cavitation persistence reached 100% in both cases. A1.5MHz HIFU system is more suitable for this study for its smaller and tighter focus and reduced risk of tissue damage.

A new active cavitation mapping technique for pulsed high-intensity focused ultrasound (pHIFU) applications termed bubble Doppler is proposed and its feasibility tested in tissue-mimicking gel phantoms. Based on a fusion of the adaptations of three Doppler techniques that had been previously developed for imaging of ultrasound contrast agents – color Doppler, pulse inversion Doppler, and decorrelation Doppler, a new ultrasound imaging protocol was demonstrated to detect microbubbles induced by pHIFU using a modification of Doppler pulse sequences. Color Doppler was able to image the decrease in bubble sizes after the HIFU pulse. Pulse inversion could capture the nonlinearity of the bubbles. Interleaving Doppler, different from decorrelation Doppler was most sensitive to the mere presence of bubbles among all techniques. Therefore, with the combination of the techniques, bubble Doppler quantifies the bubble nonlinearity and map bubble presence at the same time. The method was also shown to provide sensitivity superior to that of existing cavitation detection methods, and at the same time can spatially resolve bubble location, similarly to conventional Doppler imaging.

5.2 Future Work

Survival studies may be carried out to evaluate including finding the right focus for pHIFU enhanced drug delivery and potential application using endoscopic ultrasound guided HIFU.

5.3 Using Harmonics Imaging to Locate HIFU Focus

5.3.1 Introduction

Since the cavitation induction heavily depends on *in situ* pressure amplitude, it is useful to control the latter in real-time during treatment or before the start of treatment. Currently, there are no well-defined quantitative methods to measure that yet. The magnetic resonance guided

and conventional ultrasound guided monitoring techniques are accepted in clinic as standard methods. But they don't offer the capability to localize HIFU focus before ablative temperature is reached, neither do they detect bubbles before they grow large enough to appear as hyperechoeic regions in conventional ultrasound imaging [27]. Here, a new method is also proposed for the future work to indicate whether the threshold for non-linear propagation at certain tissue depth is reached and therefore whether the pressure level at the HIFU focus is sufficient to induce cavitation without beam distortion by any defects in the tissue.

Harmonic waves are generated as ultrasound wave insonated tissues in the body and become nonlinearly distorted [98]. In HIFU wave propagation, the generation of harmonics increases as the pulse intensity increases and it's the greatest at the HIFU focus [99]. During HIFU, the backscattered signal within higher harmonic band could be enhanced at the lesion site relative to the surrounding tissues. Studies have shown that the second harmonics could be used to improve visualization of HIFU lesion site [100]. Recently, harmonic motion imaging for focused ultrasound was developed for HIFU treatment monitoring [101]. It's been demonstrated for monitoring and mapping tissue viscoelastic response changes during and after HIFU treatment. However, as it measures the displacement resulted from tissue softening/stiffening during ablation, the HIFU focal region cannot be localized before it make any tissue mechanical properties and won't be able to monitor cavitation since there is minimal thermal ablation or tissue denature. In this study, harmonic imaging of the pHIFU focus will be for precise treatment targeting and planning before treatment.

5.3.2 Using Harmonics Imaging to Locate HIFU Focus

A annular focused 1.24MHz HIFU transducer (64 mm aperture and radius of curvature) is coaxially aligned with a B-mode imaging probe (P7-4 phased array, fc = 5MHz) and is mounted at a water tank, filled with degassed water. The HIFU transducer was first driven by a 30 cycle sinusoidal bursts produced by a function generator together with a power amplifier, which is in turn connected to a 50 ohm matching network. The imaging probe is connected to a commercial ultrasound machine – Verasonics Ultrasound Engine (VUE, Verasonics, Redmonds, WA), which could provide the access to the raw RF signals of each channel from the imaging probe.

As shown in Fig. 5.1, a fiber optic pressure hydrophone (FOPH 2000, RP Acoustics, Leutenbach, Germany) was used for HIFU field measurement. The FOPH probe was connected to a three-dimensional positioning system (Velmex Inc, bloomfield, NY). The output of the FOPH was first recorded by a digital oscilloscope (LeCroy wavesurfer, Chestnut, NY) at 100MHz sampling frequency and then transferred to a PC for off-line pressure conversion and analysis.

For harmonics imaging of ex vivo bovine liver, the fiber optic tip holder was replaced by a custom designed tissue holder. Pieces of liver was selected to avoid big blood vessels and was cut into a dimension of 8 cm wide by 8 cm tall by 4 cm deep with its capsule layer contained. After degassing the liver for 1hr, it was fitted in the tissue holder with the side of capsule facing the HIFU transducer. The imaging probe (P7-4) was used to guide the positioning of the tissue holder so that HIFU focus was placed 1.5cm to 2cm in depth inside the liver.

In the practical cases, tissues are not usually homogeneous. There are conditions that defects exist on the side region or in the prefocal region of the HIFU focus. In order to find out how it influences the nonlinearity of the HIFU focus, defects were created manually like this: two pieces of liver were combined together with the side of capsule facing each other. In this way, the capsules from each piece are combined and create a 'defect'. In order to create the defect on the side, the combined piece of liver were rotated with an angle of around 20 degrees. The focus was placed inside the tissue of 2cm depth but was very close to the defect. In order to create the defect in the prefocal region, the combined piece of liver was placed so that the defect was positioned closer than the focus by the guidance of the B-mode image. Post image processing was carried out to reconstruct image from different harmonics and find out the impact of the defects and pressure levels on HIFU nonlinearity at the focus.

5.3.3 Experimental Procedures of Harmonics Imaging

The 1.24MHz HIFU transducer was driven by a 30 cycle burst with a peak to peak voltage (Vpp) output of 200mV from the function generator. The focus of the HIFU transducer was determined by searching for the location of maximum signal strength with a burst delay time of $\sim 42\,\mu$s, which is the time needed for HIFU wave to propagate from the surface to the focus of the HIFU

transducer. Acoustic field characterization of the HIFU transducer was then carried out by line scan across x y z coordinate system.

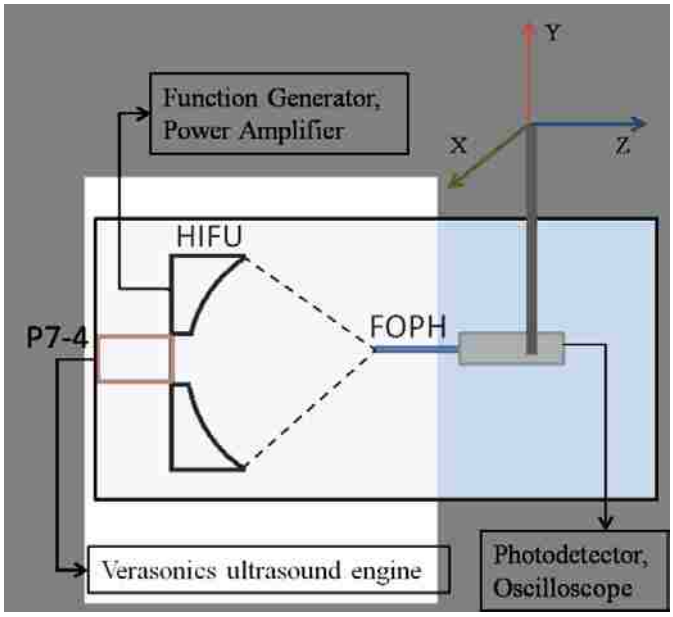

Figure 5.1 Schematic of HIFU treatment system. A 1.24MHz HIFU transducer and imaging probe (P7-4) are coaxially aligned. Fiber optical pressure hydrophone (FOPH) was positioned at the HIFU focus after 3D mapping with the 3D positioning system. In the subsequent experiments, the FOPH was replaced by an *ex vivo* tissue sample.

After the focus is located, the number of cycles is reduced to 2 cycles burst so that the HIFU wave is shortest for imaging but was still able to become nonlinear and form a shock front as the input power increases. The one cycle burst was too short to become shocked in the range of the power levels applied to the transducer. Peak positive pressure varied from 1.8MPa to 55.1MPa within the range of power applied to HIFU (Fig. 5.2). Pressure waveforms changed from linear to nonlinearly distorted and to a shock front shown in Figures 5.2a to 5.2c. The acquired signals were Fourier transformed into frequency domain. Figures 5.2d to 5.2f clearly demonstrated that as the pressure increases, more harmonics generated. At the higher level used in the study, up to 6^{th} harmonic was generated.

The P7-4 imaging probe consisted of 64 elements spanning an aperture of 25mm. Each element had a 0.2 mm width and a 0.16 mm spacing between elements. VUE was connected to the probe

and was triggered to acquire RF signals from each change at the same time HIFU burst was transmitted into the FOPH tip. The VUE system operated P7-4 probe in passive mode (no active pulse) and the collected RF data were used to post processing. B-mode images of the FOPH tip were also collected for future guidance of HIFU focus positioning in an *ex vivo* tissue sample.

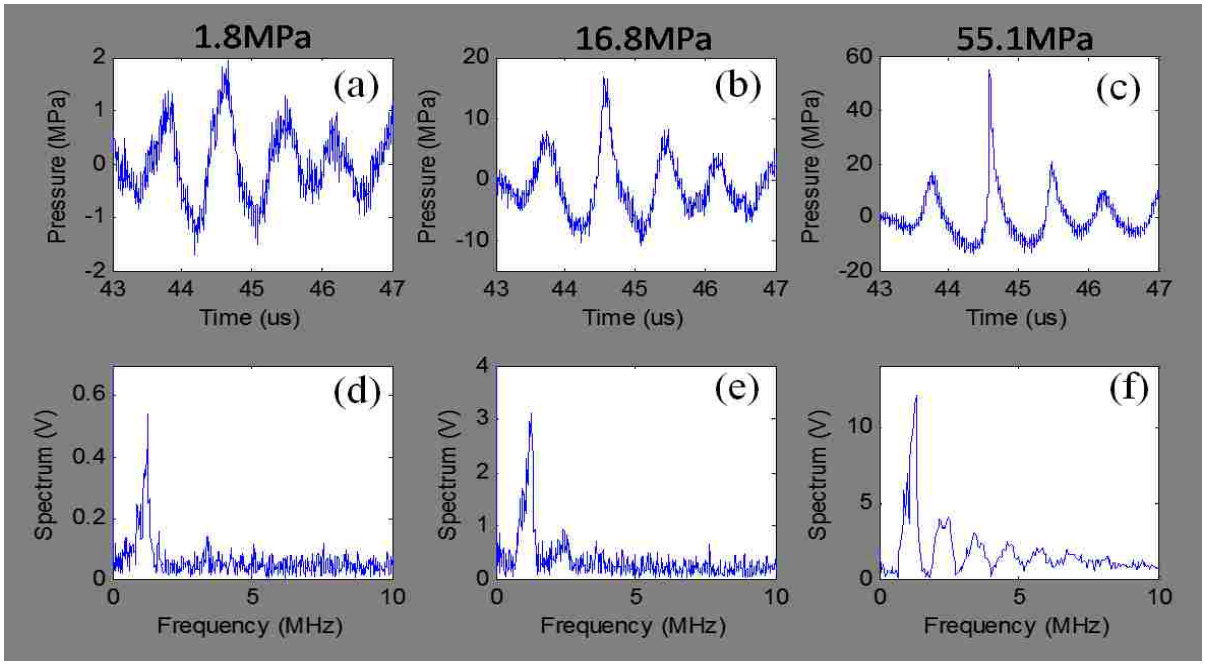

Figure 5.2 2-cycle HIFU waveforms were measured by FOPH in water and converted to pressure in time domain. Pressure waveforms are shown in Fig a, Fig b and Fig c with the increase of HIFU power. The signals were also Fourier transformed in frequency domain and shown in Figs. 5.2d, 5.2e and 5.2f correspondingly. With input eletrical powers varied from low to high, the pressure waves first become nonlinearly distorted and then become shocked. Peak positive pressure varied at 1.8MPa, 16.8MPa and 55.1MPa. The spectrum of FOPH signals show more and more harmonics develped as pressure increases, the highest pressure level of 55.1MPa has up to 6^{th} harmonics.

Signals acquired from the reflected signal of FOPH tip, and signals acquired from the backscattered signal of an piece of ex vivo liver (with intact capsule layer on the surface) are first filtered at 1st to 6th harmonic of the HIFU center frequency and then reconstruted into images for analysis. The image intensity at the focus location in lateral and axial direction are plotted and compared across different harmonics.

In a separate sets of experiment, one piece of liver is combined with another piece of liver with their capsule layers facing each other. This combined capsule layers will induce an artificially introduced strong reflection of the backscattered signal, and thus will be used to manually generate a defect in the image and will be used to test how the defect influence the restructed image and the nonlinearity of the beamformed signal. The combined capsule layer is positioned either prior to the HIFU focus or behind the HIFU focus at an small angle.

5.3.4 Beamforming for Harmonic Imaging

After RF data acquisition, the B-mode and passively acquired channel data were transferred to a personal computer and converted to a high-level technical computing language (Matlab, R2010b; Mathworks, Natick, Massachusetts). B-mode signals are reconstructed using a custom developed beamforming algorithm. For the passively acquired channel data, The transmit distance was estimated base on the HIFU transducer geometry. And receive delay was estimated base on the imaging probe. In this study, the phased P7-4 array is used in receive mode and the beamforming (delay and sum) algorithm uses it as a linear array with elements at (X_i,0,0) on the X axis and focused in the X Z plane, shown Fig. 5.3.

$H_i(x, z, t)$ is the back propagated signal $Hi(x, z, t) = \alpha(di(x, z))P_i(t*c + D_i(x, z))$ with Pi(t) being the pressure sensed by array element i at time t (assumed proportional to recorded voltage), c the speed of sound. t*c is the transmit distance from the nearest point at the surface of the HIFU transducer to a point in the image plane, (X, Z). Whereas, Di the propagation distance from the point (X, Z) to array element i. $Di(X, Z) = [Z^2 + (X_i - X)^2]^{1/2}$ and $\alpha(di)$ a receiver spatial sensitivity compensation term. The only difference between the B-mode and the passively acquired signal is the transmit delay.

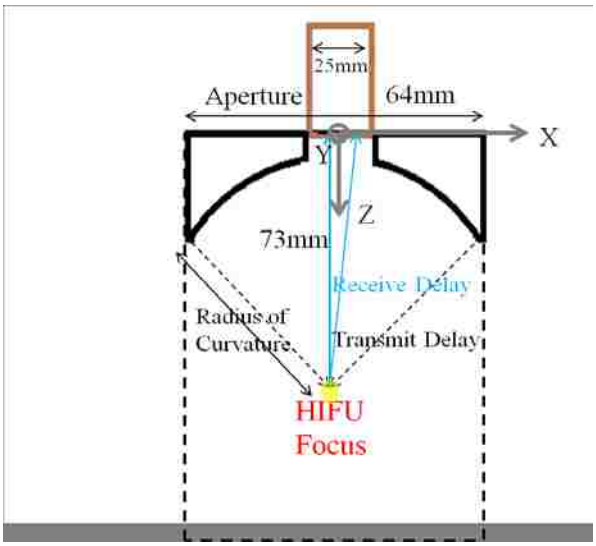

Figure 5.3 Schematic of harmonic imaging, the center of the imaging probe is the origin of the imaging plane (X-Z plane), Y axis is perpendicular to the imaging plane. The aperture of the HIFU transducer is 64mm, so is the radius of curvature. The surface of the imaging probe is 73mm away from the HIFU focus.

5.3.5 Signal Processing of Harmonic Imaging

The signal processing of the harmonic imaging was shown in the flow diagram (Fig. 5.4). The passively acquired RF signals from all 64 channels were digitally filtered by using Matlab function of *filtfilt*. Six frequency bands, centered from 1st to 6th harmonic of the HIFU center frequency 1.24MHz were used to bandpass the RF signals with a bandwidth of 1.24MHz. The filtered signals was then fed through the previously described passive beamforming algorithm. They were then quadrature demodulated by Hilbert transform, the in-phase and quadrature data are obtained. Envelope detection is performed followed by compression to reduce the dynamic range of the received signal for efficient display. Finally grey color image is displayed.

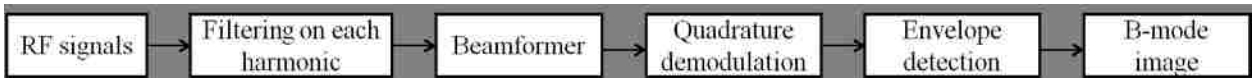

Figure 5.4 Flow diagram for reconstructing image of HIFU focus. Unbeamformed RF raw signals were acquired through VUE at each channel in receive mode. RF signals were first filtered to separate the harmonic contents from 1st to 6th harmonic. Then they were fed into a passive beamforming algorithm, quadrature demodulation, and envelope detection and form a B-mode image.

5.3.6 Results of Harmonic Imaging

After FOPH tip is located at the focus of the HIFU transducer. A 2 cycle HIFU wave travels to the fiber-optic pressure hydrophone (FOPH) tip. The output from the FOPH was first converted by a photo detector, recorded by the digital Oscilloscope and was transferred into a personal computer. At the same position, the reflected HIFU wave from the FOPH tip back to one of the channels in P7-4 probe was acquired and the raw RF signals were stored in the VUE system. Figure 5.5 shows the waveforms measured by FOPH in water at different power levels and was converted in to frequency domain by fast Fourier transform.

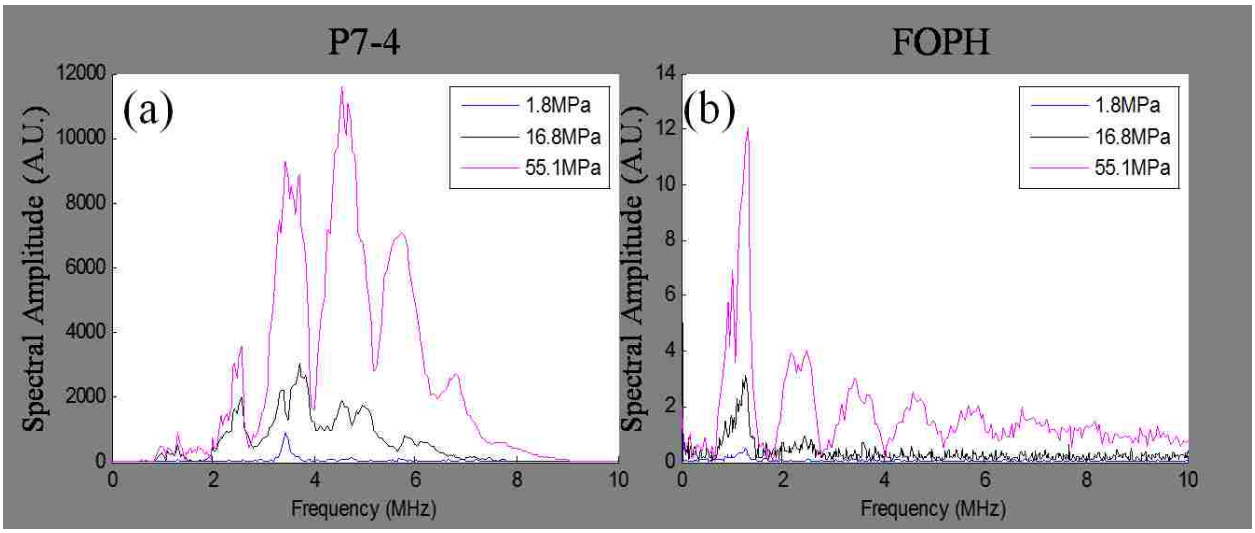

Figure 5.5 Spectrum of the RF signal acquired by a single element of P7-4 probe (a) or by FOPH (b). Signals in blue, black and magenta corresponds to HIFU peak positive pressures at 1.8MPa, 16.8MPa and 55.1MPa. As the pressure increases, more and more harmonics are induced, and the power at each harminic are elevated. Y axis are spectral amplitude in arbitrary unit.

In order to find out how the P7-4 response compare with the FOPH response, the signal from FOPH ouput and the signal acquired from one of the channels of P7-4 at the highest pressure are plotted together. The overlapped plot show that the harmonics from both had the same center frequency (Fig. 5.6). The P7-4 probe has a higher sensitivity at 5MHz since its highest sensitivity span from 4MHz to 7MHz, whereas the FOPH has a bandwidth spans from 0 up to 150MHz.

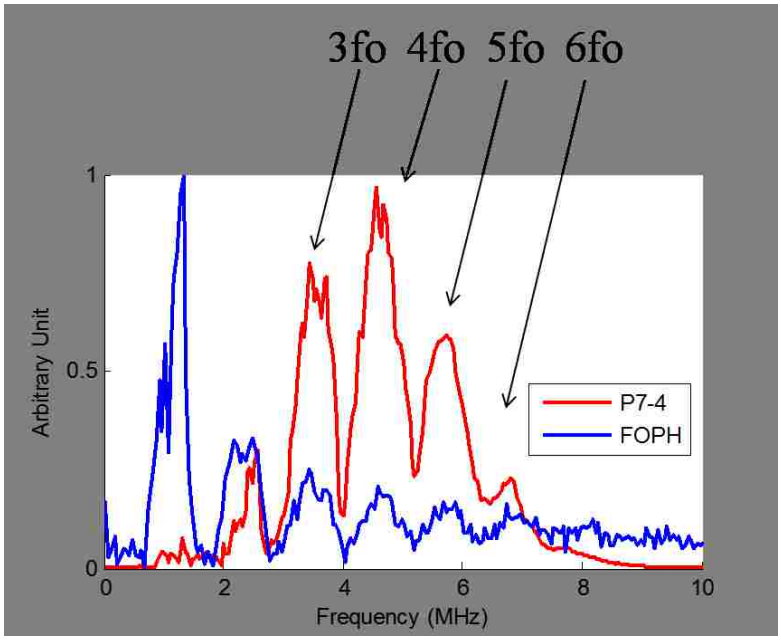

Figure 5.6 The two spectrums from FOPH and P7-4 received signal at 55.1MPa HIFU peak positive pressure are overlaped on the same harmonics. Both could detect up to 6th harmonic of the signal. The P7-4 has higher sensitivity from 4MHz to 7MHz. FOPH has a relatively constant sensitivity across the frequency range (0 to half of the sampling frequency, 20MHz)

After RF signals are filter at every harmonic from fundamental to the 6th harmonic, image are recontructed from each harmonic. The 3rd and 6th harmonic reconstructed images are shown in Fig. 5.7a and 5.7b. The intensities at the depth of focus in lateral direction and axial direction are plotted and are normalized at the highest intensity, along lateral direction (Fig. 5.7c), and along axial direction (Fig. 5.7e). The half maximum widths are ploted versus the number of harmonics. In the lateral direction, the half maximum width decreased with the number of harmonics, and it's almost inversely proportional with the harmnics (Fig. 5.7d, blue line). A ftted curve with inversely propotional function is plotted in red line, which has a correlation coefficient of 99.88% in respect with the actual half maximum width curve (Fig. 5.7d, red line). In the axial direction, the half maximum width becomes smaller from fundamental to the 3rd harmonic of the signal. However, from 3rd to 6th harmonic, the widths didn't become smaller but stays at a relative constant (Fig. 5.7f). Since the axial resolution is dependent on the transmit wave (the HIFU transmit wave), this is likely because that the amplitude of HIFU waveform is not optimized and

the filtering of harmonics is not optimized either. In the future work, harmonic imaging literature will be reviewed and use the available techniques to address the problems.

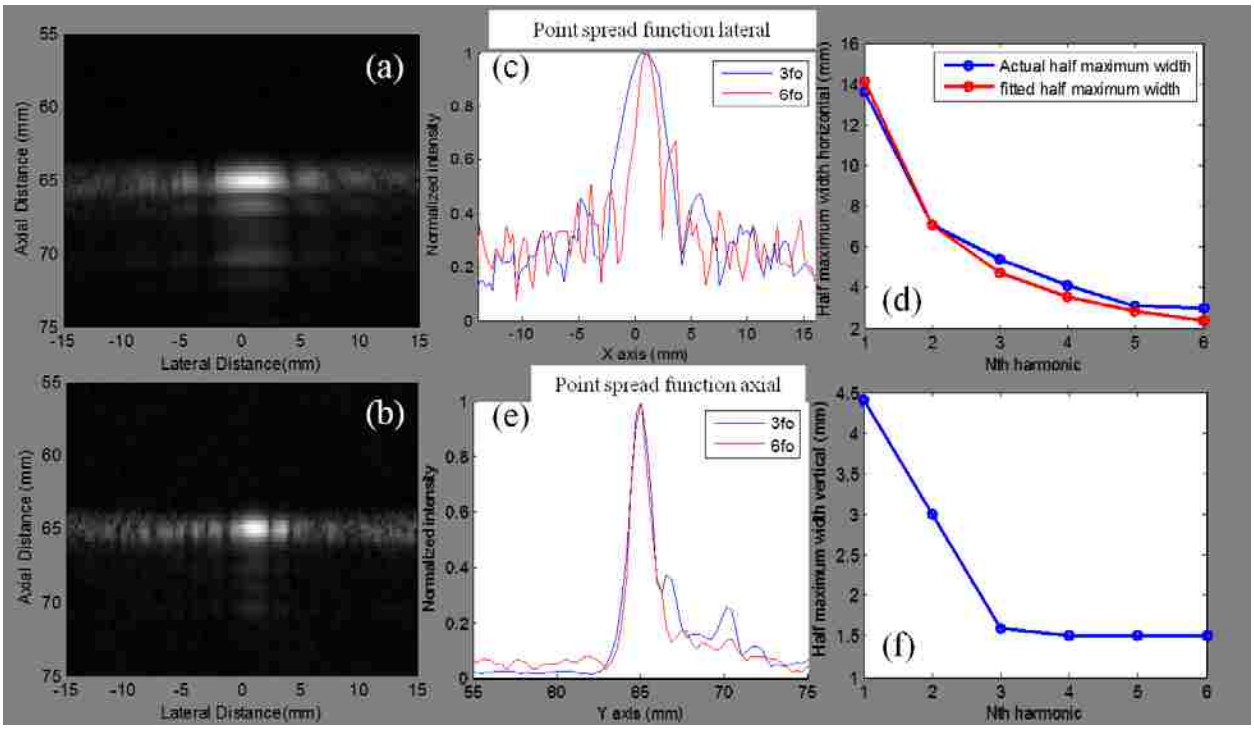

Figure 5.7 Reconstructed images of FOPH tip, transmitted by 2-cycle HIFU wave, passively received by P7-4. Radiofrequency signals are filtered at 3rd and 6th harmonics and beam-formed into individual images. fig (a) and fig (b) are reconstructed image of the FOPH tip. fig (c) and fig (e) are plot of the nomarlized image intensity along the axial and lateral direction at the FOPH tip location, in other words, it's the point spread function laterally and axially. Along the lateral axis, the half maximum width become smaller as number of harmonics increase, it could be fitted into a inversely proportaional relationship with the harmonics, shown in fig (d). Fig (f) shows the half maximum width along axial direction also became smaller as harmonics increase and saturate after 3rd harmonic, it's likely due to the unoptimized filtering of the signal.

When the FOPH tip was replaced by a sample of *ex vivo* boving liver, signals are collected and individual harmonics were reconstrucrted in the same way. Figures 5.8a to 5.8c showed that the images reconstructed from the reflected HIFU wave from FOPH tip at 2nd, 4th, and 6th harmonic. The width of the point spread function changed from 7mm, 5mm to 3mm. On the other hand, Figures 5.8d to 5.8f showed images reconstructed from the backscattered HIFU wave from a piece of *ex vivo* liver sample at 2nd, 4th, and 6th harmonic.. The HIFU focus was place

1.5cm below the surface of the liver. The images show increased intensity at the same depth (~65mm) as the FOPH images, which is the anticipated focus location (Figs. 5.8e to 5.8f). The side lobes are also stronger in the liver due to the backscatter signals, whereas there's none in the water. The images also show a strong inensity on one spot at the surface of the liver. This is likely due to a small bubble trapper in the capsule layer of the liver surface. This is likely why the up right side of the focus has reduced side lobes.

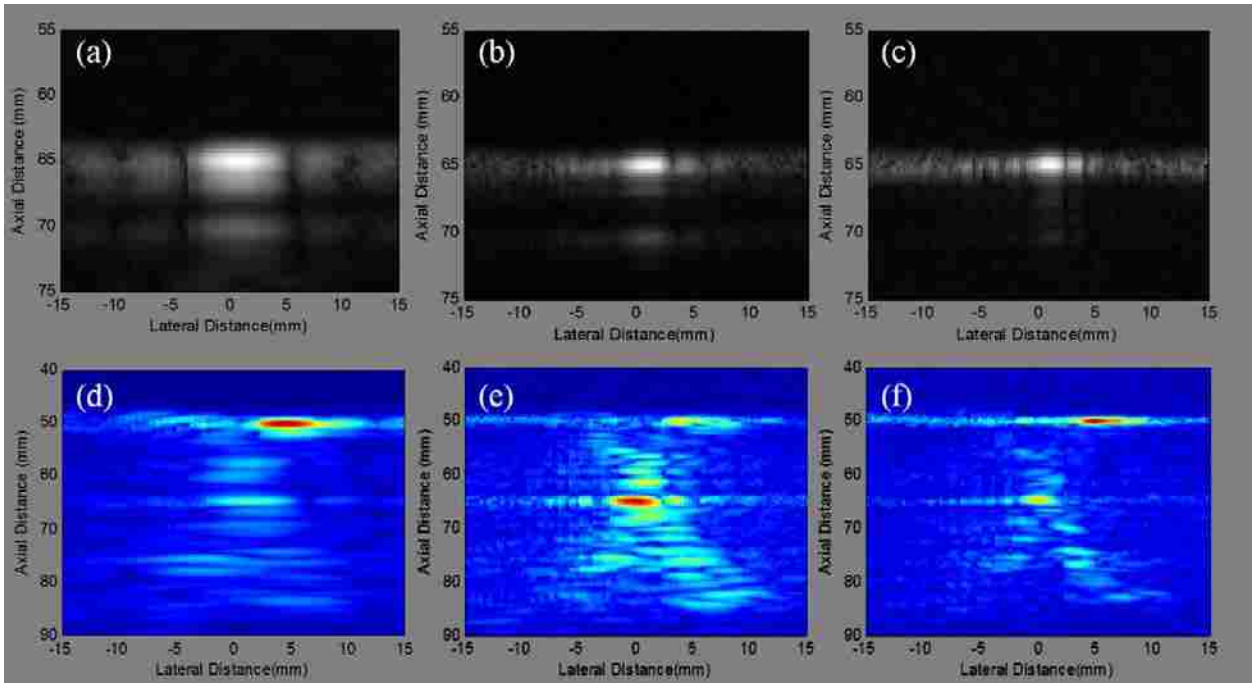

Figure 5.8 From (a) to (e) are the reconstructed images of FOPH tip reflected HIFU wave filtered at 2nd, 4th and 6th harmonics. From (d) to (f) are the reconstructed images of ex vivo liver sample from the backscattered signals filtered at 2nd, 4th and 6th harmonics. The results shows a little distortion of focus due reflection from surface on the right. It is likely due to a bubble trapped on the surface of the liver capsule layer.

There was a major limitation of set up, which is the small aperture of probe. At the highest level of pressure, the 6th harmonic image showed a focus of 3mm in lateral direction for the 100um FOPH tip. At the *ex vivo* liver experiment. The width was around 5mm where as the actual focus width was around 1mm. Although, it doesn't reflect the true width of the HIFU focus, the results showed how much HIFU become nonlinear and if the energy was delivered to the HIFU focus, or it's distorted by any defect in the path.

In the defect experiments, the focus was place around 2cm deep from the surface of the liver. This time, because the capsule layer of one piece of liver was fliped to be combined with another piece of the liver to manually create a detect postfocal and prefocal, the capsule layer was not on the surface anymore. The images from postfocal and prefocal defects were reconstructed at the 4th harmonic in Figs. 5.9a and 5.9b. The sidelobes before the focus were not as strong as the no defect images, it was likely due to the lack of the capsule layer. From both figues, the anticipated focus could be clearly identified at the same depth of the FOPH tip location. There were also enhanced intensity at the anticipated location of the defect in the side of postfocal region Fig. 5.9a and defect in the prefocal region Fig.5.9b.

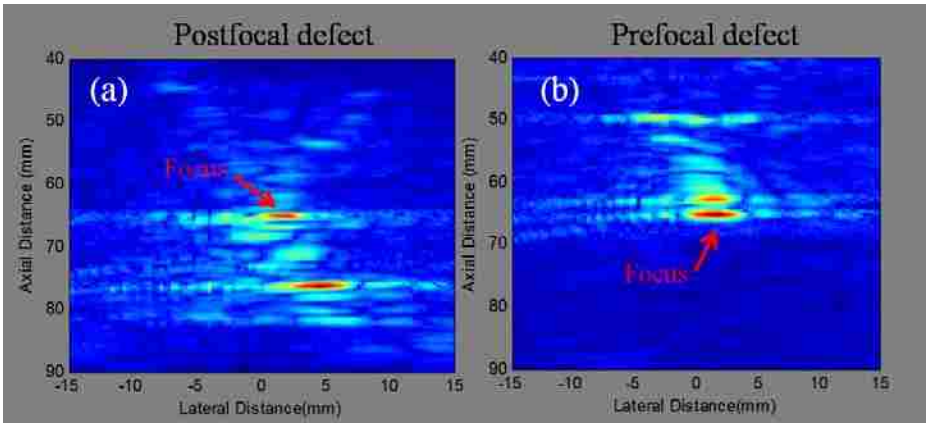

Figure 5.9 (a) was an example that defect is at the side of the focus, which is also a postfocal detect. (b) demonstrated an example where a defect is located prior to the focus, which generated a larger reflected signal before the focs then after the focus. The red arrow was pointed to anticipated HIFU focus.

5.3.7 Discussion on Harmonic Imaging Method

Short HIFU pulses could generate enough nonlinearity at the focus to image a fiber tip with harmonic imaging. It also detects the preexisting bubbles on tissue surface. Harmonic imaging of the pHIFU focus could be used for precise treatment targeting and planning before treatment. It could potentially verify the HIFU focus location before it starts causing irreversible tissue damage and overtreatment is needed.

5.4 Potential Application Using Endoscopic Ultrasound (EUS) Guided HIFU Treatment

5.4.1 Introduction

High intensity focused ultrasound (HIFU) is an promising non-invasive technology, in which high amplitude ultrasound (US) waves are focused inside the human body to thermally ablate or mechanically disrupt the tissue at the focus without affecting surrounding tissues. The thermal ablation effect of HIFU has been used for treatment of benign and malignant tumors including pancreatic cancer[62], [102], [103] and liver cancer[104], [105]. Recent studies also found that mechanical effect of HIFU can enhance targeted drug delivery [3], [74], [77] and stimulate anti-tumor immune responses[106], [107] in many tumors including liver[108] and pancreatic tumors[109]. However, targeting of these tumors using an extracorporeal source is quite challenging due to the lack of acoustic window. HIFU waves cannot penetrate through the bowel gas to reach pancreas. High energy sound waves can be reflected before they reach the target and burns can be produced in the intervening tissue[110]. Targeting of livers is also difficult because some areas of the liver are adjacent to a rib, which distorts the focused beam and redistribute the energy much larger than focal region.

An endoscopic device with integration of a miniature HIFU transducer and a EUS imaging probe is beneficial for image guided therapeutic ablation of peri-lumenal lesions. The development of EUS-guided HIFU device could avoid gas and bones that oppose penetration of HIFU and provide direct ultrasound visualization of the targeted treatment. It brings many potential benefits including improved targeting, decreased energy requirements, and decreased potential for injury

---

Work published part in:

Li T, Khokhlova TD, Maloney E, Morrison K, Keilman G, Wang Y-N, Hwang JH (2014), "Endoscopic ultrasound guided high intensity focused ultrasound therapeutic ablation", Digestive disease week 2014, Chicago, IL.

Maloney E, **Li T**, Khokhlova TD, Wang Y-N, Morrison K, Keilman G, Hwang JH (2014), "Update on eus-guided high intensity focused ultrasound", 14th International Symposium on Therapeutic Ultrasound, Las Vegas, NV.

to intervening structures. Therefore, the aim of the study is to demonstrate experimentally the feasibility of precise ablation by using the EUS guided HIFU device on gel phantoms, *ex vivo* tissues and *in vivo* porcine model.

5.4.2 The Development of EUS Guided HIFU Device

The EUS guided HIFU device is a spherically curved HIFU transducer with diameter of 12 mm and radius of curvature of 35 mm, operating at 2.64MHz and 3.73MHz (Sonic Concepts, Bothell, WA). B-mode imaging probe at frequency of 10MHz (Olympus America, Center Valley, PA) provides image guidance (Fig. 5.10a). They were fitted into a metal housing and were aligned

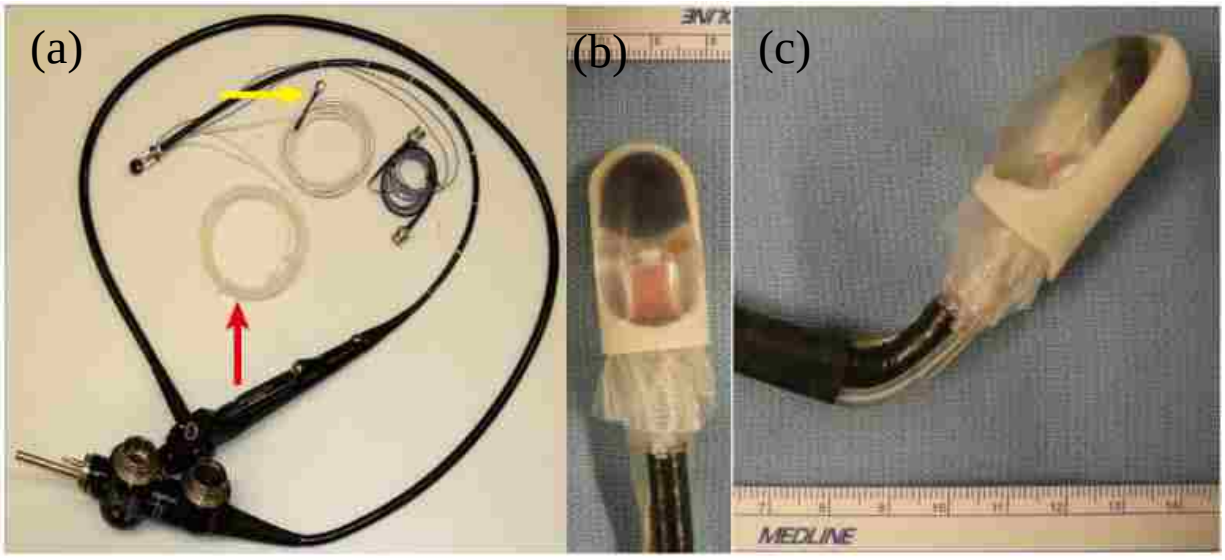

Figure 5.10 (A) Photograph of the prototype of the EUS guided HIFU apparatus. The additional lines attached to the endoscope head were a pair of water tubes for inflating and deflating the water balloon (red arrow), a power line for the HIFU transducer (yellow arrow) and a pair of connecting cables for miniature passive cavitation detectors. (B) The front view of the EUS imaging probe (pink) integrated with the HIFU transducer (black) with inflated water balloon for US coupling. The white plastic cover capping the device ensures the frontal inflation of the balloon for the adjustment of the depth of HIFU focus in tissue. (C) The side view of the distal end of the endoscope demonstrated the bending capability for improved *in vivo* maneuvering.

so that the focus of the HIFU transducer lies on the center of the US image, of which the total depth was 4 cm. Before the experiment, the two transducers were fixed in position mechanically to avoid displacement from the twist force applied during clinical procedures. The metal housing

is covered and sealed with a condom filled with degassed water as a water balloon for US coupling (Fig. 5.10b). There were two water channels on the side of the metal housing, through which the balloon were inflated or deflated with degassed water. A custom made plastic cover was placed outside the water balloon, which ensures the water balloon was only inflated at the front side of transducer. In this way, the depth of HIFU focus was controlled through the inflation and deflation of the water balloon. The whole device has full flexibility of bending (Fig. 5.10c). During experiment, the transducer was connected to a matching network for maximum power transfer and a power amplifier (ENI 400B; ENI, Rochester, NY).

5.4.3 Characterization of the Endoscopic HIFU Transducer

The dimensions of focal areas produced by the HIFU transducer (- 6 dB level) in water were measured to be 20 mm X 0.9 mm for 3.73MHz and 22 mm X 1.6 mm for 2.64MHz by a fiber optic probe hydrophone (FOPH 2000; RP Acoustics, Leutenbach, Germany). The focal waveform at 2.64MHz at the highest power output containing a shock front was used in all the experiments with P^+ = 17 MPa and P^- = 9 MPa (Fig. 5.11). A pulsing protocol of 0.1 s pulse duration, 0.2 s pulse repetition period, and exposure duration of 30 s was used for gel phantoms, *ex vivo* bovine liver and *in vivo* porcine liver and pancreas.

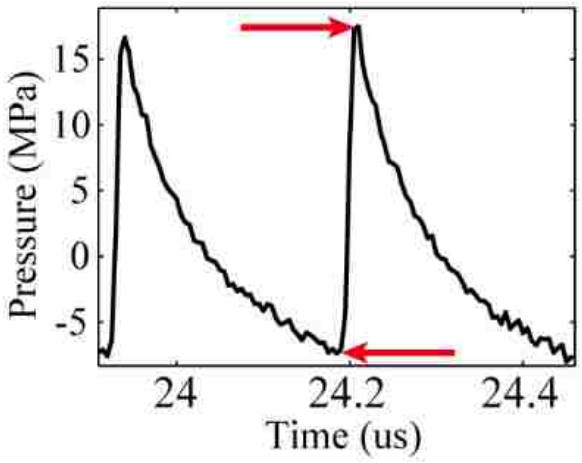

Figure 5.11 Focal pressure waveforms produced by HIFU at 3.73 MHz operating frequency, 144 Watt electric power and measured in water by fiber optic probe hydrophone. The peak-compressional and rarefactional focal pressure levels were 17 MPa and 9 MPa, correspondingly. The waveform contained a sharp rise in pressure – a shock front (red arrows) formed due to

nonlinear ultrasound propagation effects. Shock waves allowed depositing ultrasound energy in a very localized fashion and very rapidly, so that the boiling temperature of water was reached in a matter of milliseconds. The resulting boiling bubble activity was readily seen on B-mode ultrasound as bright hyperecho, and was used for therapy monitoring and guidance.

After measuring the acoustic properties, characterization of lesion formation was first performed using gel phantoms. The gel phantoms were composed of 5 % w/v polyacrylamide (PA) hydrogels and 7 % w/v bovine serum albumin (BSA) that becomes optically opaque when denatured [111]. To prepare the gel phantom samples, the liquid mixture of PA gel constituents as well as BSA were degassed for 1 h in a desiccant chamber and then poured into a custom mold (5 cm wide by 5 cm tall by 8 cm deep) for polymerization. The polymerized gel was optically transparent, which made it convenient to observe thermal lesions.

To characterize the lesion formation in *ex vivo* tissue, *ex vivo* bovine liver tissue was obtained from an abattoir on the same day as experiments and stored in phosphate buffered saline and on ice until experiments were performed. The tissue was cut into samples to fit in a custom-designed tissue holder (8 cm wide by 8 cm tall by 2.7 cm deep) and was brought to room temperature and degassed for 1 h in a desiccant chamber immediately prior to experiments. During experiment, the endoscopic device was place so that the focus was 15 mm deep below the surface for both gel phantoms and liver.

In the end, preliminary *in vivo* studies were performed to assess the ergonomics of the transducer design and demonstrate the feasibility of targeting and creating lesions in the porcine pancreas. To test the device in an *in vivo* setting, a pig model was chosen because of its similarity to the human digestive anatomy. During the *in vivo* study, the pigs were given general anesthetics. The stomach was imaged, flushed and cleaned with degassed water by a gastrointestinal videoscope (Olympus America, Center Valley, PA). The EUS guided HIFU device was inserted through the esophagus and placed against the stomach wall with the inflated water balloon for US coupling (Fig. 5.12). The US image was used to identify the location of pancreas and liver.

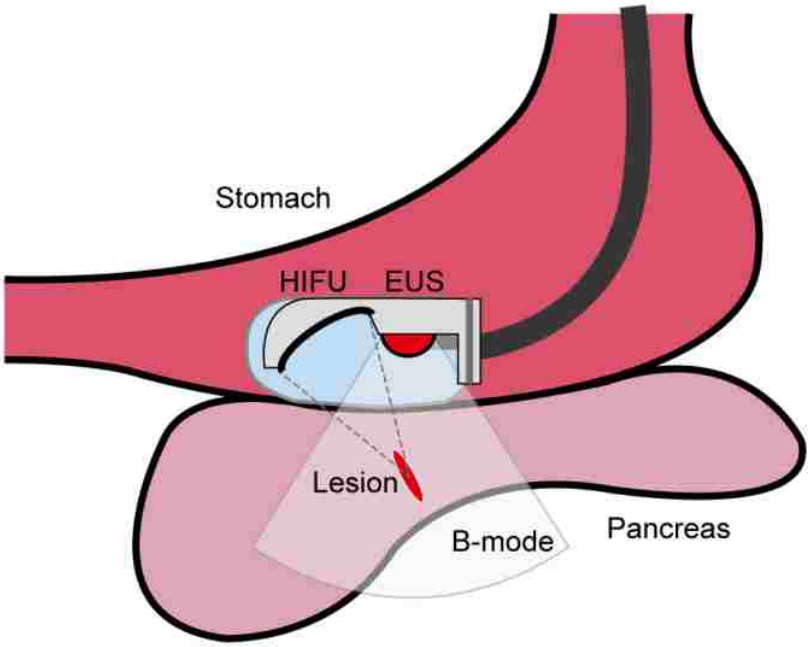

Figure 5.12 Illustration of the EUS guided HIFU apparatus placement in the stomach during HIFU ablation of the pancreas. The device was coupled to the stomach wall by the distended water balloon. The HIFU transducer and the EUS imaging probe were aligned so that the HIFU focus was at the center of the B-mode image that allowed monitoring lesion formation in real time.

After a treatment location is chosen, the pig was stopped breathing and HIFU waves were delivered. In each pig, HIFU exposure was applied to 4-5 locations in liver and pancreas by moving the endoscopic device along the stomach wall. After the treatment, the pigs were imaged again by videoscope to identify any surface lesions and were sacrificed immediately afterwards. The lesions were collected for histological analysis to evaluate the damage.

The samples of pancreas and liver which contained a lesion were embedded for histological evaluation. In order to characterize the thermal damage to tissue, the consecutive tissue slices were sectioned. They were stained with hematoxylin and eosin (H&E) to visualize tissue structure and mechanical disruption, as well as nicotinamide adenine dinucleotide diaphorase (NADH-d) to evaluate the extent of thermal damage.

5.4.4 Attenuation of the Stomach Wall

In order to evaluate the attenuation from the stomach wall to the focal waveform, the following experiment was set up (Fig. 5.13)

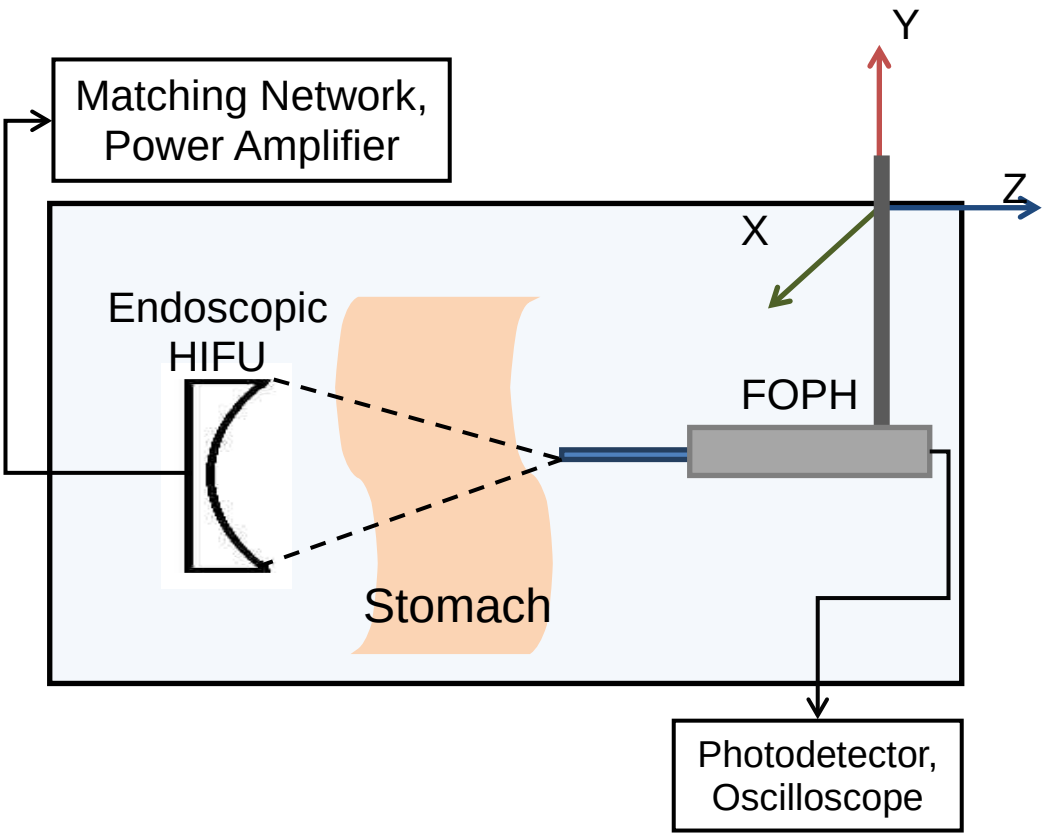

Figure 5.13 Illustration of experimental setup for measuring attenuation of stomach wall. FOPH was placed at the focus of the endoscopic HIFU transducer by field mapping. A piece of stomach wall placed in between the tip of the FOPH and the transducer.

First, FOPH is aligned with the HIFU focus. Then, a piece of fresh stomach wall, which was excised right after a pig was sacrificed, was placed in between the tip of the hydrophone and the transducer (Fig. 5.13). The focal pressure waveforms from the groups of water, fresh stomach wall, and rinsed stomach wall (slime was removed), were acquired. The following plots showed the relationship between the peak negative pressure and peak positive pressure versus the input driving voltage (Figs. 5.14a and 5.14b).

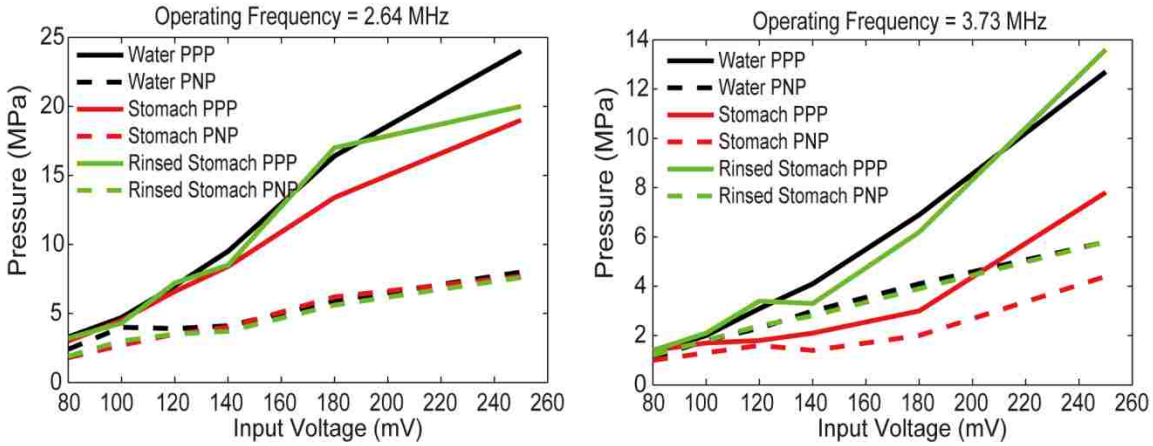

Figure 5.14 The relationship between the peak positive (solid line) and peak negative (dashed line) pressure levels change versus input driving voltage under different media. Black, green and red lines correspond to pressure acquired when the media is water, fresh stomach wall and rinsed stomach wall. Left figure are results acquired when frequency is 2.64MHz (a). Right figure are results acquired when frequency is 3.73MHz (b).

From the results, we could see that the fresh stomach wall has the highest attenuation. The rinsed stomach wall only attenuates a little, suggesting that the slime on top of the stomach wall could lead to heat deposition prefocal. The attenuation extent is less with the 2.64MHz frequency than 3.73MHz.

5.4.5 Thermal Lesions in BSA Polyacrylamide Gel Phantoms

HIFU exposure of a transparent PA-BSA gel phantom resulted in the formation of an elongated, tadpole-shaped opaque region (Fig. 5.15a) that corresponded to the area of thermal denature of the BSA protein. The tadpole shape of the lesion was due to the formation of boiling and cavitation bubbles at the HIFU focus and subsequent backscattering of the incident ultrasound waves that were absorbed prefocally. B-mode ultrasound image (Fig. 5.15b) showed a hyperechoic region in the middle of the screen within 1 second after the start of HIFU exposure due to the boiling bubble formation at the HIFU focus. The region gradually elongated towards the transducer in a stripe shape throughout the exposure indicating the area of bubble activity. After HIFU was turned off, the hyperecoic region persisted and gradually shrunk. The size and shape of the echogenic region corresponded well to the size of the thermal lesion.

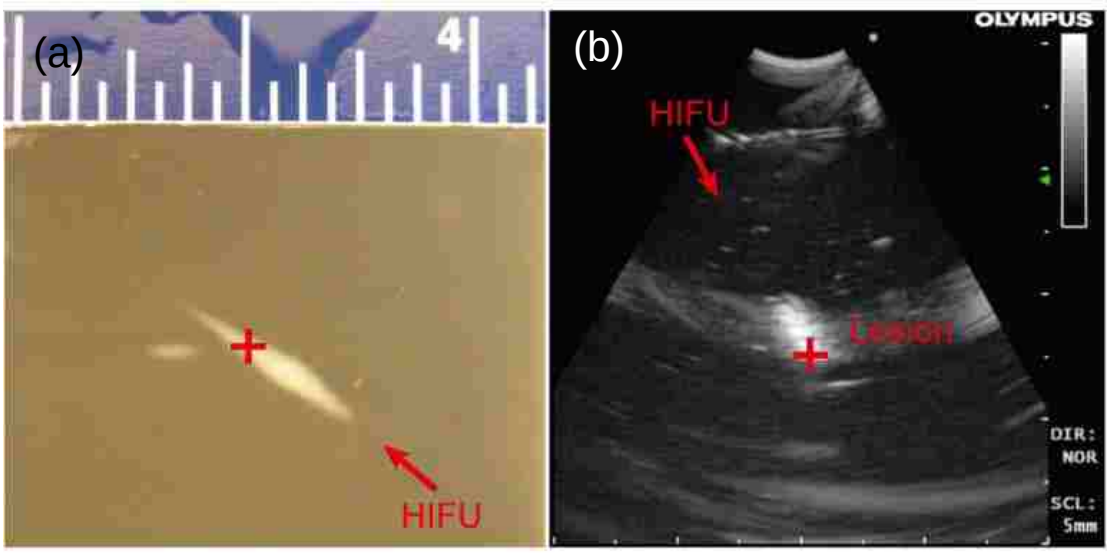

Figure 5.15 (a) Thermal lesion created by HIFU in the transparent tissue-mimicking PA gel phantom embedded with BSA. The lesion corresponded to the elongated opaque region in the middle of the image which resulted from thermal denature of the BSA. The red arrow shows the direction of incidence of the HIFU wave, and the red cross marks the HIFU focus location. b) A hyperechoic region was observed during HIFU ablation in B-mode EUS image. The size and location of the hyperechoic region corresponded well with the thermal lesion. The hyperechogenicity was due to the presence of HIFU-induced cavitation and boiling bubbles that were highly reflective.

5.4.6 Thermal Lesions in *Ex Vivo* Bovine Tissue

Similarly to the experiments in the gel phantoms, pulsed HIFU exposure of the *ex vivo* bovine liver samples resulted in well-defined tadpole-shaped thermal lesions with small vacuoles in the middle of the prefocal region (Fig. 5.16a). The vacuoles corresponded to the location of the boiling bubbles, as indicated by the hyperechoic region that appeared in the B-mode image 2 seconds after the start of HIFU exposure (Fig. 5.16b). The hyperechoic region expanded in direction towards the transducer throughout the exposure, demonstrating preferential energy deposition in the prefocal region due to the ultrasound scattering by the boiling bubbles. The size and shape of the hyperechoic region corresponded well to these of the resulting lesion, thus demonstrating the capability of B-mode ultrasound to monitor the treatment.

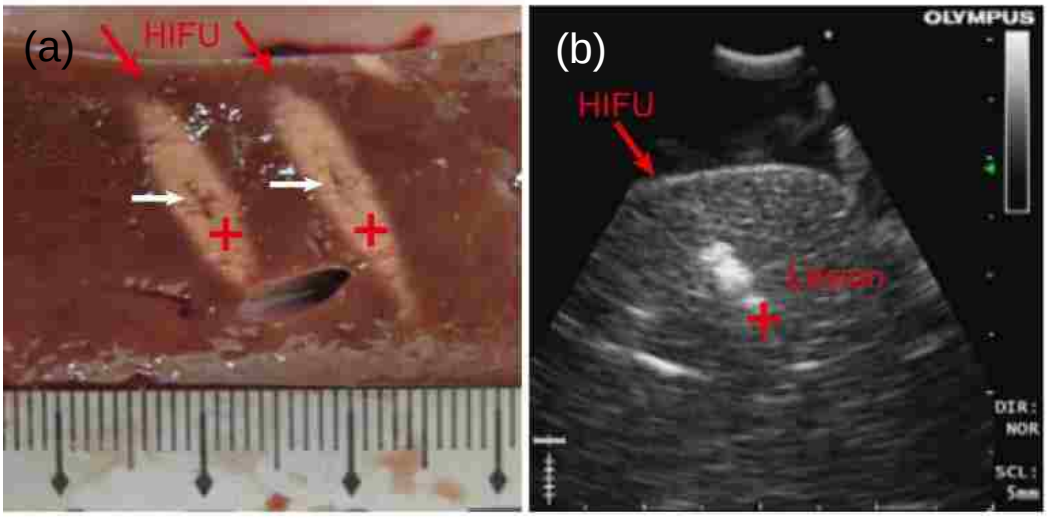

Figure 5.16 (a) Two separate thermal lesions in bovine liver, seen as regions of whitening, were created with the same HIFU exposure protocol as the lesions in the gel phantom. Small cavities in the middle of the thermal lesions (white arrows) resulted from HIFU-induced bubble activity. (b) Formation of the hyperechoic region during the HIFU exposure was observed by B-mode ultrasound, similarly to the gel phantom experiments. The red arrow shows the direction of incidence of the HIFU wave, and the red cross marks the HIFU focus location.

5.4.7 Thermal lesions in Liver and Pancreas of *In Vivo* Pig Study

In vivo study results

HIFU ablation of the porcine liver and pancreas *in vivo* caused the appearance of the area of slightly enhanced tissue echogenicity as observed on the B-mode images (Figs. 5.17a, 5.17b, 5.17d, 5.17e). However, this change in echogenicity was far less pronounced and localized than that observed *ex vivo*, and it formed closer to the HIFU transducer surface. Immediately after the ablation, the videoscope observations showed surface lesioning on the stomach wall corresponding to the treatment locations. The solid thermal lesions found in the excised liver and pancreas (Figs. 5.17c and 5.17f) were larger in diameter than in the *ex vivo* case and involved a large area of the tissue surface, which corresponded to the prefocal area of the HIFU transducer. This preferential heating of the pre-focal area was likely due to the increased attenuation of the intervening tissues - gastric wall and mucosa – that could still harbor residual bubbles. The presence of the bubbles is also suggested by the increased brightness of the stomach wall surface on the B-mode image after the HIFU exposure. The partial blocking of the HIFU beam by the bubbles prevented the tissue at the focus from reaching the boiling temperature.

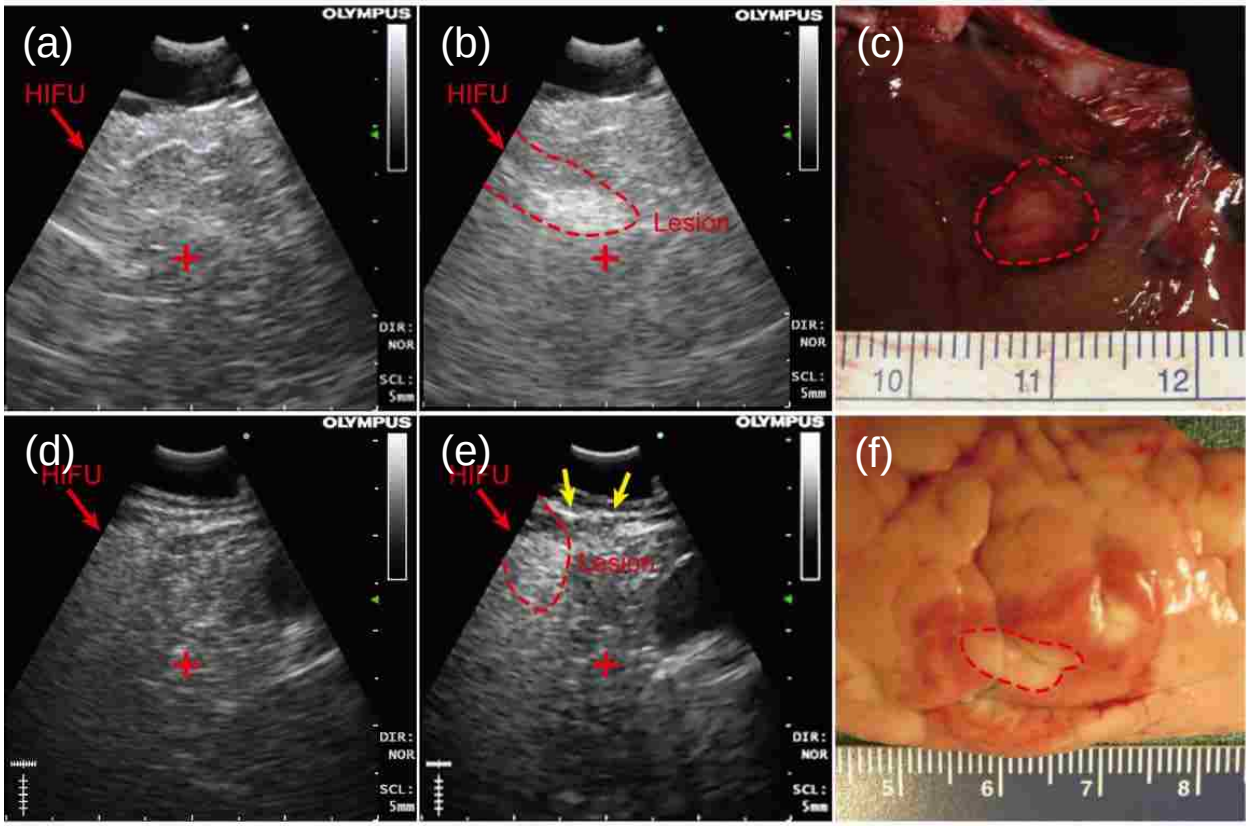

Figure 5.17 The B-mode EUS images were acquired before and after HIFU ablation of liver (a), (b) and pancreas (d), (e), correspondingly, in an *in vivo* porcine model. The red arrow shows the direction of incidence of the HIFU wave, and the red cross marks the HIFU focus location. The increase in brightness corresponding to the region of ablation (red dashed lines in a, e), was considerably lower than that observed in the experiments in gel phantoms and *ex vivo* tissue, suggesting that the boiling temperature was not reached at the focus. This is likely due to enhanced attenuation of the intervening tissues – gastric wall and mucosa. The corresponding area of the interior surface of the gastric wall (yellow arrows) has an increased brightness after HIFU exposure, suggesting the presence of bubbles in the mucosa, that are reflective to ultrasound and partially block the HIFU penetration to the focal area After the animal was euthanized, the liver (c) and pancreas (f) were excised to photograph the thermal lesions.

Histology Analysis

An example of NADH-d stained slices showed a surface damage on porcine pancreas tissue (Fig. 5.18a), where the damaged area appears more white than undamaged area, and a larger thermal damage on the porcine liver tissue (Fig. 5.18c), where the lesion boundaries are clear shown. H&E stained slices showed the histological structure was disrupted in the treated area in

pancreas and liver (Fig. 5.18b and 5.18d). Both of liver and pancreas showed both mechanical and thermal damage.

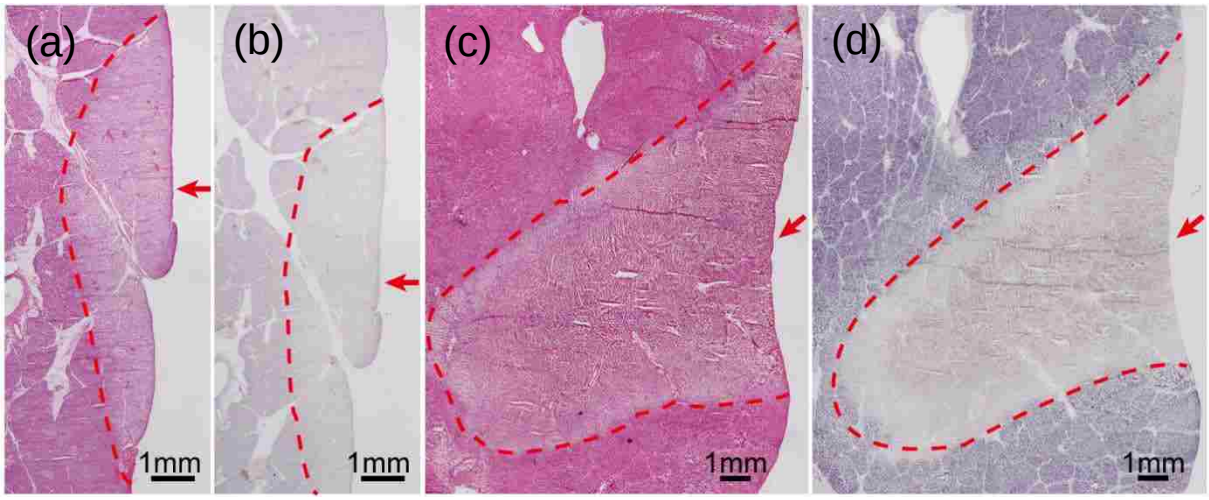

Figure 5.18 H&E stained histological sections of the HIFU lesions ((a) and (c)) revealed no structural disruption in either pancreas or liver, but evidence of coagulative necrosis was seen in the treated region (red dashed line). Consecutive NADH-d stained histological sections of the same samples in both the pancreas (b) and liver (d) showed whitening in the treated area (red dashed line), indicating complete thermal necrosis of tissue. The direction of incidence of the HIFU wave is from the right of the images (red arrows).

5.4.8 Discussion

In this article, we have demonstrated the feasibility of using an endoscopic HIFU device for making trangastric lesions under the guidance of EUS imaging. The device is particularly useful for inducing necrosis in peancreas and liver tumor, which is often associated with difficulty to resect and tendency to metastases. Treatment planning and monitoring was achieved by transgastric US images. Our findings in BSA PA gel phantoms, *ex vivo* bovine liver and *in vivo* procine studies show that lesions can be created in deep seated tissues transgastrically in a realistic anatomy.

In the gel phantoms and ex vivo tissue studies, the dimensions of the lesions formed in BSA PA gel phantoms and ex vivo bovine liver samples corresponded well with the echogenic region on B-mode EUS images. The lesion is likely to result from a mixed thermal and mechanical effect.

Histological analysis from H&E and NADH-d staining confirmed both effects occurred. The lesions were formed shallower in bovine liver than the gel phantoms, likely because attenuation coefficient in liver is about 60% more than in BSA[112].

In the *in vivo* studies, the device successfully induced lesions in pancreas and liver through gastric wall with no immediate adverse effects to surrounding organs. The lesion is formed in the pre-focal region and grows into surface. The lesions appeared to be bigger and shallower than the *ex vivo* case. It is likely due to the high attenuation from the stomach. Previous literature showed an attenuation coefficient of 0.6-5.2 dB/cm/MHz for stomach wall [38], which is already higher than liver 0.37 dB/cm/MHz. The presence of the gas bubbles in the slime made the HIFU waves attenuate even more.

To evaluate the influence of the mucous deposits in the pig's stomach on the outcome of HIFU treatment, thermal lesions were induced in porcine liver through the gastric wall immediately post euthanasia, in an open abdomen. The stomach was opened, and the stomach wall was thoroughly rinsed with degassed saline prior to HIFU exposures. B-mode images (Fig. 5.19a) acquired during HIFU exposures and the subsequent gross observations (Fig. 5.19b) showed that the lesions were successfully induced in depth of the liver, without damage to the liver surface or gastric wall. The histological analysis of the lesion confirmed that both structural damage and thermal effect were contained in the liver tissue (Figs. 5.19c and 5.19d), which was consistent with the previous findings from our group [113]. Thus, to reduce the chance of surface damage, special attention should be paid to cleaning of the stomach before HIFU treatment, and removing mucous deposits. A HIFU transducer with higher focusing gain would allow further eliminating the attenuation and reflection effects in the acoustic pathway and make the ablation safer, more predictable and more rapid. Given the required depth of ablation, this would imply using a transducer with a larger aperture, which may not be acceptable for endoscopic use. Foldable or expandable HIFU transducers may represent a viable solution, and are currently under development.

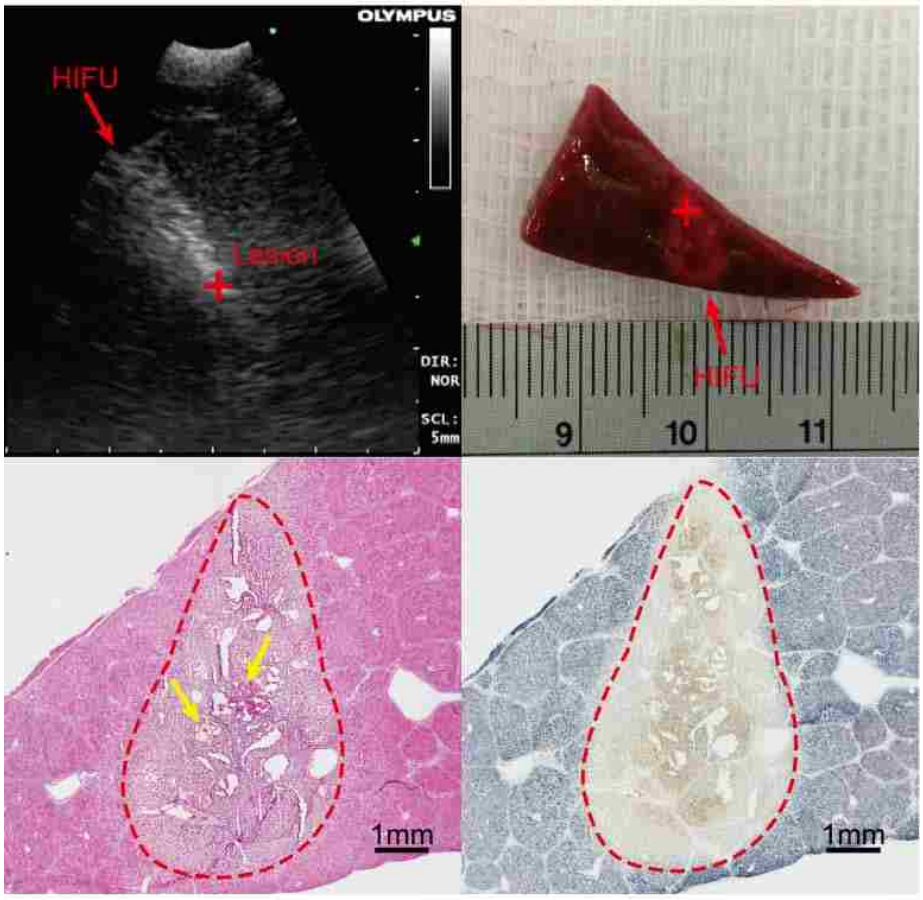

Figure 5.19 (A) B-mode EUS image acquired during ablation of liver through gastric wall in an open pig. Hyperechoic region (red arrow) identified the region of ablation, which started 2.5cm and grows toward the surface of the tissue. (B) The corresponding in depth lesion was resulted. NADH-d (C) and H&E (D) stained liver slices showed both thermal and mechanical effects were resulted.

5.4.9 Conclusions

An EUS-guided HIFU transducer successfully created lesions in BSA PA gel phantoms, *ex vivo* bovine livers, and *in vivo* porcine liver and pancreas. Compared with other imaging guidance modalities such as magnetic resonance imaging (MRI), the EUS-guided HIFU device provides immediate visualization of HIFU ablation directed by its orientation. Further development of this technology allows endoscopists to perform therapeutic ablation of peri-lumenal tumors without the need for surgery, in which case significant inflammation can be induced. Potential applications of this technology include ablation of perilumenal tumors in the liver (hepatocellular

carcinoma, metastatic liver lesion), pancreas (adenocarcinoma, neuroendocrine) and bile duct. In addition, EUS-guided HIFU can be used to perform ablation of the celiac plexus for palliation of pain. Furthermore, it could also be used for enhancing targeted drug delivery of chemotherapy by using mechanical effect of HIFU to improve tissue permeability.

References

[1] V. Frenkel, "Ultrasound mediated delivery of drugs and genes to solid tumors.," *Adv. Drug Deliv. Rev.*, vol. 60, pp. 1193–208, Jun. 2008.

[2] E. C. PUA and P. ZHONG, "Ultrasound-Mediated Drug Delivery," *IEEE Eng. Med. Biol. Mag.*, vol. 28, pp. 64–75, 2009.

[3] S. Mo, C. Coussios, L. Seymour, and R. Carlisle, "Ultrasound-enhanced drug delivery for cancer," *Expert Opin. Drug Deliv.*, vol. 9, pp. 1525–1538, 2012.

[4] K. Ferrara, R. Pollard, and M. Borden, "Ultrasound microbubble contrast agents: fundamentals and application to gene and drug delivery.," *Annu. Rev. Biomed. Eng.*, vol. 9, pp. 415–47, Jan. 2007.

[5] A. D. Maxwell, C. A. Cain, T. L. Hall, J. B. Fowlkes, and Z. Xu, "Probability of cavitation for single ultrasound pulses applied to tissues and tissue-mimicking materials.," *Ultrasound Med. Biol.*, vol. 39, pp. 449–465, Mar. 2013.

[6] M. Bazan-Peregrino, C. D. Arvanitis, B. Rifai, L. W. Seymour, and C. C. Coussios, "Ultrasound-induced cavitation enhances the delivery and therapeutic efficacy of an oncolytic virus in an in vitro model," *J. Control. Release*, vol. 157, no. 2, pp. 235–242, 2012.

[7] K. D. Watson, C.-Y. Lai, S. Qin, D. E. Kruse, Y.-C. Lin, J. W. Seo, R. D. Cardiff, L. M. Mahakian, J. Beegle, E. S. Ingham, F.-R. Curry, R. K. Reed, and K. W. Ferrara, "Ultrasound Increases Nanoparticle Delivery by Reducing Intratumoral Pressure and Increasing Transport in Epithelial and Epithelial-Mesenchymal Transition Tumors," *Cancer Research*, vol. 72, no. 6. pp. 1485–1493, 2012.

[8] C. C. Coussios, C. H. Farny, G. T. E. R. Haar, and R. A. Roy, "Role of acoustic cavitation in the delivery and monitoring of cancer treatment by high-intensity focused ultrasound (HIFU)," *Engineering*, vol. 23, pp. 105–120, 2007.

[9] J. McLaughlan, I. Rivens, T. Leighton, and G. Ter Haar, "A study of bubble activity generated in ex vivo tissue by high intensity focused ultrasound.," *Ultrasound Med. Biol.*, vol. 36, pp. 1327–1344, Aug. 2010.

[10] S. I. Madanshetty and R. E. Apfel, "Acoustic microcavitation: enhancement and applications.," *J. Acoust. Soc. Am.*, vol. 90, pp. 1508–14, Sep. 1991.

[11] J. H. Hwang, J. Tu, A. A. Brayman, T. J. Matula, and L. A. Crum, "Correlation between inertial cavitation dose and endothelial cell damage in vivo.," *Ultrasound Med. Biol.*, vol. 32, pp. 1611–1619, Oct. 2006.

[12] W.-S. Chen, T. J. Matula, A. A. Brayman, and L. A. Crum, "A comparison of the fragmentation thresholds and inertial cavitation doses of different ultrasound contrast agents," *J. Acoust. Soc. Am.*, vol. 113, pp. 643–651, 2003.

[13] Z. Kyriakou, M. I. Corral-Baques, A. Amat, and C.-C. Coussios, "HIFU-induced cavitation and heating in ex vivo porcine subcutaneous fat.," *Ultrasound Med. Biol.*, vol. 37, pp. 568–579, Apr. 2011.

[14] T. D. Khokhlova, M. S. Canney, D. Lee, K. I. Marro, L. a Crum, V. a Khokhlova, and M. R. Bailey, "Magnetic resonance imaging of boiling induced by high intensity focused ultrasound.," *J. Acoust. Soc. Am.*, vol. 125, no. 4, pp. 2420–31, Apr. 2009.

[15] P. I. Bortezomib, J. A. Poff, C. T. Allen, B. Traughber, Z. Chen, and B. J. Wood, "Pulsed High-Intensity Focused Ultrasound Enhances Apoptosis and Growth Inhibition of Squamous Cell Carcinoma Xenografts with Purpose : Methods : Results : Conclusion :," vol. 248, no. 2, pp. 485–491, 2008.

[16] A. Rahmouni, R. Bargoin, A. Herment, N. Bargoin, and N. Vasile, "Color Doppler twinkling artifact in hyperechoic regions.," *Radiology*, vol. 199, no. 1, pp. 269–271, 1996.

[17] W. Lu, O. A. Sapozhnikov, M. R. Bailey, P. J. Kaczkowski, and L. A. Crum, "Evidence for Trapped Surface Bubbles as the Cause for the Twinkling Artifact in Ultrasound Imaging," *Ultrasound Med. Biol.*, vol. 39, no. 6, pp. 1026–1038, 2013.

[18] B. E. O'Neill, H. Vo, M. Angstadt, K. P. C. Li, T. Quinn, and V. Frenkel, "Pulsed High Intensity Focused Ultrasound Mediated Nanoparticle Delivery: Mechanisms and Efficacy in Murine Muscle," *Ultrasound Med. Biol.*, vol. 35, no. 3, pp. 416–424, 2009.

[19] A. C. Society, "Cancer Facts & Figures 2013," in *Cancer Facts & Figures 2013*, Society, American Cancer, 2013.

[20] K. P. Olive, M. A. Jacobetz, C. J. Davidson, A. Gopinathan, D. Mcintyre, D. Honess, B. Madhu, M. A. Goldgraben, M. E. Caldwell, D. Allard, K. K. Frese, G. Denicola, C. Feig, C. Combs, S. P. Winter, H. Ireland-zecchini, S. Reichelt, W. J. Howat, A. Chang, M. Dhara, L. Wang, F. Rückert, R. Grützmann, C. Pilarsky, K. Izeradjene, S. R. Hingorani, and P. Huang, "Inhibition of Hedgehog signaling enhances delivery of chemotherapy in a mouse model of pancreatic cancer," *Science (80-.).*, vol. 324, pp. 1457–1461, 2009.

[21] R. K. Jain, "An Indirect Way to Tame Cancer," *Sci. Am.*, vol. 310, no. 2, pp. 46–53, Jan. 2014.

[22] V. P. Chauhan and R. K. Jain, “Strategies for advancing cancer nanomedicine.,” *Nat. Mater.*, vol. 12, no. 11, pp. 958–62, Nov. 2013.

[23] S. Dromi, V. Frenkel, A. Luk, M. Bur, J. Poff, J. Xie, S. K. Libutti, K. C. P. Li, and B. J. Wood, “Pulsed-High Intensity Focused Ultrasound and Low Temperature − Sensitive Liposomes for Enhanced Targeted Drug Delivery and Antitumor Effect Pulsed-High Intensity Focused Ultrasound and Low Temperature ^ Sensitive Liposomes for Enhanced T argeted Drug Deli,” *Clin. Cancer Res.*, 2007.

[24] R. Rao and S. Nanda, “Sonophoresis: recent advancements and future trends.,” *J. Pharm. Pharmacol.*, vol. 61, no. 6, pp. 689–705, 2009.

[25] J. H. Hwang, J. Tu, A. A. Brayman, T. J. Matula, and L. A. Crum, “Correlation between inertial cavitation dose and endothelial cell damage in vivo.,” *Ultrasound Med. Biol.*, vol. 32, pp. 1611–1619, Oct. 2006.

[26] Y.-S. Tung, F. Vlachos, J. J. Choi, T. Deffieux, K. Selert, and E. E. Konofagou, “In vivo transcranial cavitation threshold detection during ultrasound-induced blood-brain barrier opening in mice.,” *Phys. Med. Biol.*, vol. 55, pp. 6141–6155, Oct. 2010.

[27] C. C. Coussios, M. Gyongy, R. Ritchie, I. Webb, S. Nandlall, E. Jackson, C. Arvanitis, M. Bazan-Peregrino, and M. Arora, “Passive mapping for real-time monitoring of ultrasound therapy.,” *J. Acoust. Soc. Am.*, vol. 128, no. 4, p. 2416, 2010.

[28] N. Vykhodtseva, “Histologic effects of high intensity pulsed ultrasound exposure with subharmonic emission in rabbit brain in vivo,” *Ultrasound Med. Biol.*, vol. 21, pp. 969–979, 1995.

[29] M. J. Stone, V. Frenkel, S. Dromi, P. Thomas, R. P. Lewis, K. C. P. Li, M. Horne, and B. J. Wood, “Pulsed-high intensity focused ultrasound enhanced tPA mediated thrombolysis in a novel in vivo clot model, a pilot study.,” *Thromb. Res.*, vol. 121, pp. 193–202, Jan. 2007.

[30] C. C. Church, “Spontaneous homogeneous nucleation, inertial cavitation and the safety of diagnostic ultrasound,” *Ultrasound Med. Biol.*, vol. 28, pp. 1349–1364, 2002.

[31] C. K. Holland and R. E. Apfel, “Thresholds for transient cavitation produced by pulsed ultrasound environment,” *Jounal Acoust. Soc. Am.*, vol. 88, pp. 2059–2069, 1990.

[32] L. Somaglino, G. Bouchoux, J. L. Mestas, and C. Lafon, “Validation of an acoustic cavitation dose with hydroxyl radical production generated by inertial cavitation in pulsed mode: Application to in vitro drug release from liposomes,” *Ultrason. Sonochem.*, vol. 18, no. 2, pp. 577–588, 2011.

[33] T. D. Khokhlova, M. S. Canney, D. Lee, K. I. Marro, L. A. Crum, V. A. Khokhlova, and M. R. Bailey, "Magnetic resonance imaging of boiling induced by high intensity focused ultrasound.," *J. Acoust. Soc. Am.*, vol. 125, no. 4, pp. 2420–31, Apr. 2009.

[34] A. Jensen, "Calculation of pressure fields from arbitrarily shaped, apodized, and excited ultrasound transducers," *IEEE Trans. Ultrason. Ferroelectr. Freq. Control*, vol. 39, pp. 262–267, 1992.

[35] K. Hynynen, "Ultrasound for drug and gene delivery to the brain.," *Adv. Drug Deliv. Rev.*, vol. 60, pp. 1209–1217, Jun. 2008.

[36] T. D. Khokhlova, M. S. Canney, V. A. Khokhlova, O. A. Sapozhnikov, L. A. Crum, and M. R. Bailey, "Controlled tissue emulsification produced by high intensity focused ultrasound shock waves and millisecond boiling," *J. Acoust. Soc. Am.*, vol. 130, pp. 3498–3510, 2011.

[37] K. J. Parker, "The thermal pulse decay technique for measuring ultrasonic absorption coefficients," *Jounal Acoust. Soc. Am.*, vol. 74, pp. 1356–1361, 1983.

[38] F. Duck, *Physical properties of tissue: a comprehensive reference book*. Academic, London, 1990, pp. 9–137.

[39] J. McLaughlan, I. Rivens, T. Leighton, and G. Ter Haar, "A study of bubble activity generated in ex vivo tissue by high intensity focused ultrasound.," *Ultrasound Med. Biol.*, vol. 36, pp. 1327–1344, Aug. 2010.

[40] A. Rose, *Human and electronic vision*. New York: Plenum Press, 1974.

[41] V. A. Khokhlova, M. R. Bailey, J. A. Reed, B. W. Cunitz, P. J. Kaczkowski, and L. A. Crum, "Effects of nonlinear propagation, cavitation, and boiling in lesion formation by high intensity focused ultrasound in a gel phantom," *J. Acoust. Soc. Am.*, vol. 119, p. 1834, 2006.

[42] C. Lafon, V. Zderic, M. L. Noble, J. C. Yuen, P. J. Kaczkowski, O. A. Sapozhnikov, F. Chavrier, L. A. Crum, and S. Vaezy, "Gel phantom for use in high-intensity focused ultrasound dosimetry.," *Ultrasound Med. Biol.*, vol. 31, pp. 1383–1389, Oct. 2005.

[43] Y. Liu and P. Zhong, "P2G-6 High Intensity Focused Ultrasound Induced Transgene Activation in a Cell-Embedded Tissue Mimicking Phantom," *2006 IEEE Ultrason. Symp.*, pp. 1746–1749, 2006.

[44] A. D. Maxwell, T.-Y. Wang, L. Yuan, A. P. Duryea, Z. Xu, and C. A. Cain, "A tissue phantom for visualization and measurement of ultrasound-induced cavitation damage.," *Ultrasound Med. Biol.*, vol. 36, pp. 2132–2143, Dec. 2010.

[45] J. Gateau, J.-F. Aubry, D. Chauvet, a-L Boch, M. Fink, and M. Tanter, “In vivo bubble nucleation probability in sheep brain tissue.,” *Phys. Med. Biol.*, vol. 56, pp. 7001–7015, Nov. 2011.

[46] T. G. Leighton, *The acoustic bubble*. Academic Press Inc, 1994, p. 335.

[47] M. Monziols, M. Bonneau, A. Davenel, and M. Kouba, “Comparison of the lipid content and fatty acid composition of intermuscular and subcutaneous adipose tissues in pig carcasses.,” *Meat Sci.*, vol. 76, pp. 54–60, May 2007.

[48] W. O’Brien, *The role of collagen in determining ultrasonic propagation properties in tissue*. New York: Plenum Publishing Corporation, 1977, pp. 37–50.

[49] Z. Kyriakou, M. I. Corral-Baques, A. Amat, and C. C. Coussios, “HIFU-induced cavitation and heating in ex vivo porcine subcutaneous fat.,” *Ultrasound Med. Biol.*, vol. 37, pp. 568–579, Apr. 2011.

[50] L. R. Nyman, E. Ford, A. C. Powers, and D. W. Piston, “Glucose-dependent blood flow dynamics in murine pancreatic islets in vivo.,” *Am. J. Physiol. Metab.*, vol. 298, pp. E807–E814, May 2010.

[51] A. Vincent, J. Herman, R. Schulick, R. H. Hruban, and M. Goggins, “Pancreatic cancer.,” *Lancet*, vol. 378, no. 9791, pp. 607–20, Aug. 2011.

[52] A. Jimeno, G. Feldmann, A. Suárez-Gauthier, Z. Rasheed, A. Solomon, G.-M. Zou, B. Rubio-Viqueira, E. García-García, F. López-Ríos, W. Matsui, A. Maitra, and M. Hidalgo, “A direct pancreatic cancer xenograft model as a platform for cancer stem cell therapeutic development.,” *Mol. Cancer Ther.*, vol. 8, no. 2, pp. 310–314, 2009.

[53] H. a Burris, M. J. Moore, J. Andersen, M. R. Green, M. L. Rothenberg, M. R. Modiano, M. C. Cripps, R. K. Portenoy, a M. Storniolo, P. Tarassoff, R. Nelson, F. a Dorr, C. D. Stephens, and D. D. Von Hoff, “Improvements in survival and clinical benefit with gemcitabine as first-line therapy for patients with advanced pancreas cancer: a randomized trial.,” *J. Clin. Oncol.*, vol. 15, no. 6, pp. 2403–13, Jun. 1997.

[54] E. Matano, P. Tagliaferri, A. Libroia, V. Damiano, A. Fabbrocini, S. De Lorenzo, and A. R. Bianco, “Gemcitabine combined with continuous infusion 5-fluorouracil in advanced and symptomatic pancreatic cancer: a clinical benefit-oriented phase II study.,” 2000.

[55] P. E. Oberstein and K. P. Olive, “Pancreatic cancer: why is it so hard to treat?,” *Therap. Adv. Gastroenterol.*, vol. 6, no. 4, pp. 321–37, Jul. 2013.

[56] M. Hidalgo, “Pancreatic cancer.,” *N. Engl. J. Med.*, vol. 362, no. 17, pp. 1605–17, Apr. 2010.

[57] M. A. Jacobetz, D. S. Chan, A. Neesse, T. E. Bapiro, N. Cook, K. K. Frese, C. Feig, T. Nakagawa, M. E. Caldwell, H. I. Zecchini, M. P. Lolkema, P. Jiang, A. Kultti, C. B. Thompson, D. C. Maneval, D. I. Jodrell, G. I. Frost, H. M. Shepard, J. N. Skepper, and D. A. Tuveson, "Hyaluronan impairs vascular function and drug delivery in a mouse model of pancreatic cancer," *Gut*. 2012.

[58] M. Erkan, S. Hausmann, C. W. Michalski, A. a Fingerle, M. Dobritz, J. Kleeff, and H. Friess, "The role of stroma in pancreatic cancer: diagnostic and therapeutic implications.," *Nat. Rev. Gastroenterol. Hepatol.*, vol. 9, no. 8, pp. 454–67, Aug. 2012.

[59] K. P. Olive and D. a Tuveson, "The use of targeted mouse models for preclinical testing of novel cancer therapeutics.," *Clin. Cancer Res.*, vol. 12, no. 18, pp. 5277–87, Sep. 2006.

[60] G. Feldmann, S. Dhara, V. Fendrich, D. Bedja, R. Beaty, M. Mullendore, C. Karikari, H. Alvarez, C. Iacobuzio-Donahue, A. Jimeno, K. L. Gabrielson, W. Matsui, and A. Maitra, "Blockade of hedgehog signaling inhibits pancreatic cancer invasion and metastases: a new paradigm for combination therapy in solid cancers.," *Cancer Res.*, vol. 67, no. 5, pp. 2187–96, Mar. 2007.

[61] A. D. Rhim, P. E. Oberstein, D. H. Thomas, E. T. Mirek, C. F. Palermo, S. A. Sastra, E. N. Dekleva, T. Saunders, C. P. Becerra, I. W. Tattersall, C. B. Westphalen, J. Kitajewski, M. G. Fernandez-Barrena, M. E. Fernandez-Zapico, C. Iacobuzio-Donahue, K. P. Olive, and B. Z. Stanger, "Stromal Elements Act to Restrain, Rather Than Support, Pancreatic Ductal Adenocarcinoma," *Cancer Cell*, pp. 1–13, May 2014.

[62] T. D. Khokhlova and J. H. Hwang, "HIFU for palliative treatment of pancreatic cancer.," *J. Gastrointest. Oncol.*, vol. 2, no. 3, pp. 175–84, 2011.

[63] C. C. Coussios and R. A. Roy, "Applications of Acoustics and Cavitation to Noninvasive Therapy and Drug Delivery," *Annu. Rev. Fluid Mech.*, vol. 40, no. 1, pp. 395–420, Jan. 2008.

[64] W. G. Pitt, G. A. Husseini, and B. J. Staples, "Ultrasonic drug delivery – a general review," *Nature*, pp. 37–56, 2004.

[65] A. Khaibullina, B.-S. Jang, H. Sun, N. Le, S. Yu, V. Frenkel, J. A. Carrasquillo, I. Pastan, K. C. P. Li, and C. H. Paik, "Pulsed high-intensity focused ultrasound enhances uptake of radiolabeled monoclonal antibody to human epidermoid tumor in nude mice.," *J. Nucl. Med.*, vol. 49, no. 2, pp. 295–302, 2008.

[66] S. Tinkov, C. Coester, S. Serba, N. A. Geis, H. A. Katus, G. Winter, and R. Bekeredjian, "New doxorubicin-loaded phospholipid microbubbles for targeted tumor therapy: In-vivo characterization," *J. Control. Release*, vol. 148, no. 3, pp. 368–372, 2010.

[67] E. L. Yuh, S. G. Shulman, S. A. Mehta, J. Xie, L. Chen, V. Frenkel, M. D. Bednarski, and K. C. P. Li, "Delivery of systemic chemotherapeutic agent to tumors by using focused ultrasound: study in a murine model.," *Radiology*, vol. 234, no. 2, pp. 431–437, 2005.

[68] T. Li, H. Chen, T. Khokhlova, Y.-N. Wang, W. Kreider, X. He, and J. H. Hwang, "Passive Cavitation Detection during Pulsed HIFU Exposures of Ex Vivo Tissues and In Vivo Mouse Pancreatic Tumors.," *Ultrasound Med. Biol.*, no. Ferrara 2007, pp. 1–12, 2014.

[69] T. Li, H. Chen, T. Khokhlova, Y.-N. Wang, W. Kreider, X. He, and J. H. Hwang, "Passive cavitation detection during pulsed HIFU exposures of ex Vivo tissues and in vivo mouse pancreatic tumors.," *Ultrasound Med. Biol.*, vol. 40, no. 7, pp. 1523–1534, Mar. 2014.

[70] A. H. Fischer, K. A. Jacobson, J. Rose, and R. Zeller, "Hematoxylin and eosin staining of tissue and cell sections.," *CSH Protoc.*, vol. 2008, p. pdb.prot4986, 2008.

[71] A. Vonlaufen, S. Joshi, C. Qu, P. A. Phillips, Z. Xu, N. R. Parker, C. S. Toi, R. C. Pirola, J. S. Wilson, D. Goldstein, and M. V Apte, "Pancreatic stellate cells: partners in crime with pancreatic cancer cells.," *Cancer Res.*, vol. 68, no. 7, pp. 2085–2093, 2008.

[72] A. M. Al-Abd, N. H. Kim, S.-C. Song, S. J. Lee, and H.-J. Kuh, "A simple HPLC method for doxorubicin in plasma and tissues of nude mice.," *Arch. Pharm. Res.*, vol. 32, no. 4, pp. 605–611, 2009.

[73] R Development Core Team, "R: A language and environment for statistical computing. R Foundation for Statistical Computing, Vienna, Austria. URL http://www.R-project.org/.," *R Foundation for Statistical Computing, Vienna, Austria*. 2013.

[74] S. Ibsen, M. Benchimol, D. Simberg, and S. Esener, "Ultrasound mediated localized drug delivery.," *Adv. Exp. Med. Biol.*, vol. 733, pp. 145–53, Jan. 2012.

[75] N. Nomikou and A. P. McHale, "Exploiting ultrasound-mediated effects in delivering targeted, site-specific cancer therapy.," *Cancer Lett.*, vol. 296, no. 2, pp. 133–143, Oct. 2010.

[76] B. Krasovitski, V. Frenkel, S. Shoham, and E. Kimmel, "Intramembrane cavitation as a unifying mechanism for ultrasound-induced bioeffects.," *Proc. Natl. Acad. Sci. U. S. A.*, vol. 108, no. 8, pp. 3258–3263, 2011.

[77] C. C. Coussios and R. A. Roy, "Applications of Acoustics and Cavitation to Noninvasive Therapy and Drug Delivery," *Annu. Rev. Fluid Mech.*, vol. 40, pp. 395–420, Jan. 2008.

[78] D. M. Hallow, A. D. Mahajan, T. E. McCutchen, and M. R. Prausnitz, "Measurement and correlation of acoustic cavitation with cellular bioeffects," *Ultrasound Med. Biol.*, vol. 32, no. 7, pp. 1111–1122, 2006.

[79] S. Vaezy, X. Shi, R. W. Martin, E. Chi, P. I. Nelson, M. R. Bailey, and L. A. Crum, "Real-time visualization of high-intensity focused ultrasound treatment using ultrasound imaging," *Ultrasound in Medicine & Biology*, vol. 27, no. 1. pp. 33–42, 2001.

[80] B. A. Rabkin, V. Zderic, and S. Vaezy, "Hyperecho in ultrasound images of HIFU therapy: Involvement of cavitation," *Ultrasound Med. Biol.*, vol. 31, no. 7, pp. 947–956, 2005.

[81] B. A. Rabkin, V. Zderic, L. A. Crum, and S. Vaezy, "Biological and physical mechanisms of HIFU-induced hyperecho in ultrasound images," *Ultrasound Med. Biol.*, vol. 32, no. 11, pp. 1721–1729, 2006.

[82] R. G. H. and R. A. R. Constantin -C. Coussios, Caleb H. Farny, Charles R. Thomas, Robin O. Cleveland, "Cavitation detection during and following HIFU exposure in vitro," *Acoust. Soc. Am. J.*, vol. 115, no. 5, p. 2448, 2001.

[83] J. R. Crowe, B. M. Shapo, D. N. Stephens, D. Bleam, M. J. Eberle, E. Ignacio Cespedes, C. C. Wu, D. M. Muller, J. A. Kovach, R. J. Lederman, and M. O'Donnell, "Blood speed imaging with an intraluminal array.," *IEEE Trans. Ultrason. Ferroelectr. Freq. Control*, vol. 47, no. 3, pp. 672–681, 2000.

[84] J. R. Crowe and M. O'Donnell, "Quantitative blood speed imaging with intravascular ultrasound.," *IEEE Trans. Ultrason. Ferroelectr. Freq. Control*, vol. 48, no. 2, pp. 477–487, 2001.

[85] H. Ernst, E. G. Hahn, T. Balzer, R. Schlief, and N. Heyder, "Color doppler ultrasound of liver lesions: signal enhancement after intravenous injection of the ultrasound contrast agent Levovist," *J Clin Ultrasound*, vol. 24, no. 1, pp. 31–35, 1996.

[86] A. Boussuges, "Detection of right-to-left shunts by transcranial contrast Doppler ultrasound.," *Bull. Med sub hyp*, no. 9(suppl), pp. 61–66, 1999.

[87] S. K. Aytaç and H. Ozcan, "Effect of color Doppler system on the twinkling sign associated with urinary tract calculi.," *J. Clin. Ultrasound*, vol. 27, no. 8, pp. 433–439, 1999.

[88] D. H. Simpson, C. T. Chin, and P. N. Burns, "Pulse inversion Doppler: a new method for detecting nonlinear echoes from microbubble contrast agents.," *IEEE Trans. Ultrason. Ferroelectr. Freq. Control*, vol. 46, no. 2, pp. 372–382, 1999.

[89] P. Frinking, "Multi-pulse ultrasound contrast imaging based on a decorrelation detection strategy," *IEEE Ultrason. Symp. Proc.*, vol. 2, pp. 1787–1790, 1998.

[90] K. Tiemann, C. Pohl, T. Schlosser, J. Goenechea, M. Bruce, C. Veltmann, S. Kuntz, M. Bangard, and H. Becher, "Stimulated acoustic emission: Pseudo-Doppler shifts seen

during the destruction of nonmoving microbubbles," *Ultrasound Med. Biol.*, vol. 26, no. 7, pp. 1161–1167, 2000.

[91] R. Daigle, "Sequence programming manual." Verasonics, pp. 64–65, 2011.

[92] O. A. Sapozhnikov, T. Li, T. D. Khokhlova, M. O'Donnell, V. A. Khokhlova, and J. H. Hwang, "A new active cavitation mapping technique for pulsed hifu applications – bubble Doppler," *Int. Soc. Ther. Ultrasound*, 2014.

[93] D. H. Evans and W. N. McDicken, *Doppler Ultrasound - physics, instrumentation and clinical applications.* 2000.

[94] C. Kasai, K. Namekawa, A. Koyano, and R. Omoto, "Real-time two-dimensional blood flow imaging using an autocorrelation technique," *IEEE Trans. Sonics Ultrason.*, vol. 32, no. 3, pp. 458–464, May 1985.

[95] J. M. Rubin, T. A. Tuthill, and J. B. Fowlkes, "Volume flow measurement using doppler and grey-scale decorrelation," *Ultrasound Med. Biol.*, vol. 27, no. 1, pp. 101–109, 2001.

[96] G. Montaldo, M. Tanter, J. Bercoff, N. Benech, and M. Fink, "Coherent plane-wave compounding for very high frame rate ultrasonography and transient elastography.," *IEEE Trans. Ultrason. Ferroelectr. Freq. Control*, vol. 56, no. 3, pp. 489–506, 2009.

[97] M. Tanter and M. Fink, "Ultrafast imaging in biomedical ultrasound.," *IEEE Trans. Ultrason. Ferroelectr. Freq. Control*, vol. 61, no. 1, pp. 102–19, 2014.

[98] S. Choudhry, B. Gorman, J. W. Charboneau, D. J. Tradup, R. J. Beck, J. M. Kofler, and D. S. Groth, "Comparison of tissue harmonic imaging with conventional US in abdominal disease.," *Radiogr. a Rev. Publ. Radiol. Soc. North Am. Inc*, vol. 20, no. 4, pp. 1127–1135, 2000.

[99] Y. Zhou, L. Zhai, R. Simmons, and P. Zhong, "Measurement of high intensity focused ultrasound fields by a fiber optic probe hydrophone.," *J. Acoust. Soc. Am.*, vol. 120, no. 2, pp. 676–685, 2006.

[100] F. Tranquart, N. Grenier, V. Eder, and L. Pourcelot, "Clinical use of ultrasound tissue harmonic imaging," *Ultrasound Med. Biol.*, vol. 25, no. 6, pp. 889–894, 1999.

[101] G. Y. Hou, F. Marquet, S. Wang, and E. E. Konofagou, "Multi-parametric monitoring and assessment of high-intensity focused ultrasound (HIFU) boiling by harmonic motion imaging for focused ultrasound (HMIFU): an ex vivo feasibility study.," *Phys. Med. Biol.*, vol. 59, no. 5, pp. 1121–45, 2014.

[102] F. Wu, Z.-B. Wang, H. Zhu, W.-Z. Chen, J.-Z. Zou, J. Bai, K.-Q. Li, C.-B. Jin, F.-L. Xie, and H.-B. Su, "Feasibility of US-guided high-intensity focused ultrasound treatment in patients with advanced pancreatic cancer: initial experience.," 2005.

[103] H. J. Jang, J.-Y. Lee, D.-H. Lee, W.-H. Kim, and J. H. Hwang, "Current and Future Clinical Applications of High-Intensity Focused Ultrasound (HIFU) for Pancreatic Cancer.," *Gut Liver*, vol. 4 Suppl 1, pp. S57–S61, 2010.

[104] J. E. Kennedy, F. Wu, G. R. Ter Haar, F. V. Gleeson, R. R. Phillips, M. R. Middleton, and D. Cranston, "High-intensity focused ultrasound for the treatment of liver tumours," in *Ultrasonics*, 2004, vol. 42, no. 1–9, pp. 931–935.

[105] C.-X. Li, G.-L. Xu, Z.-Y. Jiang, J.-J. Li, G.-Y. Luo, H.-B. Shan, R. Zhang, and Y. Li, "Analysis of clinical effect of high-intensity focused ultrasound on liver cancer.," *World J. Gastroenterol.*, vol. 10, no. 15, pp. 2201–4, 2004.

[106] F. Wu, L. Zhou, and W. R. Chen, "Host antitumour immune responses to HIFU ablation.," *Int. J. Hyperthermia*, vol. 23, no. 2, pp. 165–171, 2007.

[107] Z. Hu, X. Y. Yang, Y. Liu, G. N. Sankin, E. C. Pua, M. A. Morse, H. K. Lyerly, T. M. Clay, and P. Zhong, "Investigation of HIFU-induced anti-tumor immunity in a murine tumor model.," *J. Transl. Med.*, vol. 5, p. 34, 2007.

[108] F. Wu, Z.-B. Wang, P. Lu, Z.-L. Xu, W.-Z. Chen, H. Zhu, and C.-B. Jin, "Activated anti-tumor immunity in cancer patients after high intensity focused ultrasound ablation.," *Ultrasound Med. Biol.*, vol. 30, no. 9, pp. 1217–1222, 2004.

[109] X. Wang and J. Sun, "High-intensity focused ultrasound in patients with late-stage pancreatic carcinoma.," *Chin. Med. J. (Engl).*, vol. 115, no. 9, pp. 1332–1335, 2002.

[110] Y.-F. Zhou, "High intensity focused ultrasound in clinical tumor ablation.," *World J. Clin. Oncol.*, vol. 2, no. 1, pp. 8–27, 2011.

[111] C. Lafon, V. Zderic, M. L. Noble, J. C. Yuen, P. J. Kaczkowski, O. A. Sapozhnikov, F. Chavrier, L. A. Crum, and S. Vaezy, "Gel phantom for use in high-intensity focused ultrasound dosimetry.," *Ultrasound Med. Biol.*, vol. 31, no. 10, pp. 1383–9, Oct. 2005.

[112] M. J. Choi, S. R. Guntur, K. I. L. Lee, D. G. Paeng, and A. Coleman, "A Tissue Mimicking Polyacrylamide Hydrogel Phantom for Visualizing Thermal Lesions Generated by High Intensity Focused Ultrasound," *Ultrasound Med. Biol.*, vol. 39, no. 3, pp. 439–448, 2013.

[113] Y.-N. Wang, T. Khokhlova, M. Bailey, J. H. Hwang, and V. Khokhlova, "Histological and biochemical analysis of mechanical and thermal bioeffects in boiling histotripsy

lesions induced by high intensity focused ultrasound.," *Ultrasound Med. Biol.*, vol. 39, no. 3, pp. 424–38, 2013.

APPENDIX A

Doppler Processing

During the Doppler processing, the raw RF signals were analyzed to obtain maps of bubble presence using a custom-made program by MatLab (MATLAB 2010b, The MathWorks, Natick, MA, USA) as follows. First, consider Doppler ensemble pulses is consisted of N pulses. We define slow time as the time from one Doppler pulse to the next, determined by the pulse repetition period. And fast time is defined as the time along the reception of each pulse, i.e. along the time of flight from transmit to receive. In VUE, the default number of pulses is 14 [Daigle 2011]. However, the first two pulses are omitted to avoid possible electronic instability and efficient filtering. Therefore, at the first step, the last 12 pulses were plotted along slow time and fast time. Then the signals were beamformed by using the conventional "delay-and-sum" beamforming method. Consider the received beamformed slow time signal $E(n)$, which could be represented as $E(n) = R_e\{Z(n)e^{j\omega_o n}\}$, where $Z(n)$ is the complex envelop of the $E(n)$ and n is the sample point ([94]Kasai et al, 1985). By using a quadrature detector, the real and imaginary parts of $Z(n)$ could be separately obtained. In this case, Hilbert transform was used as a quadrature detector.

Therefore, the signal $Z(n)$ can be represented as $Z(n) = x(n) + jy(n)$, where $x(n)$and $y(n)$ are the real and imaginary parts respectively.

Next, wall filtering was performed to remove the stationary signals along slow time. To do that, the 1st order regression filter was applied to the analytic signal [Evans and McDicken, 2000] and signal echoes from stationary scatters will be reduced; only the Doppler residuals will be left. In the pulse inversion Doppler case, an additional filtering along slow time was applied. A low pass filter with a cut-off frequency of PRF/4 (Matlab function *sgolayfilt*) was applied to the analytic signal so that the resulting signals are only associated with the nonlinear scatters.

After wall filtering, we used the most common method for velocity and Doppler power estimation in modern systems, the autocorrelation algorithm [94]. If $P(\omega)$ is the power Doppler

function along slow time, the relation between the mean angular frequency $\bar{\omega}$ of the power Doppler $P(\omega)$ is defined as:

$$\bar{\omega} = \frac{\int_{-\infty}^{\infty} \omega P(\omega) d\omega}{\int_{-\infty}^{\infty} P(\omega) d\omega}$$

Where $\bar{\omega}$ gives the mean Doppler frequency shift and the mean velocity can be derived as following:

$$\bar{v} = \frac{\bar{\omega} c}{\omega_o 2 \cos\theta}$$

ω_o is the angular frequency of carrier signal; c is the velocity of sound; and θ is the angle between the sound beam and the direction of the flow, which is zero in our case. So if $\bar{\omega}$ is known, the velocity can be calculated. By the Wiener-Khinchine's theorem, the following relationship pertains between the autocorrelation function $R(n)$ of the slow time signal and power Doppler $P(\omega)$:

$R(n) = \int_{-\infty}^{\infty} P(\omega) e^{j\omega n} d\omega,$

$R(0) = \int_{-\infty}^{\infty} P(\omega)\, d\omega,$

$-j\dot{R}(0) = -j\frac{dR}{dn}|_{n=0} = \int_{-\infty}^{\infty} \omega P(\omega) d\omega$

$$\therefore \omega = -j\left[\frac{\dot{R}(0)}{R(0)}\right]$$

If the autocorrelation function could be represented as $(n) = A(n)e^{j\phi(n)}$, where the amplitude function A(n) is an even function and the phase $\phi(n)$ is a odd function of time, the derivative of $R(t)$ becomes

$$\dot{R}(n) = \frac{dA(n)}{dn} e^{j\phi(n)} + jA(t)\frac{d\phi(n)}{dt} e^{j\phi(n)}$$

At $t = 0$, $\dot{R}(0) = [\dot{A}(0) + jA(0)\dot{\phi}(0)]e^{j\phi(0)}$

Since A(t) is even→ $\dot{A}(0) = 0$,

Since $e^{j\phi(t)}$is odd, → $e^{j\phi(0)} = 1$

$$\therefore \dot{R}(0) = jA(0)\dot{\phi}(0) \rightarrow \bar{\omega} = \frac{-j[jA(0)\dot{\phi}(0)]}{A(0)} = \dot{\phi}(0)$$

For discrete signals, the derivative of the autocorrelation phase at lag zero could be approximated as: $\dot{\phi}(0) = \frac{\phi(1)-\phi(-1)}{2} = \frac{2\phi(1)}{2} = \phi(1)$, since $\phi(n)$ is a odd function.

As there were N pulses within each Doppler ensemble, the autocorrelation for 0 delay and one pulse repetition period delay are:

R(0) = $\sum_{i=1}^{N} \mathrm{Z(i)Z^{*}(i)}$

R(1) = $\sum_{i=1}^{N-1} \mathrm{Z(i-1)Z^{*}(i)}$

R(1) is the autocorrelation at lag one, which is at a lag of one pulse repetition period. Therefore, the mean Doppler frequency shift, which is equal to the derivative of the autocorrelation phase at lag zero, can be approximate as:

$\bar{\omega} = \dot{\phi}(0) = \phi(1) = \arg \mathrm{R(1)} = \arg \sum_{i=1}^{N-1} \mathrm{Z(i-1)Z^{*}(i)}$

In this way, Doppler frequency shift and velocity could be estimated. At the final step, the color to be displayed on the image is determined by a threshold. It was defined the same way as Lu [17]. The background noise level was defined as the average of the Doppler powers over all pixels in the entire image. If the Doppler power exceeded more than 6 dB the background noise level, the corresponding pixel was displayed as color.

Curriculum Vitae

Tong Li

Tong Li was born in Beijing, China. She received her B.E. degree in Electronic Engineering in 2009 from Chinese University of Hong Kong, Hong Kong. She is a Ph.D. student in Bioengineering at the University of Washington, Seattle, from 2009 to present. She is also a research assistant at Center for Industrial and Medical Ultrasound (CIMU) with research interests in image guided high-intensity focused ultrasound (HIFU), pulsed HIFU induced cavitation and related clinical applications such as drug delivery in pancreatic cancer. Her research is focused on cavitation monitoring and spatial mapping for pulsed high-intensity focused ultrasound enhanced drug delivery in pancreatic cancer.

Education

2014 Ph.D. Department of Bioengineering, University of Washington

2009 B.E. Department of Electronic, Chinese University of Hong Kong

Academic Awards

2014 Student travel grant recipient for the 14th International Symposium on Therapeutic Ultrasound, Las Vegas, NV

2013 Best presentation award and Student travel grant recipient for the 13th International Symposium on Therapeutic Ultrasound, Shanghai, China

2013 Student travel grant recipient for the 166th Meeting of the Acoustical Society of America, San Francisco, CA

Peer-Reviewd Publications

Tong Li, Hong Chen, Tatiana Khokhlova, Yak-Nam Wang, Wayne Kreider, Xuemei He, Joo Ha Hwang, “Passive cavitation detection during pulsed HIFU exposures of *ex vivo* tissues and *in vivo* mouse pancreatic tumors”, Ultrasound in Medicine and Biology (Published).

Tong Li, Tatiana Khokhlova, Oleg Sapozhnikov, Joo Ha Hwang, "Bubble Doppler on monitoring cavitation in tissue during high-intensity focused ultrasound therapy", IEEE transactions on Ultrasonics, Ferroelectrics and Frequency Control (Accepted).

Tong Li, Tatiana Khokholova, Ezekiel Maloney, Yak-Nam Wang, Kyle Morrison, Navid Farr, George Keilman, Samantha D'Andrea, Frank Starr, Joo Ha Hwang, "Endoscopic high-intensity focused ultrasound – technical aspects and in vivo studies", Gastrointestinal Endoscopy (Submitted).

Tong Li, Yak-Nam Wang, Tatiana Khokhlova, Samantha D'Andrea, Frank Starr, Hong Chen, Jeannine McCune, Linda Risler, Afshin Mashadi-Hossein, Joo Ha Hwang, "Cavitation enhanced uptake of doxorubicin delivery *in vivo* mouse pancreatic tumors", Cancer Research (In Preparation).

Conference Abstracts and Proceedings

Li T, Khokhlova TD, Maloney E, Morrison K, Keilman G, Wang Y-N, Hwang JH (2014), "Endoscopic ultrasound guided high intensity focused ultrasound therapeutic ablation", Digestive disease week 2014, Chicago, IL.

Li T., Khokhlova TD, Wang Y-N, D'Andrea S, Starr F, Hwang JH (2014), "In vivo cavitation enhanced delivery of doxorubicin in mouse pancreatic tumors",14th International Symposium on Therapeutic Ultrasound, Las Vegas, NV.

Sapozhnikov OA, **Li T,** Khokhlova TD, O'Donnell M, Khokhlova VA, Hwang JH, "A new active cavitation mapping technique for pulsed HIFU applications – Bubble Doppler ", The 14th International Symposium on Therapeutic Ultrasound, Las Vegas, NV. (April 14)

Li T., Khokhlova TD, Sapozhnikov OA, Hwang JH, "Twinkling artifact of Doppler imaging for cavitation detection during high-intensity focused ultrasound therapy: sensitivity and resolution", 166th Meeting of Acoustic Society of America, San Francisco, CA. (Dec 13)

Li T., Chen H, Khokhlova TD, Wang Y-N, Hwang JH, "Passive cavitation detection during pulsed high-intensity focused ultrasound exposures of ex vivo tissues and in vivo mouse model of pancreatic tumors",13th International Symposium on Therapeutic Ultrasound, Shanghai, China. (May 13)

Sapozhnikov OA, **Li T**, Khokhlova TD, Hwang JH (2013), "The use of twinkling artifact of Doppler imaging to monitor cavitation in tissue during HIFU therapy", The 13th International Symposium on Therapeutic Ultrasound, Shanghai, China.

Conference Proceedings

Khokhlova TD, **Li T**, Sapozhnikov OA, Hwang JH (2013). "The use of twinkling artifact of Doppler imaging to monitor cavitation in tissue during high intensity focused ultrasound therapy." The Journal of the Acoustical Society of America 133(5):3315.

Owen NR, Kaczkowski PJ, **Li T**, Gross D, Postlewait SM, Curra FP (2010). "Multilayer array transducer for nonlinear ultrasound imaging. The 10th International Symposium on Therapeutic Ultrasound." AIP Conference Proceedings 1359: 206-210.